Circulation Agreement

In presenting this dissertation/thesis as a partial fulfillment of the requirements for an advanced degree from Emory University, I agree that the Library of the University shall make it available for inspection and circulation in accordance with its regulations, governing materials of this type. I agree that permission to copy from, or to publish, this thesis/dissertation may be granted by the professor under whose direction it was written, or, in his/her absence, by the Dean of the Graduate School when such copying or publication is solely for scholarly purposes and does not involve potential financial gain. It is understood that any copying from, or publication of, this thesis/dissertation which involves potential financial gain will not be allowed without written permission.

_____

Yong Jiang

Molecular simulations of lipid systems:

Edge stability and structure in pure and mixed bilayers

By

Yong Jiang

Doctor of Philosophy

Department of Chemistry

_____

Dr. James T. Kindt
Advisor

_____

Dr. Joel M. Bowman
Committee Member

_____

Dr. Tianquan Tim Lian
Committee Member

Accepted:

_____

Lisa A. Tedesco, Ph.D.
Dean of the Graduate School

_____

Date

Molecular simulations of lipid systems:

Edge stability and structure in pure and mixed bilayers

By

Yong Jiang

B.S., Peking University, 2001

Advisor: James T. Kindt, Ph.D.

An Abstract of
A dissertation submitted to the Faculty of the Graduate
School of Emory University in partial fulfillment
of the requirements for the degree of
Doctor of Philosophy

Department of Chemistry

2007

Abstract

Understanding the structural, mechanical and dynamical properties of lipid self-assembled systems is fundamental to understand the behavior of the cell membrane. This thesis has investigated the equilibrium properties of lipid systems with edge defects through various molecular simulation techniques. The overall goal of this study is to understand the free energy terms of the edges and to develop efficient methods to sample equilibrium distributions of mixed-lipid systems.

In the first main part of my thesis, an atomistic molecular model is used to study lipid ribbon which has two edges on both sides. Details of the edge structures, such as area per lipid and tail torsional statistics are presented. Line tension, calculated from pressure tensor in MD simulation has good agreement with result from other sources. To further investigate edge properties on a longer timescale and larger length scale, we have applied a coarse-grained forcefield on mixed lipid systems and try to interpret the edge fluctuations in terms of free energy parameters such as line tension and bending modulus. We have identified two regimes with quite different edge behavior: a high line tension regime and a low line tension regime. The last part of this thesis focuses on a hybrid Molecular dynamics and Configurational-bias Monte Carlo (MCMD) simulation method in which molecules can change their type by growing and shrinking the terminal acyl united carbon atoms. A two-step extension of the MCMD method has been developed to allow for a larger difference in the components' tail lengths. Results agreed well with previous one-step mutation results for a mixture with a length difference of four carbons. The current method can efficiently sample mixtures with a length difference of eight

carbons, with a small portion of lipids of intermediate tail length. Preliminary results are obtained for “bicelle”-type (DMPC/DHPC) ribbons.

Molecular simulations of lipid systems:

Edge stability and structure in pure and mixed bilayers

By

Yong Jiang

B.S., Peking University, 2001

Advisor: James T. Kindt, Ph.D.

A dissertation submitted to the Faculty of the Graduate
School of Emory University in partial fulfillment
of the requirements for the degree of
Doctor of Philosophy

Department of Chemistry

2007

Acknowledgement

First and foremost, I would like to thank my advisor, Dr. James Kindt for all his dedicated guidance and support through my study at Emory University. He has always patiently explained theoretical principles and techniques used in experiments. He has given me expert advice in solving the research problems and steered me down the right path. He always encourages me to work independently while very willing to discuss my research and offering guidance without giving any pressure. I feel fortunate to have him as my Ph.D. advisor.

I am also indebted to my committee members, Dr. Joel Bowman and Dr. Tim Lian, for their tutorship in course lectures and their constant advice and support in my research career afterwards. Their questions and comments in yearly report presentations are very constructive and lead me to a deeper understanding of my project.

I would like to thank Dr. Jason de Joannis for his numerous constructive suggestions to my research on a daily basis. He offered insights and raised questions in group meeting which stimulated me into deep understanding of my projects. I enjoyed discussing science or even politics with him during lunch time and learned a lot in American culture. He organized a walleyball team that brought many people to the sport to release the pressure felt as an academic researcher. Also, he was always ready to provide help in my postdoctoral application. He has left so much joyful moments that I will cherish forever in my memory.

During my years at Emory, I have benefited from many faculty members. I should thank Professor Keiji Morokuma, Professor MC Lin for teaching Physical Chemistry graduate courses in my early years at Emory. I thank Professor Fereydoon Family for teaching me Statistical Physics in my third year and help me to clarify some technical details when I prepared for my oral defense. I should also thank Dr. James Snyder for teaching me a course in molecular modeling and I enjoyed participating in a small project and learned a lot hand-on experience in modeling protein systems.

My labmates also help me a lot during my research at Emory. Dr. Hao Wang, the postdoc in our group and also my very good friend, has been given my countless suggestions on successfully balancing my academic research and personal life. He is very considerate and comforted me when I have been frustrated. He has been very patient listening to my practice talks, giving suggestions for improvements and taking me to the airport for job interviews. Another graduate student in our group, Mr. Xinjiang Lv, is very active in exchanging ideas with me regarding research topics, computer skills and

improving English as a foreigner. I should thank Mr. Fuchang Yin for sharing his extraordinary computer expertise. I learned a lot from him about python scripting language which greatly improves the efficiency in analyzing simulation data. Also, I must thank Mr. Patrick Coppock for his invaluable help for proofreading my manuscript, correcting my grammar error and giving me suggestions on preparing my slides. His forever smiling and sense of humor expels all the fatigue and keeps me working very happily.

My appreciation extends to many people among whom I can only mention a few. I thank Dr. Jamal Musaev, Dr. Stephan Irle and Dr. Alex Kaledin for the excellent maintenance of Emerson Center computers and softwares. I thank previous Emerson Center administrative assistant, Ms.Jianli Zhao for her kind advice on the administrative issues.

Finally I should thank my parents Ms. Baoyun Dai and Mr.Xingguo Jiang for their forever unconditional love. I could not have achieved my work without their support. This dissertation is dedicated to them.

TABLE OF CONTENTS

List of Figures

Chapter 1: Introduction

Chapter 2: Atomistic Simulation of lipid Bilayer edge

Chapter 3: Coarse-grained MD simulation of mixed bilayer systems: Understanding the in-plane fluctuation of bilayer edge

Chapter 4: Two-step hybrid Configurational-bias Monte Carlo and Molecular dynamics simulations of mixed lipid bilayer

List of Tables

Chapter 1: Introduction

Chapter 2: Atomistic Simulation of lipid Bilayer edge

Chapter 3: Coarse-grained MD simulation of mixed bilayer systems: Understanding the in-plane fluctuation of bilayer edge

Chapter 4: Two-step hybrid Configurational-bias Monte Carlo and molecular dynamics simulations of mixed lipid bilayer

Chapter One

Introduction

INTRODUCTION

Lipid bilayers are the main components of biological membranes. In eukaryotic cells, phospholipids are the most common lipid type. As lipids have both hydrophilic and hydrophobic moieties, their assemblies show various morphologies and phases in water. The most biologically relevant phase is the lipid bilayer in liquid crystalline phase (Lα phase) in which lipid molecules are not trapped in the local regions within bilayers but can diffuse laterally within the bilayer. Experimentally, X-ray diffraction techniques are used to elucidate the detailed structural properties such as the area per lipid, electron density profile and bilayer thickness [1]. However, X-ray based techniques have the shortcoming of not being able to resolve accurate electron density profile at higher order, especially for the fully hydrated Lα phase. The higher order intensities from the diffraction signal are reduced due to the bilayer fluctuation and protrusion and therefore lead to large uncertainties. Detailed structure and dynamics can also be extracted from solid-state deuterium and phosphorus NMR experiments [2, 3]. The dynamics of internal atomic motion and rotational diffusion of the lipid can be inferred by measuring the motional correlation time involving deuterated atoms. Order parameters S^{CD}, a characteristic measurement of orientational order of membrane lipid can also be calculated directly from quadrupolar splitting. NMR is powerful, nevertheless insufficient to trace the dynamics and structure of individual molecules in a disordered bilayer. Complementary to experimental limitations, molecular dynamics simulation of lipid systems has been a powerful tool to understand their equilibrium properties. In molecular dynamics, systems are subject to a forcefield and evolve with time based on Newton's equation of motion. The integration of motion is solved numerically. System

configurations are recorded periodically, each representing one particular point in phase space. It is reasonable to assume that a macroscopic observable A is the time average of instantaneous properties of the configuration along the trajectory:

$$A_{obs} = \left\langle A(\Gamma(t)) \right\rangle_{time} = \lim_{t \to \infty} \frac{1}{t_{obs}} \int_0^{obs} A(\Gamma(t)) dt$$

where Γ stands for a particular point in phase space and its time evolution is classically governed by Newton's equations of motion. That is exactly what MD simulation do: sequentially and numerically solve these equations on a step-by-step basis. We clearly cannot run MD simulation for infinitely long time; however a reasonably long time is sufficient for many biological systems on nanometer scale. The current time-scale limitation of atomistic MD simulation is on the order of a few hundred nanoseconds and the size of the system is under a million atoms. These boundaries limit its applications on systems such as phase transitions, bilayer fusion or folding of large proteins.

Due to the fact that MD simulation is based on step-by-step integration, algorithms that accurately predict the trajectory path for all the particles do not exist. It has been established that however close initially, two configurations will diverge exponentially as time progresses. This is called the Lyapunov instability; because of it, small inaccuracies in integration grow into large differences in configurations[4]. However, the Lyapunov instability has not raised many concerns and worries as considerable numerical evidence has supported that numerical trajectory for a reasonable amount of time can still reproduce, at least statistically, the system properties at equilibrium. As we cannot experimentally know or control the exact configuration of a

system with many atoms anyhow, it is the statistical properties that interest us more than any single trajectory.

Despite the limitations above, with the improvement of forcefield and increasing computational power, molecular dynamics simulation has become an indispensable tool to investigate nanoscale biological process. Its application to lipid bilayers has become common [5-7]. However, the properties of lipid bilayer edge have not been investigated thoroughly. Lipid bilayer edge is usually considered unstable as its existence will increase the free energy of lipid assemblies per unit length of the edge (namely, line tension) and therefore reflect the resistance of the bilayer to damage or bisection. However, some compound, eg. short-tail lipids, when introduced to pure lipid bilayer systems, will greatly reduce the line tension and leads to disruption of the bilayer into disks, ribbons or porous structures[8]. These phase morphologies are closely related to the free energy of lipid bilayer edge and distributions of different lipid types.

This thesis describes my graduate work at Emory University which is consists of three parts. (1) Atomistic simulations of lipid bilayer edge (2) Coarse-grained simulation of lipid bilayer edge and its fluctuation analysis (3) Hybrid configurational-bias Monte Carlo and molecular dynamics simulation method and its applications.

Atomistic simulations of lipid bilayer edge

In the first part, atomistic model of DMPC[a] and POPE[b] lipids are used to investigate the properties of the edge of pure bilayers. In the starting configuration, edges are present with the hydrophobic tails exposed to solvents. Within 2ns, the DMPC headgroups migrated to the edge region and formed a rounded cap to exclude the direct contact between solvents and hydrophobic tails. A similar process is observed in POPE edges, however the migration process is much longer. The stability of the edge is characterized by line tension, defined as the free energy penalty per unit edge length. The line tension is a mechanical indicator of system durability under external disturbance. A typical positive line tension for membrane lipids is on the order of 10~30pN, equivalent to 2.5~7.5k_BT/nm, large enough to close any transient pores and to keep the system from breaking into disks. It is observed that line tension is largely affected by the system composition. By adding some edge-active agents (e.g. detergents or lipids that have shorter tail length), line tension can be greatly reduced, leading to a variety of stable morphologies, including disks, perforated bilayers and perforated vesicles. In some cases, these lipid mixtures have the property of being able to align with the presence of magnetic field and therefore they are used as media in NMR studies on large biomolecules such as trans-membrane proteins[9, 10].

Line tension can be measured through aspiration of vesicles with a pore into a micropipette [11]. In experiment, a liposome larger than a micropipette radius is attached and an electric pulse is applied to induce a pore on the vesicle. With advanced techniques

[a]DMPC : dimyristoylphosphatidylcholine, systematic name: 1,2-Dimyristoyl-*sn*-Glycero-3-Phosphocholine
[b]POPE : palmitoyloleoylphosphatidylethanolamine, systematic name: 1-Palmitoyl-2-Oleoyl-*sn*-Glycero-3-Phosphoethanolamine

of video imaging, the size and lifespan of pore can be measured and line tension can be inferred by the balance of surface tension of the vesicle that tends to increase the pore size and line tension of the pore that tends to reduce the pore size. In this computational study, a ribbon geometry of lipid assembly is used to simplify the calculation of lipid line tension. Line tension is calculated from the difference of pressure tensor in the edge direction and the directions perpendicular to it. We have observed that line tension is highly sensitive to electrostatic treatments of charged groups. Line tension calculated from this study is on the order of 10-30pN and agrees well with experimental measurement. Structural and dynamical properties are also investigated. Our research indicates that the presence of bilayer edge could potentially accelerate the flip-flop events.

Coarse-grained simulation of lipid bilayer edge and its fluctuation analysis

The second part of this thesis aims to infer the physical parameters that control the free energy of the edge by fluctuation analysis. Edges are frequently observed in mixed lipid system since the line tension is greatly reduced as short-tail lipid moves towards the edge covering the most part of the rim. Sanders and Schwonek[10] first introduced the mixed lipid assemblies, called “bicelles”, to NMR studies of membrane-associate macromolecules. Bicelles can align nematically with the magnetic field which gives rise to non-zero dipole-dipole coupling signals. These signals contain information about the relative positions of heavy atoms and therefore bicelles are widely used in NMR studies. Cryo-TEM experiments [12] show that bicelles’ microscopic morphologies vary with system composition and temperature. A thorough investigation of individual components

in free energy of the edge would be crucial to understand these morphological transformations. The free energy of the edge would result from line tension effect which tends to reduce the edge length and, we hypothesize, from bending effect which tends to reduce the curvature effect. It is reasonable to assume that the second effect would become dominant at certain binary lipid composition when line tension is small. However to investigate the fluctuation of the edge of mixed lipid systems through conventional atomistic models in MD simulation require time-scale that is much larger than current affordability to reach equilibrium. Coarse-grained (CG) models, in which a group of atoms are mapped into one CG particle, can be used to overcome this dynamic barrier. In these models, the degrees of freedom are reduced and since each CG particle is much "heavier" than real atoms the time step in numerical integration is also increased by a factor of 10. In this study, a coarse-grained forcefield [13] is used to fully sample the edge fluctuation behavior at equilibrium at longer length scale and time scale. Structural properties and line tension can be well reproduced using these models. As expected, line tension values have set the systems into 2 categories: high line tension and low line tension regime. Our results show that at high line tension, a single parameter is sufficient to explain the bilayer edge fluctuation statistics. On the other hand, when the line tension approaches to zero, bilayer edge fluctuates under the apparent effect of elasticity modulus and a harmonic energy term with a preferred edge length. This study, combined with a Monte Carlo model and theoretical formulas, has shed light on the how line tension and bending modulus would affect the edge properties and distribution of lipid molecules from different types.

Two-step hybrid Configurational-bias Monte Carlo and Molecular dynamics

In many biologically-relevant systems, mixed lipid assemblies do not have a uniform distribution of different lipid types. For instance, previous simulations [14, 15] show that lipid edge would prefer a preponderance of short tail lipid on and near the edge with the bulk part mainly occupied with long-tail lipid. With fluorescence intensity measurement techniques, lactose permease, a integral membrane protein, shows preference for lipid whose hydrophobic tail length matches its trans-membrane hydrophobic domains[16]. The protein/lipid hydrophobic matching has been considered to have impact on protein activity and membrane organization[17]. As it is hard to measure the microscopic distribution of different lipids, it is useful to apply simulation to study lipid mixtures.

As the diffusion of lipid in liquid crystalline phase is slow (on the order of 1 $nm^2/\mu s$), the timescale required to approach equilibrium distribution of mixed lipid systems, starting from completely random mixture, is on the order of μs. Therefore atomistic simulation of mixed lipid systems at equilibrium using conventional MD is prohibitive. To take advantage of the capability of bypassing the barrier in phase space using artificial stochastic moves, MC and mixed MC-MD methods are developed to improve the sampling in the atomistic lipid bilayer simulations. For example, the hybrid MC-MD method developed by Chiu et al[18] has used a block of configurational-bias Monte Carlo (CBMC) steps alternating with a block of regular MD steps.

Configurational-bias Monte Carlo[19-22] has the advantage of sampling the configurations of chain molecules at different length. In CBMC, the Rosenbluth weight is used to bias the generation of trial conformations with corrected Boltzmann distribution recovered through Monte Carlo scheme. In contrast to the method of Chiu et al, in which only local tail rearrangement were performed using CBMC, we have used CBMC to switch lipid type through varying the tail length. In this semi-grand ensemble approach(see [23] for more details), DPPC and DLPC lipids, which differ by 4 carbons in each of its tail, will attempt to exchange its identity by growing or shrinking carbon atoms along the tails according to this procedure, and the acceptance ratio of these attempts depends on the tail length difference between the two lipids types. Based on previous established CBMC, we integrated this method into Gromacs MD codes and applied to binary mixed DPPC[c]-DLPC[d] systems at various compositions[24]. This CBMC step allows simulation to investigate the distribution of different lipid types more easily without following the true dynamics of each atom in the system. Between CBMC steps, molecular dynamics steps are performed so that lipid tail configurations can be sampled locally and to equilibrate the lipid headgroups and solvents. The successful rate of MC mutation in the DPPC/DLPC system is approximately 0.1%, which enables the composition of 128 lipid system to converge within 1 ns, a great improvement over pure MD simulations. However, we found the acceptance ratio to be unacceptably low when the above scheme is applied to more relevant applications such as "bicelles", which are composed of DMPC[e]/DHPC[f] mixture. Described in previous section, bicelles are used as

[c] DPPC: dipalmitoylphosphatidylcholine, systematic name: 1,2-Dipalmitoyl-*sn*-Glycero-3-Phosphocholine
[d] DLPC: dilauroylphosphatidylcholine, systematic name: 1,2-Dilauroyl-*sn*-Glycero-3-Phosphocholine
[e] DMPC: dimyristoylphosphatidylcholine, systematic name: 1,2-Dimyristoyl-*sn*-Glycero-3-Phosphocholine
[f] DHPC: dihexanoylphosphatidylcholine, systematic name: 1,2-Diheptanoyl-*sn*-Glycero-3-Phosphocholine

media solvent which aligns with magnetic field while not disrupting big biomolecules', such as membrane protein, activity in NMR studies. The low acceptance of mutation attempts are on account of the large difference of tail length (8 carbons in each tail) between the two lipid types. To solve this dilemma, we developed a two-step mutation scheme: an intermediate species is introduced to facilitate the transforming of long-tail lipid to the short-tail lipid. This two-step mutation resembles in some respects the "expanded ensemble" method[25] in which intermediate states between initial and final states are sampled through configurational bias Monte Carlo methods; each intermediate states has a preweighting factor that is predetermined iteratively and its exponential is included in the partition function of extended ensemble. In the current two-step MCMD method, only one intermediate is introduced and its weighting factor is determined by its chemical potential difference with the long tail lipid. The intermediate species helps to establish two equilibria: intermediate/L and intermediate/S. The activity ratios, the parameters that determine the relative ratio between two species of the equilibrium, are carefully chosen to keep a low level of intermediate species so that the system is still largely composed of components L and S. This two-step MCMD method has been successfully applied to DMPC/DHPC system with edge defects. Distribution profiles and line tension calculation from CBMC-MD simulations are consistent with coarse-grained simulations and previous atomistic simulations. The most unique advantage of this method is that it enables fast approaching to the equilibrium distribution among the lipid types while reproducing the structural and mechanical properties without losing the atomic details.

REFERENCE

1. Nagle, J.F. and S. Tristram-Nagle, *Structure of lipid bilayers.* Biochimica Et Biophysica Acta-Reviews on Biomembranes, 2000. **1469**(3): p. 159-195.
2. Dufourc, E.J., et al., *Dynamics of Phosphate Head Groups in Biomembranes - Comprehensive Analysis Using P-31 Nuclear-Magnetic-Resonance Lineshape and Relaxation-Time Measurements.* Biophysical Journal, 1992. **61**(1): p. 42-57.
3. Aussenac, F., et al., *Detailed structure and dynamics of bicelle phospholipids using selectively deuterated and perdeuterated labels. H-2 NMR and molecular mechanics study.* Langmuir, 2003. **19**(25): p. 10468-10479.
4. Frenkel, D. and B. Smit, *Understanding molecular simulation : from algorithms to applications*. 2nd ed. Computational science: from theory to applications ; v. 1. 2002, San Diego, Calif. London: Academic Press. xxii, 638 p.
5. Tieleman, D.P., S.J. Marrink, and H.J.C. Berendsen, *A computer perspective of membranes: molecular dynamics studies of lipid bilayer systems.* Biochim. Biophys. Acta., 1997. **1331**: p. 236.
6. Jakobsson, E., *Computer simulation studies of biological membranes: progress, promise and pitfalls.* Trends in Biochemical Sciences, 1997. **22**(9): p. 339-344.
7. Pastor, R.W., *Molecular-Dynamics and Monte-Carlo Simulations of Lipid Bilayers.* Current Opinion in Structural Biology, 1994. **4**(4): p. 486-492.
8. Katsaras, J., et al., *"Bicellar" lipid mixtures as used in biochemical and biophysical studies.* Naturwissenschaften, 2005. **92**(8): p. 355-366.

9. Tjandra, N. and A. Bax, *Direct Measurement of Distances and Angles in Biomolecules by NMR in a Dilute Liquid Crustalline Medium.* Science, 1997. **278**: p. 1111.

10. Sanders, C.R. and J.P. Schwonek, *Characterization of Magnetically Orientable Bilayers in Mixtures of Dihexanoylphosphatidylcholine and Dimyristoylphosphatidylcholine by Solid-State Nmr.* Biochemistry, 1992. **31**(37): p. 8898-8905.

11. Zhelev, D.V. and D. Needham, *Tension-Stabilized Pores in Giant Vesicles - Determination of Pore-Size and Pore Line Tension.* Biochimica Et Biophysica Acta, 1993. **1147**(1): p. 89-104.

12. van Dam, L., G. Karlsson, and K. Edwards, *Direct observation and characterization of DMPC/DHPC aggregates under conditions relevant for biological solution NMR.* Biochimica Et Biophysica Acta-Biomembranes, 2004. **1664**(2): p. 241-256.

13. Marrink, S.J., A.H. de Vries, and A.E. Mark, *Coarse grained model for semiquantitative lipid simulations.* Journal of Physical Chemistry B, 2004. **108**(2): p. 750-760.

14. Jiang, F.Y., Y. Bouret, and J.T. Kindt, *Molecular dynamics simulations of the lipid bilayer edge.* Biophysical Journal, 2004. **87**(1): p. 182-192.

15. de Joannis, J., F.Y. Jiang, and J.T. Kindt, *Coarse-grained model simulations of mixed-lipid systems: Composition and line tension of a stabilized bilayer edge.* Langmuir, 2006. **22**(3): p. 998-1005.

16. Dumas, F., M.C. Lebrun, and J.F. Tocanne, *Is the protein/lipid hydrophobic matching principle relevant to membrane organization and functions?* Febs Letters, 1999. **458**(3): p. 271-277.

17. Killian, J.A., et al., *Modulation of membrane structure and function by hydrophobic mismatch between proteins and lipids.* Pure and Applied Chemistry, 1998. **70**(1): p. 75-82.

18. Chiu, S.W., et al., *Application of combined Monte Carlo and molecular dynamics method to simulation of dipalmitoyl phosphatidylcholine lipid bilayer.* Journal of Computational Chemistry, 1999. **20**(11): p. 1153-1164.

19. Stubbs, J.M. and J.I. Siepmann, *Aggregation in dilute solutions of 1-hexanol in n-hexane: A Monte Carlo simulation study.* Journal of Physical Chemistry B, 2002. **106**(15): p. 3968-3978.

20. Siepmann, J.I. and I.R. Mcdonald, *Monte-Carlo Simulations of Mixed Monolayers.* Molecular Physics, 1992. **75**(2): p. 255-259.

21. Martin, M.G. and J.I. Siepmann, *Predicting multicomponent phase equilibria and free energies of transfer for alkanes by molecular simulation.* Journal of the American Chemical Society, 1997. **119**(38): p. 8921-8924.

22. Siepmann, J.I. and D. Frenkel, *Configurational Bias Monte-Carlo - a New Sampling Scheme for Flexible Chains.* Molecular Physics, 1992. **75**(1): p. 59-70.

23. Kofke, D.A., *Advances in Chemical Physics: Monte carlo methods in chemical physics*, ed. D.M. Ferguson, J.I. Siepmann, and D.G. Truhlar. Vol. 105. 1998: Interscience. 405-441.

24. Joannis, J., et al., *Equilibrium distributions of dipalmitoyl phosphatidylcholine and dilauroyl phosphatidylcholine in a mixed lipid bilayer: Atomistic semigrand canonical ensemble simulations.* Journal of Physical Chemistry B, 2006. **110**(51): p. 25875-25882.

25. Escobedo, F.A. and J.J. Depablo, *Monte-Carlo Simulation of the Chemical-Potential of Polymers in an Expanded Ensemble.* Journal of Chemical Physics, 1995. **103**(7): p. 2703-2710.

Chapter Two

Molecular Dynamics Simulations of the Lipid Bilayer Edge

INTRODUCTION

Many physical and biochemical properties of lipid bilayers are important to the bilayer's fundamental role as the basis of biological membranes. These properties are now commonly investigated by atomistic molecular dynamics (MD) simulation (for general reviews of atomistic simulation of lipid bilayers, see [1-6]). Some of these properties include elastic moduli for bending and stretching [7-9], diffusion constants[10, 11], electrostatic and dielectric properties [12, 13], intrinsic permeability to ions and small molecules[14-16], influence on solvating water [17, 18], mechanisms of fusion [19, 20], and influences on membrane-associated macromolecules [21-27]. Simulation has been useful for providing detailed insight into how complex molecular interactions lead to experimentally observable behavior.

Free edges are infrequently observed in bilayer or membrane systems. At equilibrium, edges will typically be eliminated from bilayer systems either through the assembly of extended lamellar sheets or of closed-shell vesicle structures. Nonetheless, several motivations exist for studying the bilayer edge. Edge defects are formed transiently by mechanical or electrical impulses (e.g., osmotic stress or electroporation) as a means of introducing DNA or other material into living cells. Spontaneously formed pore edges have been proposed to play roles in bilayer fusion [28] [29] and transleaflet "flip-flop" lipid diffusion [30]. Edges are presumably present during the initial stages of lipid assembly into lamellar or vesicle structures [31]. The typical instability of the edge can be characterized by a positive free energy per unit length (or line tension) that experiment and theory place on the order of 10^{-11} N. Early experiments relied on indirect

measurements such as vesicle leakage rates [32], the shapes of open-ended bilayer tubes [33], or the voltage-dependent rate of electroporation [34] to calculate the line tension. With the achievement of video imaging of giant vesicles [35, 36], line tensions have been measured somewhat more directly through aspiration of pore-containing vesicles into a pipette (in which case the dynamics of the vesicle could be related to the dynamics of water efflux through the pore) [37, 38] and through the direct observation of pore resealing dynamics[39].The edge can be stabilized by the addition of a variety of "edge-active agents" [40] that can reduce or eliminate the line tension, as observed experimentally, e.g., in the formation of stable bicelle disks used in macromolecular NMR[41] and in the formation of stable channels by some ceramides[42].

From early accounts [46] onward, the microscopic structure of the edge has been envisioned as a rounded, hemicylindrical rim of hydrophilic headgroups that protects the hydrophobic bilayer interior from contact with water. In the absence of experimental methods for the study of such a transient structure, few attempts have been made to add more detail to this picture. Computer simulations of pore formation in a lattice-based model of a diblock-copolymer bilayer have been reported [47] showing that, except for very small pore sizes, the expected reconstructed hydrophilic edge picture was valid and that a line tension could be obtained by relating bilayer surface tension to the pore size for sufficiently large pores. Very small pores, with lifetimes on the order of 15 ns, were observed during atomistic simulation of the self-assembly of the phospholipid dipalmitoylphosphatidylcholine (DPPC) into a bilayer [48]; these had the character of point defects rather than one-dimensional edges. The formation of small pores in the bilayer, through mechanical tension or applied electric field, has recently been modeled at

the atomistic level[49] showing that headgroups do line the aqueous interior of the pore. A phenomenological theoretical study[50] has modeled the edge by treating lipids as incompressible yet elastically deformable objects whose energy depends on chain extension length as well as headgroup packing density curvature. This calculation yielded the line tension of the edge as a function of a lipid shape parameter (in good general agreement with experimental estimates) as well as a description of the optimal shape profile of the membrane rim. Pande et al.[43] have investigated DMPC lipid assemblies with gap filled with waters. In den Otter's paper, line tension is estimated about (3.5–4.0)$\times 10^{-11}$ J/m through coarsed-grained model for stable pores [44, 45]. This line tension is obtained by calculating the free energy profile at various pore sizes. However, although these line tension agreed with experiments, the curvature of pore is not considered thoroughly and deducted from these values. In addition, their line tension shows virtually no dependence on rather small pores, which is more or less artificial.

In attempting to model a bilayer edge, one might begin with a bilayer disk structure or a bilayer containing a large pore; in either case, the radius of curvature of the edge in the bilayer plane (or equivalently, the magnitude of the Gaussian curvature of the lipid-water interface, positive for a disk and negative for a pore) depends on the size of the system simulated. In this investigation, we have chosen instead to simulate a system with zero mean curvature along the direction of the edge, a continuous bilayer ribbon, or rather a 2D array of ribbons in which the ribbon edges continue across periodic boundaries in a unique direction that we will call *z*. Apart from the avoiding the uncertainty of the dependence of edge properties on curvature (an interesting question, but one requiring a series of simulations), this arrangement facilitates the calculation of

the line tension from the anisotropy of pressure in z versus x and y. Lipid bilayer ribbons studied were composed either of dimyristoylphosphatidylcholine (DMPC) or palmitoyl-oleoylphosphatidylethanolamine (POPE).

In these simulations, the migration of headgroups around the DMPC edge to form a rounded, reconstructed structure appears complete within 2 ns, whereas for POPE the process is significantly slower and continued throughout a 14-ns simulation. Edge structure and line tension are significantly influenced by long-ranged electrostatic forces. The line tensions calculated for DMPC ribbons simulated using the particle mesh Ewald (PME) algorithm [51, 52] ranged between 12 and 35 pN (within qualitative agreement with experimental estimates for several lipids) but rose by an order of magnitude when an electrostatic truncation method was used. The edge profile of the DMPC ribbon in the simulation displayed bulges at the edges when electrostatic forces were treated fully but not when truncation was used. The effects of electrostatics and lipid structure differences offer some insight into the general principles governing line tension and edge structure.

METHODS

The molecular dynamics simulations were carried out using GROMACS (version 3.1.3, single precision; [53, 54]. Most simulations were performed on a Beowulf-type cluster of dual-processor 1.4-GHz 1600 MP Athlon Linux nodes (Linuxlabs, Atlanta, GA), using either one or six processors; some final calculations were performed using an Intel 3.0-GHz dual processor system (Penguin Computing, San Francisco, CA). The VMD package [55] was used for visualization and molecular graphics.

The starting configurations were adapted as described below from the fluid phase DMPC and POPE bilayer coordinates made available by the Tieleman group at the University of Calgary at http://moose.bio.ucalgary.ca/Downloads/files/dmpc_npat.pdb and http://moose.bio.ucalgary.ca/Downloads/files/pope.pdb [56]

To generate a ribbon-like configuration from the intact DMPC bilayer, we first double the system size by appending its replica in the *x* direction using the GROMACS genconf utility, yielding a rectangular bilayer patch of 256 lipids with 7310 waters. Lipids whose phosphorus atom coordinates lied in a 3.4-nm band in the *y* direction were removed, leaving behind a ribbon of 183 lipids with two free edges, separated from its replica by open space. The *x* and *z* coordinates of the system were then switched so that the edges would run along the *z* axis (which will be necessary for proper pressure equilibration in GROMACS). The simulation box dimension in the *x* direction (now normal to the bilayer) was increased to prevent steric interaction of the ribbon with its replica in case it rotates around the *z* axis. The empty spaces in the simulation box were filled with water using the genbox utility; a number of waters inserted within the bilayer interior by this utility were then removed. The starting configuration of the DMPC bilayer ribbon in the context of neighboring periodic repeats, with waters omitted, is shown in Figure 2.1. The same procedure, with only details changed, was used to prepare all ribbon simulations to run. Details are listed in Table 2.1.

Run	Box dimensions (x, y, z), nm*	No. of lipids	No. of H_2O	Description	Treatment of electrostatic interaction	Simulation time (total)
1	(6.176, 6.176, 6.661)	128DMPC	3,655	Intact bilayer	PME	5 ns
2	(12.280, 12.280, 6.140)	183DMPC	24,308	Ribbon	Cutoff	19.5 ns
3	(12.280, 12.280, 6.140)	183DMPC	24,308	Ribbon	PME	8 ns
4	(6.114, 22.028, 6.176)	256DMPC	17,702	Ribbon	Cutoff first 0.5 ns then PME	5 ns
5	(8.300, 22.028, 6.176)	256DMPC	27,299	Ribbon	Cutoff first 0.5 ns then PME	7 ns
6	(12.497, 16.0, 6.141)	183DMPC	33,213	Ribbon (Lipid configuration from end of run 3)	PME	4 ns
7	(8.453, 12.694, 9.486)	340 POPE	20,867	Ribbon	Cutoff first 6 ns then PME	14.4 ns

*Box size is the size of initial configuration. The box sizes in the x and y (and for intact bilayer simulation, z, as well) direction fluctuate by a small amount during the simulation.

Table 2.1. Overview of simulation runs

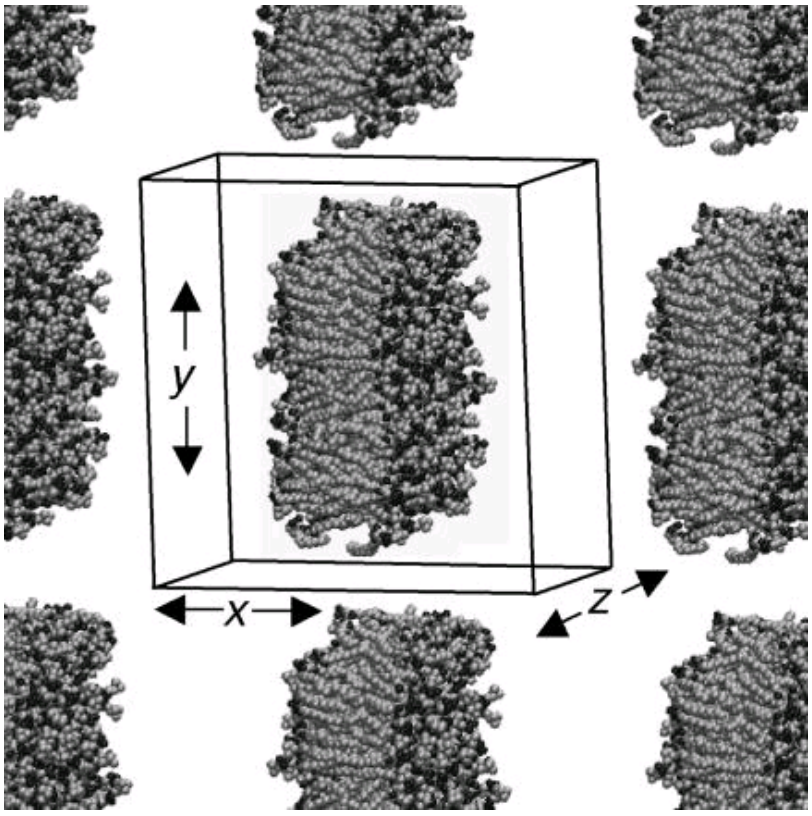

Figure 2.1. Starting geometry of 183-DMPC ribbon system. The lipid component of the system, with primary simulation box boundary and partial periodic repeats in the *x*-*y* plane, is shown. The bilayer structure is continuous in the *z* direction.

Force fields and topologies made available by the Tieleman group at http://moose.bio.ucalgary.ca/Downloads were also used. The DMPC force field uses the DPPC parameters of [57], with two methylene groups removed from each tail chain. The POPE force field uses these same interactions for the saturated tail united atom methylene and methyl groups, whereas parameters for the *cis*-double bond and partial charges are derived from the GROMOS force field [56, 58]. The flexible simple point charge (SPC) water potential [59] was used for solvent.

The integration time step was chosen as 2 fs. All bonds were constrained to a fixed length during position updates via the LINCS algorithm [60]. The center of mass motion removal was performed every 5000 steps to avoid drifting the system. In this work, we have used two methods for treating electrostatic forces. In some simulations, a dual-stage cutoff or truncation was used, with the first shell at 0.9 nm and the second shell at 1.8 nm; forces between charge sites whose distance falls between the two shells are updated only every 10 time steps. For a complete treatment of electrostatic forces in the periodic system, the particle mesh Ewald method [51, 52] was used, with a real-space cutoff of 0.9 nm, a maximal spacing of 0.12 nm for the Fourier transform grid, and fourth-order interpolation.

To keep temperature and pressure stable around the room temperature (300 K) and 1 atm, we used the Berendsen coupling algorithm [61]. Temperature scaling of solvent and lipid degrees of freedom were performed independently, both with a time constant of 100 fs. The pressure coupling scheme is dictated by the geometry of the ribbon system. The length of the box along the *z* axis (parallel to the edge) is fixed,

whereas the box dimensions in x and y are scaled jointly; the time constant for scaling is set to 500 fs, with an assumed compressibility of 4.5×10^{-5} bar^{-1}. Through this semiisotropic pressure coupling scheme, a positive line tension is supported along the edge while the system's volume is allowed to equilibrate to 1 atm pressure. In analogy to the calculation of surface tension during simulations of interfacial systems ([62, 63], the line tension Λ is derived from the diagonal elements P_{ii} of the pressure tensor, which are calculated by GROMACS. The work of extending the system along the z direction by an increment dL_z, while fixing the x and y directions, can be equated to the sum of the work of changing the system's volume and the work of changing the total length of the ribbon edge:

$$dw = -p_{zz}dV = -pdV + 2\Lambda dL_z \tag{1}$$

where P is the bulk pressure and P_{zz} is the diagonal element of the pressure tensor along the edge direction. (The factor of two multiplying the line tension arises from the presence of two edges.) The bulk pressure in this geometry is represented by the pressure perpendicular to the edge, $\frac{1}{2}(P_{xx} + P_{yy})$. As $dV/dL_z = L_xL_y$, differentiation and rearrangement of Eq. 1 gives the line tension:

$$\Lambda = \frac{1}{2}\left\langle L_xL_y[\frac{1}{2}(P_{xx} + P_{yy}) - P_{zz}]\right\rangle \tag{2}$$

No surface tension term appears in this equation because the area of the bilayer ribbon is not constrained by the box dimensions; the bilayer can therefore be considered to be at zero surface tension.

Simulations of intact bilayers, performed for comparison purposes, use more conventional semiisotropic scaling (with zero applied surface tension) in which the box dimensions parallel to the bilayer plane are jointly coupled to a pressure bath and the normal dimension is coupled separately (i.e., $NP_n\gamma T$ ensemble; [63]).

During the ribbon simulations, the ribbon can and does drift translationally in x and y and rotate in the x-y plane. To analyze the cross sectional structure of the ribbon independently of these motions, an intraribbon set of coordinates (x', y') was defined such that its origin is at the center of mass of the phosphorous atom coordinates, whereas the primary axes of inertia of the structure (defined by the set of phosphorus atoms projected onto a single x-y plane) lie along x' and y'. In other words, x' always represents the bilayer normal, whereas y' represents the direction parallel to the bilayer but normal to the edge.

RESULTS

Migration of headgroups

As the initial configuration involves a large area of hydrocarbon tail exposure to water, it is not surprising that the equilibration of the system involves the migration of polar headgroups around the edge to intervene between solvent and the solvophobic bilayer interior, as has been observed in simulations of small pores [49]. Figure 2.2 shows the number of headgroup phosphorus atoms in a slice of the edge region, defined in the ribbon internal coordinates as from $x' = -10$ Å to 10 Å, as a function of time. A constant number of headgroups in the rim region is a sign that the system has reached at least a metastable state. For DMPC, the number of headgroups in the edge region reaches a roughly constant value within 2 ns, regardless of the method used to treat the electrostatic

interactions or the width of the ribbon. However, for POPE, this process is very much slower; equilibrium was apparently not established over the 10-ns duration of the simulation. For this reason, we focus primarily on DMPC in the analysis of our results.

General morphology of the bilayer edge

Figure 2.3 shows a series of snapshots in the x'-y' plane (with solvent omitted for clarity) of DMPC ribbons modeled using both electrostatic cutoffs and PME, and of the POPE ribbon. At the early stage of the reorganization of the DMPC edge, we see some of the hydrocarbon tails of edge lipids extending into the solvent, especially in the case of the cutoff simulation. Most of these tail chains returned to the bilayer interior within 500 ps, as more and more headgroups begin to occupy the edge region. After 2 ns, this process seems to reach equilibrium. However, we observe that the packing of lipid headgroups in the edge region is still sparser than in the middle, even after 8 ns.

To better visualize the time-averaged cross sectional structure of the ribbon and its edges, we have generated scatter plots of the x' and y' coordinates of all lipid headgroups' phosphorus atoms, sampled at 10-ps intervals after the initial 3-ns equilibration of the trajectory (Figure 2.4). When truncation is used for the electrostatic interactions, the midsection of the ribbon appears as a flat bilayer, whereas the edge adopts a semielliptical profile. In contrast, when full electrostatics are used via the PME algorithm, a thickening of the bilayer ribbon near the edges (or, conversely, a pinching of the ribbon in the center) becomes apparent. This effect appears also for a wider ribbon (256 DMPC) in which the bulging edges are separated by a wider region of locally almost flat bilayer. In comparing the thickness of these ribbons near their middle (defined as the distance between the peaks in the probability density histogram for the phosphorus

atom position in the normal direction, and plotted in Figure 2.5) the larger ribbon is clearly thinner in its midsection (and thicker in the bulge near the edge) than an intact DMPC bilayer simulated under equivalent conditions.

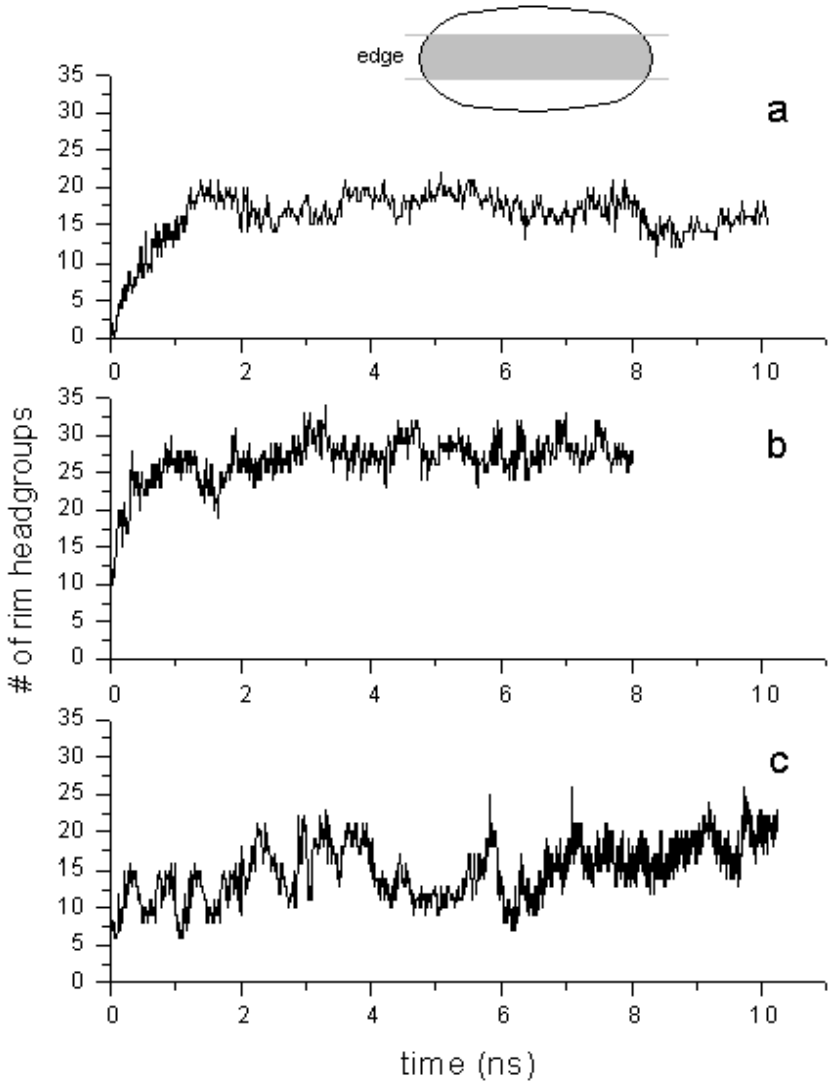

Figure 2.2 Time course of lipid headgroup migration. Variation in the number of headgroup phosphorus atoms at the bilayer edge, defined as shown in the cartoon as the region from −1.0 nm to 1.0 nm in the x' direction. (*a*) Run 2 (from Table 2.1): DMPC with truncation. (*b*) Run 3: DMPC with PME. (*c*) Run 7: POPE.

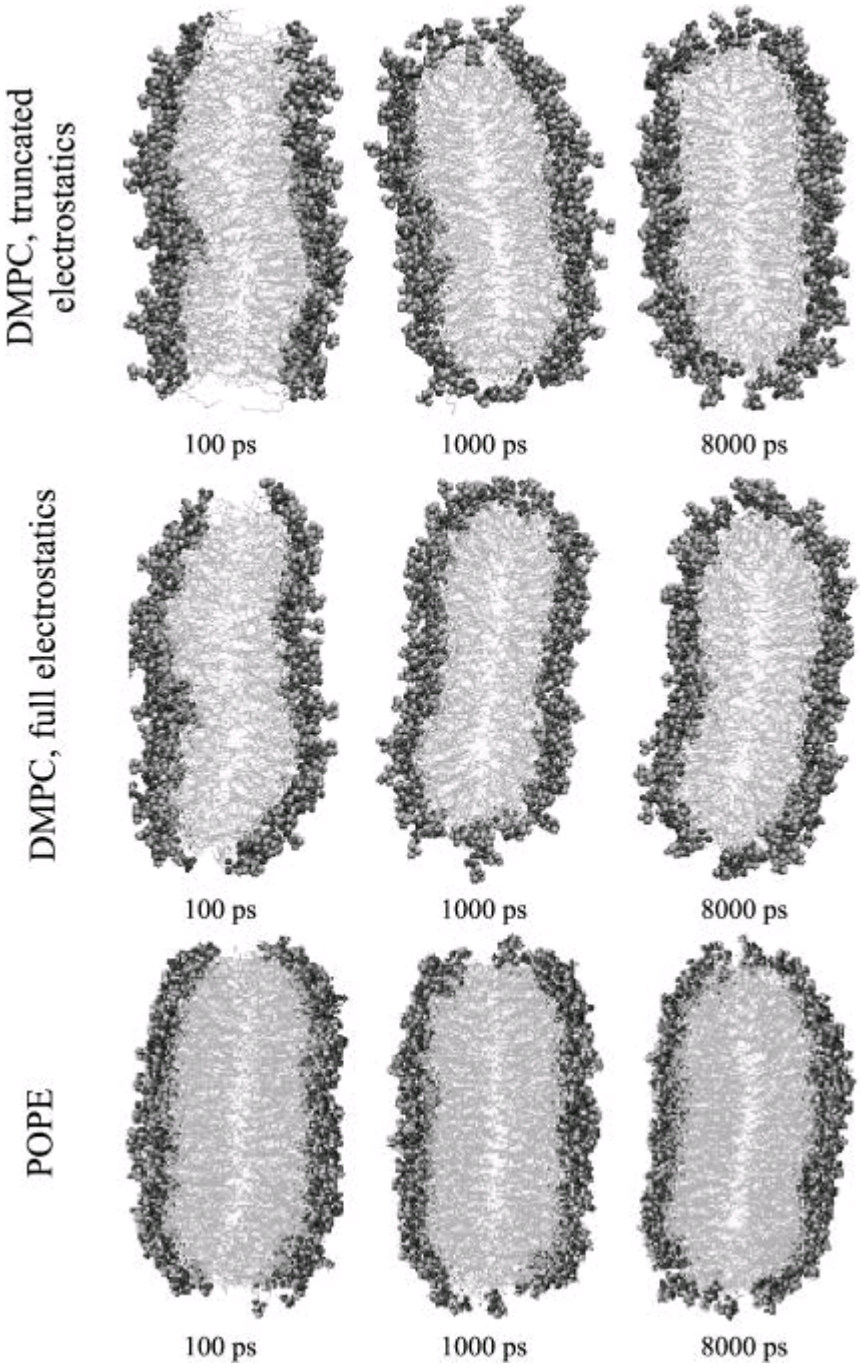

Figure 2.3**.** Evolution of cross-sectional structure of edge: simulation snapshots. (*Top*) Run 2, (*middle*) run 3, and (*bottom*) run 6 from Table 2.1.

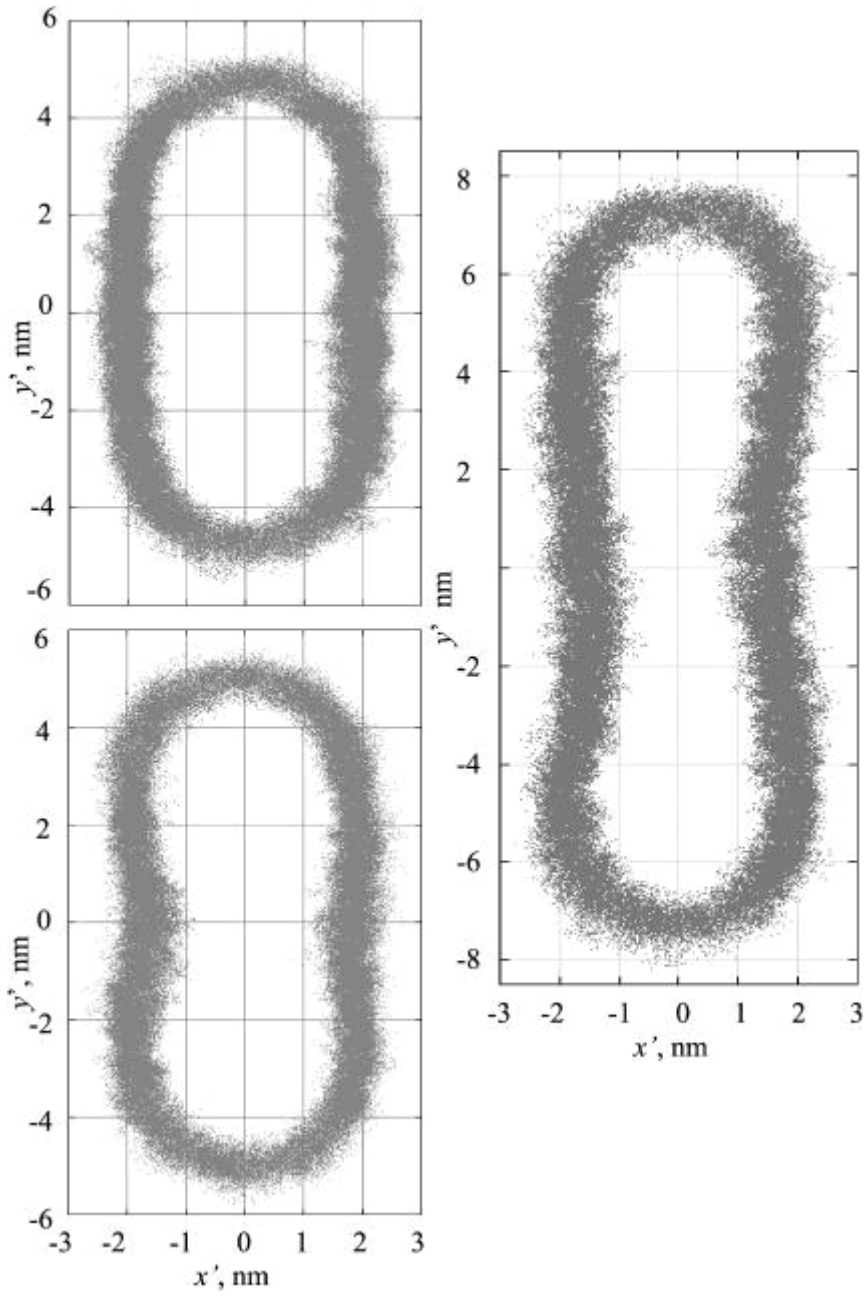

Figure 2.4. Ribbon shape profiles. Scatter plots of phosphorus atom positions generated from entire trajectories (after 3 ns equilibration), indicating the position of the headgroups. (*Top left*) Run 2, (*bottom left*) run 3, and (*right*) run 4.

The area per headgroup at the bilayer edge is not easy to define, as it requires the definition of the surface area of a curved, diffuse interface with no clear demarcation from the bilayer interior. To give a reasonable estimate, we fit the edge regions of these scatter plots to a semiellipse. The position of the center of the ellipse on the y' axis (y_0' and $-y_0'$), as well as the two diameters of the ellipse, are varied to minimize the average mean-square radial distance of the position of the lipid phosphorus site to the elliptical function. The area per headgroup is then defined as the perimeter of the ellipse, multiplied by the z dimension of the box to give an edge surface area, divided by the number of P atoms with $|y'| > y_0'$. For the flat interior sections of the bilayer ribbon and for intact bilayers, the area per headgroup is defined in the normal way. From Table 2.2, it is evident that the use of full electrostatics generally increases the area per headgroup (as found previously, e.g., by Patra et al.[64]) and that headgroups at the edge have roughly 50% greater area to occupy.

Tail conformational statistics

As any order parameter defined relative to the bilayer normal is not particularly appropriate for describing structure at a rounded edge, we concentrate on an internal measure, the fraction of *gauche* dihedral angles (defined here to be between 40° and 90°) along the saturated hydrocarbon tails, to attempt to quantify the edge's influence on tailgroup packing. As shown in Figure 2.6, in DMPC simulations performed using truncation, *gauche* defects are 20% more common at the edges of the ribbon than in its midsection, but in the more experimentally relevant simulation using the PME method the effect measured in two different simulations was an increase between 3% and 10%. For POPE, the fraction of kinks in the saturated tails was higher by 30% at the ribbon

edge than in the midsection; this may be a consequence of incomplete equilibration, however, as a high *gauche* percentage was also observed during the initial equilibration period of the DMPC ribbon (data not shown.)

System		DMPC: area per lipid ($Å^2$)	
		Truncation	PME
Intact bilayer	128 DMPC	58.9	60.4
Ribbon center	183 DMPC	61.2	66.0 (run 3) 66.1 (run 6)
	256DMPC	68.9	70.3 (run 4) 67.7 (run 5)
Ribbon edge	183 DMPC	99.4	100.7 (run 3) 95.5 (run 6)
	256 DMPC	108.8	103.6 (run 4) 97.5 (run 5)

Table 2.2 Area per lipid of DMPC from different system and different part of ribbon.

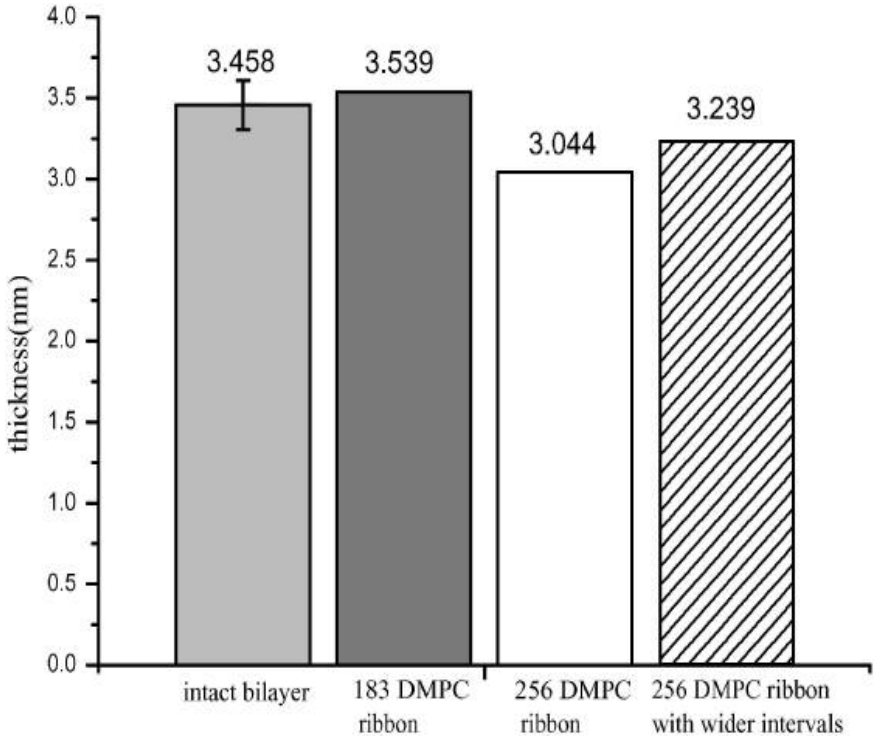

Figure 2.5. Mean bilayer thickness in different simulation runs. Thickness is defined as the distance between peaks in the probability distribution of phosphorus sites in the x' direction (or z direction for the intact bilayer.) From left to right, values are derived from runs 1, 3, 4, and 5.

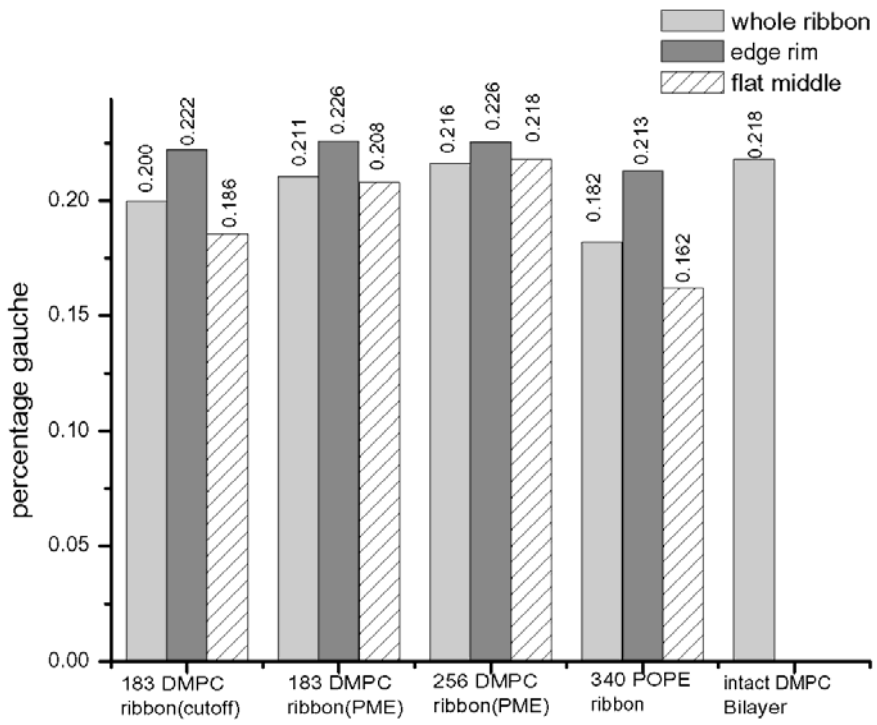

Figure 2.6. Percentage of *gauche* dihedral angles in lipid tails. All torsional angles around single bonds in lipid tails are counted.

Line tension

The line tensions of the ribbon edges, obtained using Eq. 1 from the average pressure anisotropy in the system, are presented in Table 2.3 along with some experimental values obtained for various lipid bilayer systems. The determination of the line tension with high precision is difficult. The pressure fluctuations in a finite condensed phase system are very large (on the order of 100 atm) but very rapid, yielding a precision of roughly ±30% based on the block averaging method[65] for runs of several nanoseconds. However, these large, rapid fluctuations may obscure smaller, slower fluctuations whose contributions to the line tension would not then be included in the error bars. In particular, a slow but noticeable decrease in the average line tension was observed over the course of the POPE simulation, consistent with the ongoing reconstruction that would be expected to stabilize the edge. The most striking result is that the effect of electrostatic truncation on the calculated line tension is enormous, giving results an order of magnitude above those obtained using the PME algorithm. The influences of box size and ribbon width on measured DMPC line tensions are less clear. Increasing the closest approach between bilayer periodic image edges from ~2.2 nm (run 3) to ~6 nm (run 6) gave a 30% reduction in line tension, which may or may not be statistically significant. In runs 4 and 5 with a wider ribbon, increasing the spacing between ribbons normal to the bilayer from ~2 nm to ~4 nm yielded a reduction in line tension by a factor of 3.

System	Line tension(pN)	Reference	Method
183 DMPC ribbon (run 3) 256 DMPC ribbon (run 4) 256 DMPC ribbon (run 5) 183 DMCP ribbon (run 6) 340 POPE ribbon (run 7) 183 DMPC ribbon (run 2)	24 ± 7 35 ± 10 12 ± 9 17 ± 6 57 ± 10 410 ± 40	This work	Molecular dynamics simulation
DOPC	6.9 ± 0.4	Karatekin et al. (2003)[39]	Vesicle pore closure
DOPC (different commercial source of material)	20.7 ± 3.5		dynamics
SOPC	9.2 ± 0.7	Zhelev and Needham (1993)[37]	Micropipette aspiration
SOPC with 50 mol % cholesterol	30.5 ± 1.2		
SOPC with 50 mol % cholesterol	26	Moroz and Nelson(1996) [38]	Reinterpretation of results of Zhelev and Needham
DOPC	25	Genco et al. (1993) [66]	Electroporation
DPsPC	30		
DLPC/DPsPC mixtures	21–28		
Egg lecithin	21		
Egg lecithin	42	Fromherz et al. (1986) [40]	Vesicle size distributions
Egg lecithin	8.6 ± 0.4	Chernomordik et al. (1985) [34]	Electroporation
Escherichia coli PE	16 ± 0.6		
lecithin	20	Harbich and Helfrich (1979) [33]	Observation of open
DPPC	6.5	Taupin et al. (1975) [32]	Vesicle response to osmotic stress

Table 2.3. Lipid bilayer line tension: comparison of computational and experimental results

Equilibrium dynamics

The mean-square displacement of lipid headgroups (measured at the position of the phosphorus atom) in the interior bilayer section of the ribbon is compared to that at the edge in Figure 2.7. In each case, displacement of the headgroup phosphorus atom in one of the bilayer internal coordinates is graphed; for the interior flat part of the ribbon, motion in the y' dimension across the ribbon, and for the edge, motion in the x' dimension normal to the bilayer plane. The diffusion constant derived from the limiting slope of the mean-square displacement at the edge (7.1×10^{-7} cm^2 s^{-1}) is 10-fold higher than that obtained in the normal bilayer environment (7.0×10^{-8} cm^2 s^{-1}, in reasonable agreement with simulation results by Moore et al.[10]). These are not strictly appropriate quantities to compare; flip-flop motion at the edge is on a curved surface and is bounded by the bilayer thickness, whereas diffusion parallel to the edge within the bilayer is on a flat surface and unbounded; but nonetheless the result suggests a significant enhancement in the rate of motion across the surface for lipids at the edge. Another measure of dynamics at the edge is from a positional correlation function, $c(t) = \langle x'(0)x'(t)\rangle$, evaluated for lipids at the edge as shown in Figure 2.8. Since x' changes sign from one leaflet to the other, this function will decay to 0 as lipids lose correlation with their original leaflet through random flip-flop events. From fitting the initial slope of $c(t)$ to an exponential decay, we estimate a correlation time of 18 ns for headgroup angular fluctuations around the bilayer edge.

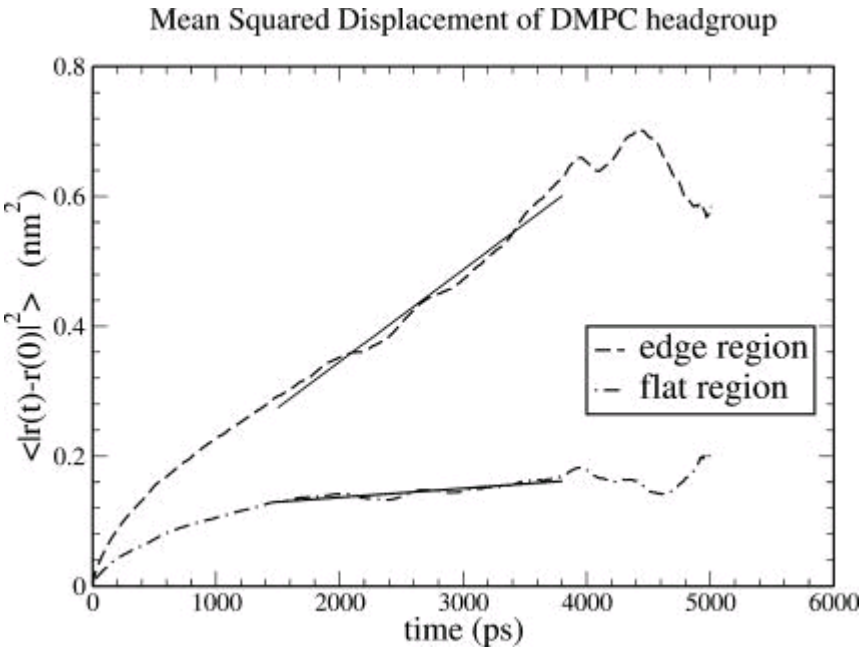

Figure 2.7. Effect of environment on mean-square displacement (MSD) of the DMPC headgroup phosphorus site. (*Dashed curve*) MSD in the x' (transleaflet) direction of lipids at the edge. (*Dot-dash curve*) MSD in the y' direction (perpendicular to the edge) for lipids in the flat center of the ribbon. Solid curves are linear least-square fits over the time range 1.5–3.8 ns. Diffusion constants D are derived from the slopes of these fits through the Einstein formula for one-dimensional diffusion, $2D = \lim_{t\to\infty} \partial/\partial t\langle(u(0) - u(t))^2\rangle$ where $u = x'$ or y'. Data obtained from simulation run 3.

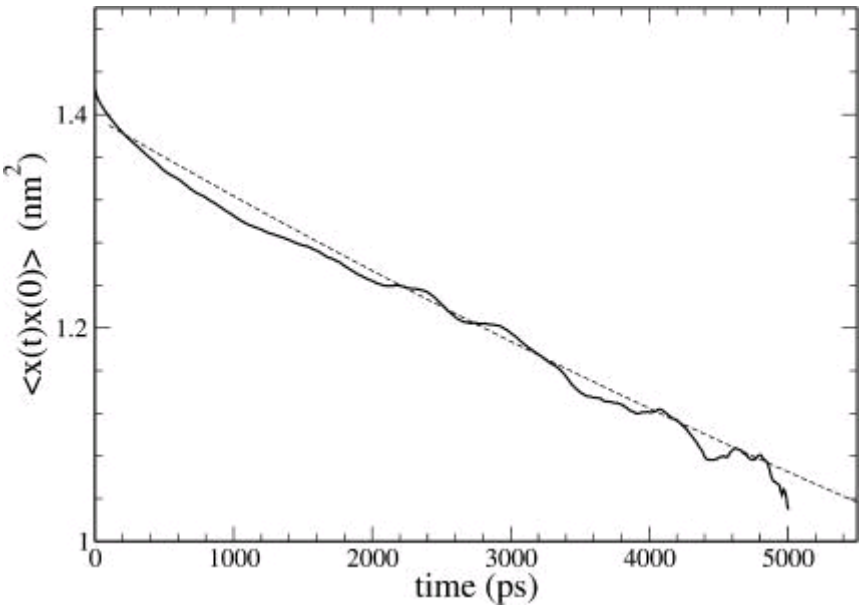

Figure 2.8. Time correlation function of the headgroup flip-flop coordinate. For lipid phosphorus atoms in the DMPC edge region, the time correlation function $c(t) = \langle x'(0)x'(t)\rangle$, where x' is the displacement from the bilayer center plane. The solid curve shows simulation data; the dashed curve shows fit to simple exponential decay, with a time constant of 18.4 ns.

DISCUSSION

Influence of electrostatics treatment on DMPC edge properties

The truncation of Coulomb interactions has been identified as a source of artifacts in biomolecular simulation in general and in lipid bilayer simulation in particular[64, 67]. In this study, a comparison of results obtained using truncation with those obtained using a superior, infinite-range method (particle mesh Ewald summation) illuminates some of the forces that determine the stability and structure of the bilayer edge.

The most dramatic result pertains to the line tension, or free energy per unit length of the edge, which is an order of magnitude greater when truncation is used (Table 2.3). Qualitatively, this most likely reflects the partial destabilization of the planar bilayer arising from long-ranged repulsions between headgroups, whose average net polarization is normal to the bilayer plane. These repulsions will be important at distances comparable to the thickness of the bilayer, but will be effectively canceled out by attractions to the dipoles on the opposite leaflet at distances much larger than the bilayer thickness. The breaking of the bilayer and the curvature of the interface at the rim partially relieve this repulsive energy.

To further investigate the effect of electrostatics treatment on line tension, we have performed four short (50 ps) simulations using PME or cutoffs on lipid ribbon starting configurations equilibrated with either method. This duration of simulation is long enough to obtain an order-of-magnitude estimate of the line tension but short enough that the initial structure is largely unaltered. The choice of electrostatics treatment used during the short simulation had a much greater effect than did the starting structure.

(Simulations using PME gave line tensions of 5 and 2×10^{-11} N, whereas simulations using cutoffs gave line tensions of 3 and 4×10^{-10} N for starting structures obtained from PME and cutoff simulations respectively.) From this we can conclude that the predominant effect of electrostatics treatment on line tension is direct, consistent with the dipolar repulsion model described above. Structural differences between model bilayers equilibrated with PME and cutoffs may be a secondary influence on line tension.

Another important effect of electrostatics treatment is the appearance of a slight thickening or bulging in the cross sectional profile of the edge when full electrostatics were used. Why might this be the case? The edge by geometric necessity has a higher area per headgroup than the flat bilayer (by a factor of two, assuming a hemicylindrical edge with a radius half the bilayer thickness, and constant lipid volume; in these simulations, by a factor of 1.6), meaning that the exposure to solvent of the hydrophobic tails is greater at the edge. Bulging or thickening at the edge lowers the area per headgroup by increasing the radius of curvature, at the expense of increasing the number of lipids in the perturbed edge environment. As we have already suggested, long-ranged dipolar repulsions lower the cost of breaking the planarity of the bilayer, so this distortion may be facilitated by extended electrostatic interactions. Furthermore, the area per headgroup is already higher (and the bilayer is thinner) when PME is employed, so the increase in exposed hydrophobic surface at the edge that drives the thickening is also somewhat greater. If our arguments based simply on long-ranged dipolar repulsions are correct, the addition of these interactions into a phenomenological model like that of May [50] should yield a bulging edge instead of the entirely convex cross section that was observed with only local interactions included.

System size scaling

The observed effects of increasing the ribbon width on the edge structure are difficult to interpret. We assume that in the limit of a very broad ribbon the middle bilayer region would have properties of an unperturbed continuous bilayer. In this simulation, the middle bilayer region is thinner than in a continuous bilayer simulated with periodic boundary conditions and semiisotropic pressure scaling with no surface tension applied, and becomes even thinner when the width of the ribbon is increased by 40% (from 183 DMPC to 256 DMPC, at a constant ribbon length). A further complicating observation is that in a separate simulation with 256 DMPC, in which the spacing between ribbons was increased, the thickness increased somewhat.

We have considered several possible explanations. One is that this thinning is a real effect that would appear in a much wider ribbon, and that the bilayer only gradually reaches an unperturbed thickness several nanometers away from the edge. Another is that the difference in thickness is a nonequilibrium effect or random fluctuation that is slow to relax on the simulation timescale [8], and that our calculated value is not converged. Finally, this result may arise from boundary conditions; as has been proposed by [68] but not conclusively corroborated by further studies [8, 9], the constraint that the bilayer be continuous across periodic boundaries in two dimensions might place the unperturbed intact bilayer under some effective lateral pressure, in which case the center of the ribbon (which is only subject to this constraint in the *z* dimension) may more closely reflect a tension-free bilayer than does the intact bilayer with full periodic boundary conditions.

Flip-flop dynamics

Transleaflet or flip-flop motion is typically considered to be an exceedingly slow process [69] with a timescale on the order of seconds or more, as it requires the disruption of the bilayer structure and removal of the polar headgroup from the water interface. At the DMPC edge, simulation results show (Figure 2.7) that translation in the flip-flop direction is significantly more rapid than is lateral diffusion in an intact bilayer; this may be the result of the lower headgroup packing density at the edge (Table 2.2). It is tempting to assign a leaflet residence timescale for lipids at the edge by assuming a simple exponential decay in the correlation of the position with respect to the bilayer normal (Figure 2.8). This may not be a valid assumption; the initial decay in the correlation function of Figure 2.8 may simply reflect local fluctuations in the headgroup position, whereas actual flip-flop motion may occur at a slower timescale due to tail entanglements or other effects. In fact, over the course of 5 ns simulation (after allowing 3 ns for initial edge reconstruction and equilibration), we observe that many lipids at the edge made significant excursions toward and away from the center line of the bilayer, but only one of ~70 edge lipids completed a clear flip-flop from one leaflet to the other, significantly fewer than an 18-ns flip-flop time would predict.

Nevertheless, even a single flip-flop event in 5 ns represents an enormous acceleration of the flip-flop rate observed experimentally in intact, unstressed bilayers. The implication for the role of pores or edges in flip-flop dynamics is that in the presence of an edge, the experimentally observed bulk flip-flop rate will probably be limited by the rate at which lipids diffuse toward and away from the edge in DMPC and not by the

actual flip-flop process at the edge. It is not surprising that the presence of an edge should greatly increase the rate of transleaflet motion; the influence of pores on flip-flop behavior in bilayers under tension has been investigated with this idea in mind [30].

Effects of lipid structure: comparison of DMPC with POPE

The timescale of edge reconstruction in POPE (as shown in Figure 2.2) is at least several times longer than for DMPC. Although the substitution of phosphatidylethanolamine for phosphatidylcholine in lipid headgroups has been shown experimentally to give to a modest decrease in probe molecule diffusion constants [70], as have substituting longer tail tail-chains [71] and introducing *cis*-double bonds [72], the combined effects of these substitutions would not be expected to give a 10-fold decrease in lateral diffusion constant at equilibrium. The most probable explanation for the pronounced difference in this study is that reconstruction of the edge (unlike lateral diffusion) involves a net increase in the spacing between headgroups, requiring a greater activation energy for the migration of PE headgroups (which allow hydrogen bonding between the hydrogens of the primary amine and the phosphate oxygens) than for PC headgroups.

The line tension calculated for POPE is significantly greater than that obtained for DMPC. Although we do not place too much weight on the former value, as it was calculated during an incompletely equilibrated trajectory, the disruption of close PE headgroup associations would indeed be expected to further reduce the stability of the free edge.

Line tension: comparison with experiment and general discussion

As long as a full treatment of electrostatic effects is used, the line tension values obtained from simulation are reasonable in comparison to the experimental values listed in Table 2.3, which were determined by a range of methods for several different lipid systems. The prediction of line tension by this simulation method for the molecular dynamics run durations used in this study is not as precise as one might desire; the error bars reflecting statistical uncertainty due to the system's rapid pressure fluctuations are rather large. The discrepancies among the four DMPC runs (3–6 in Table 2.1), of different ribbon widths and interribbon spacings, do not admit a consensus value for the line tension. Whether these discrepancies arise from finite size effects or from random fluctuations that are slow to relax on the simulation lengthscale (and so are not represented in the statistical uncertainty ranges) is unclear. Comparisons of runs 2 and 4 with runs 6 and 5 suggest a trend in which increasing the amount of solvent surrounding the ribbon decreases the calculated line tension. Such a trend would be expected to result from repulsions between the ribbon and its periodic images, which would artificially inflate the line tension at small interribbon distances by increasing P_{xx} and P_{yy} in Eq. 2.

SUMMARY AND CONCLUSIONS

We have studied the behavior of lipids at the bilayer edge through simulations in a ribbon geometry. We observe that a significant reorganization of the DMPC edge, migration of polar headgroups to form a roughly hemicylindrical cap, occurs within 2 ns. However, this process is much slower in a POPE ribbon, perhaps as a result of the stronger associations between phosphatidylethanolamine headgroups. A thickening or

bulging of the bilayer near the DMPC edge is observed when long-ranged electrostatic forces are included in the calculation, but not when Coulomb forces are truncated. The edge microenvironment leads to a 50% increase in area per lipid headgroup and a roughly order-of-magnitude increase in headgroup mobility for DMPC, but a much smaller increase in the percentage of *gauche* defects in the lipid tails. Flip-flop motion at the edge is greatly enhanced compared to its experimentally determined rate in the intact bilayer, occuring on a timescale of ~18ns rather than seconds or more. The line tension (i.e., reversible work of formation of an edge) calculated from these simulations, in the range of 10s of piconewtons, are in reasonable agreement with estimates derived from various experiments, but suffer from large statistical uncertainties and possible finite size effects. Given that experimental methods of determining line tension are generally difficult, indirect, and highly sensitive to the effects of impurities segregating toward the edge and lowering the line tension [39], we conclude that with improved simulation statistics and further investigation of finite size effects, atomistic simulation will be a useful tool to predict and interpret the relationship between lipid molecular structure and this fundamental material property of bilayers and membranes.

REFERENCE

1. Scott, H.L., *Modeling the lipid component of membranes.* Current Opinion in Structural Biology, 2002. **12**(4): p. 495-502.
2. Saiz, L. and M.L. Klein, *Computer Simulation Studies of Model Biological Membranes.* Acc. Chem. Res., 2002. **35**(6): p. 482-489.
3. Feller, S.E., *Molecular dynamics simulations of lipid bilayers.* Current Opinion in Colloid & Interface Science, 2000. **5**(3-4): p. 217-223.
4. Tobias, D.J., K.C. Tu, and M.L. Klein, *Atomic-scale molecular dynamics simulations of lipid membranes.* Current Opinion in Colloid & Interface Science, 1997. **2**(1): p. 15-26.
5. Forrest, L.R. and M.S.P. Sansom, *Membrane simulations: bigger and better?* Current Opinion in Structural Biology, 2000. **10**(2): p. 174-181.
6. Tieleman, D.P., S.J. Marrink, and H.J.C. Berendsen, *A computer perspective of membranes: molecular dynamics studies of lipid bilayer systems.* Biochim. Biophys. Acta., 1997. **1331**: p. 236.
7. Ayton, G., et al., *Calculating the bulk modulus for a lipid bilayer with nonequilibrium molecular dynamics simulation.* Biophysical Journal, 2002. **82**(3): p. 1226-1238.
8. Marrink, S.J. and A.E. Mark, *Effect of Undulations on Surface Tension in Simulated Bilayers.* J. Phys. Chem. B, 2001. **105**(26): p. 6122-6127.
9. Lindahl, E. and O. Edholm, *Mesoscopic undulations and thickness fluctuations in lipid bilayers from molecular dynamics simulations.* Biophysical Journal, 2000. **79**(1): p. 426-433.

10. Moore, P.B., C.F. Lopez, and M.L. Klein, *Dynamical properties of a hydrated lipid bilayer from a multinanosecond molecular dynamics simulation.* Biophysical Journal, 2001. **81**(5): p. 2484-2494.

11. Lindahl, E. and O. Edholm, *Molecular dynamics simulation of NMR relaxation rates and slow dynamics in lipid bilayers.* Journal of Chemical Physics, 2001. **115**(10): p. 4938-4950.

12. Stern, H.A. and S.E. Feller, *Calculation of the dielectric permittivity profile for a nonuniform system: Application to a lipid bilayer simulation.* Journal of Chemical Physics, 2003. **118**(7): p. 3401-3412.

13. Pandit, S.A. and M.L. Berkowitz, *Molecular dynamics simulation of dipalmitoylphosphatidylserine bilayer with Na+ counterions.* Biophysical Journal, 2002. **82**(4): p. 1818-1827.

14. Wilson, M.A. and A. Pohorille, *Mechanism of Unassisted Ion Transport across Membrane Bilayers.* J. Am. Chem. Soc., 1996. **118**(28): p. 6580-6587.

15. Bassolinoklimas, D., H.E. Alper, and T.R. Stouch, *Mechanism of Solute Diffusion through Lipid Bilayer-Membranes by Molecular-Dynamics Simulation.* Journal of the American Chemical Society, 1995. **117**(14): p. 4118-4129.

16. Marrink, S.J. and H.J.C. Berendsen, *Simulation of Water Transport through a Lipid-Membrane.* Journal of Physical Chemistry, 1994. **98**(15): p. 4155-4168.

17. Aman, K., et al., *Structure and dynamics of interfacial water in an L-alpha phase lipid bilayer from molecular dynamics simulations.* Biophysical Journal, 2003. **84**(1): p. 102-115.

18. Rog, T., K. Murzyn, and M. Pasenkiewicz-Gierula, *The dynamics of water at the phospholipid bilayer surface: a molecular dynamics simulation study.* Chemical Physics Letters, 2002. **352**(5-6): p. 323-327.

19. Ohta-Iino, S., et al., *Fast lipid disorientation at the onset of membrane fusion revealed by molecular dynamics simulations.* Biophysical Journal, 2001. **81**(1): p. 217-224.

20. Tieleman, D.P. and J. Bentz, *Molecular dynamics simulation of the evolution of hydrophobic defects in one monolayer of a phosphatidylcholine bilayer: Relevance for membrane fusion mechanisms.* Biophysical Journal, 2002. **83**(3): p. 1501-1510.

21. Bond, P.J. and M.S.P. Sansom, *Membrane Protein Dynamics versus Environment: Simulations of OmpA in a Micelle and in a Bilayer.* Journal of Molecular Biology, 2003. **329**(5): p. 1035-1053.

22. Colombo, G., S.J. Marrink, and A.E. Mark, *Simulation of MscL Gating in a bilayer under stress.* Biophysical Journal, 2003. **84**(4): p. 2331-2337.

23. Im, W. and B. Roux, *Ions and Counterions in a Biological Channel: A Molecular Dynamics Simulation of OmpF Porin from Escherichia coli in an Explicit Membrane with 1 M KCl Aqueous Salt Solution.* Journal of Molecular Biology, 2002. **319**(5): p. 1177-1197.

24. Capener, C.E. and M.S.P. Sansom, *Molecular dynamics simulations of a K channel model: Sensitivity to changes in ions, waters, and membrane environment.* Journal of Physical Chemistry B, 2002. **106**(17): p. 4543-4551.

25. Grossfield, A. and T.B. Woolf, *Interaction of tryptophan analogs with POPC lipid bilayers investigated by molecular dynamics calculations.* Langmuir, 2002. **18**(1): p. 198-210.

26. Gullingsrud, J., D. Kosztin, and K. Schulten, *Structural determinants of MscL gating studied by molecular dynamics simulations.* Biophysical Journal, 2001. **80**(5): p. 2074-2081.

27. Bachar, M. and O.M. Becker, *Protein-induced membrane disorder: A molecular dynamics study of melittin in a dipalmitoylphosphatidylcholine bilayer.* Biophysical Journal, 2000. **78**(3): p. 1359-1375.

28. Noguchi, H. and M. Takasu, *Fusion pathways of vesicles: A Brownian dynamics simulation.* Journal of Chemical Physics, 2001. **115**(20): p. 9547-9551.

29. Muller, M., K. Katsov, and M. Schick, *New mechanism of membrane fusion.* Journal of Chemical Physics, 2002. **116**(6): p. 2342-2345.

30. Raphael, R.M., et al., *Fractional occurrence of defects in membranes and mechanically driven interleaflet phospholipid transport.* Physical Review E, 2001. **6405**(5): p. -.

31. Leng, J., S.U. Egelhaaf, and M.E. Cates, *Kinetic pathway of spontaneous vesicle formation.* Europhysics Letters, 2002. **59**(2): p. 311-317.

32. Taupin, C., M. Dvolaitzky, and C. Sauterey, *Osmotic-Pressure Induced Pores in Phospholipid Vesicles.* Biochemistry, 1975. **14**(21): p. 4771-4775.

33. Harbich, W. and W. Helfrich, *Alignment and Opening of Giant Lecithin Vesicles by Electric-Fields.* Zeitschrift Fur Naturforschung Section a-a Journal of Physical Sciences, 1979. **34**(9): p. 1063-1065.

34. Chernomordik, L.V., et al., *The Shape of Lipid Molecules and Monolayer Membrane-Fusion.* Biochimica Et Biophysica Acta, 1985. **812**(3): p. 643-655.

35. Menger, F.M. and M.I. Angelova, *Giant vesicles: Imitating the cytological processes of cell membranes.* Accounts of Chemical Research, 1998. **31**(12): p. 789-797.

36. Sandre, O., L. Moreaux, and F. Brochard-Wyart, *Dynamics of transient pores in stretched vesicles.* Proceedings of the National Academy of Sciences of the United States of America, 1999. **96**(19): p. 10591-10596.

37. Zhelev, D.V. and D. Needham, *Tension-Stabilized Pores in Giant Vesicles - Determination of Pore-Size and Pore Line Tension.* Biochimica Et Biophysica Acta, 1993. **1147**(1): p. 89-104.

38. Moroz, J.D. and P. Nelson, *Dynamically stabilized pores in bilayer membranes.* Biophysical Journal, 1997. **72**(5): p. 2211-2216.

39. Karatekin, E., et al., *Cascades of transient pores in giant vesicles: Line tension and transport.* Biophysical Journal, 2003. **84**(3): p. 1734-1749.

40. Fromherz, P., C. Rocker, and D. Ruppel, *From Discoid Micelles to Spherical Vesicles - the Concept of Edge Activity.* Faraday Discussions, 1986(81): p. 39-+.

41. Glover, K.J., et al., *Structural evaluation of phospholipid bicelles for solution-state studies of membrane-associated biomolecules.* Biophysical Journal, 2001. **81**(4): p. 2163-2171.

42. Siskind, L.J. and M. Colombini, *The lipids C-2- and C-16-ceramide form large stable channels - Implications for apoptosis.* Journal of Biological Chemistry, 2000. **275**(49): p. 38640-38644.

43. Kasson, P.M. and V.S. Pande, *Molecular dynamics simulation of lipid reorientation at bilayer edges.* Biophysical Journal, 2004. **86**(6): p. 3744-3749.

44. Tolpekina, T.V., W.K. den Otter, and W.J. Briels, *Simulations of stable pores in membranes: System size dependence and line tension.* Journal of Chemical Physics, 2004. **121**(16): p. 8014-8020.

45. Tolpekina, T.V., W.K. den Otter, and W.J. Briels, *Nucleation free energy of pore formation in an amphiphilic bilayer studied by molecular dynamics simulations.* Journal of Chemical Physics, 2004. **121**(23): p. 12060-12066.

46. Litster, J.D., *Stability of Lipid Bilayers and Red Blood-Cell Membranes.* Physics Letters A, 1975. **A 53**(3): p. 193-194.

47. Muller, M. and M. Schick, *Structure and nucleation of pores in polymeric bilayers: A Monte Carlo simulation.* Journal of Chemical Physics, 1996. **105**(18): p. 8282-8292.

48. Marrink, S.J., et al., *Simulation of the spontaneous aggregation of phospholipids into bilayers.* Journal of the American Chemical Society, 2001. **123**(35): p. 8638-8639.

49. Tieleman, D.P., et al., *Simulation of pore formation in lipid bilayers by mechanical stress and electric fields.* Journal of the American Chemical Society, 2003. **125**(21): p. 6382-6383.

50. May, S., *A molecular model for the line tension of lipid membranes.* European Physical Journal E, 2000. **3**(1): p. 37-44.

51. Darden, T., D. York, and L. Pedersen, *Particle Mesh Ewald - an N.Log(N) Method for Ewald Sums in Large Systems.* Journal of Chemical Physics, 1993. **98**(12): p. 10089-10092.

52. Essmann, U., et al., *A Smooth Particle Mesh Ewald Method.* Journal of Chemical Physics, 1995. **103**(19): p. 8577-8593.

53. Berendsen, H.J.C., D. Vanderspoel, and R. Vandrunen, *Gromacs - a Message-Passing Parallel Molecular-Dynamics Implementation.* Computer Physics Communications, 1995. **91**(1-3): p. 43-56.

54. Lindahl, E., B. Hess, and D. van der Spoel, *GROMACS 3.0: a package for molecular simulation and trajectory analysis.* Journal of Molecular Modeling, 2001. **7**(8): p. 306-317.

55. Humphrey, W., A. Dalke, and K. Schulten, *VMD: Visual molecular dynamics.* Journal of Molecular Graphics, 1996. **14**(1): p. 33-&.

56. Tieleman, D.P. and H.J.C. Berendsen, *A molecular dynamics study of the pores formed by Escherichia coli OmpF porin in a fully hydrated palmitoyloleoylphosphatidylcholine bilayer.* Biophysical Journal, 1998. **74**(6): p. 2786-2801.

57. Berger, O., O. Edholm, and F. Jahnig, *Molecular dynamics simulations of a fluid bilayer of dipalmitoylphosphatidylcholine at full hydration, constant pressure, and constant temperature.* Biophysical Journal, 1997. **72**(5): p. 2002-2013.

58. an Gunsteren, W.F., P. Krüger, S. R. Billeter, A. E. Mark, A. A. Eising, W. R. P. Scott, P. H. Hüneberger, and I. G. Tironi, *Biomolecular Simulations: The*

GROMOS96 Manual and User Guide. Biomos, Groninger, and Hochschulverlag AG an der ETH Zürich, Zürich, Switzerland., 1996.

59. Berendsen, H.J.C., et al., *In Intermolecular Forces*, ed. B. Pullman. 1981, Dordrecht, The Netherlands: D. Reidel Publishing Company. 331–342.

60. Hess, B., et al., *LINCS: A linear constraint solver for molecular simulations.* Journal of Computational Chemistry, 1997. **18**(12): p. 1463-1472.

61. Berendsen, H.J.C., et al., *Molecular-Dynamics with Coupling to an External Bath.* Journal of Chemical Physics, 1984. **81**(8): p. 3684-3690.

62. Hill, T.L., *An Introduction to statistical thermodynamics*. 1962, Reading, MA: Addison-Wesley Publishing Company, Inc.

63. Zhang, Y.H., et al., *Computer-Simulation of Liquid/Liquid Interfaces .1. Theory and Application to Octane/Water.* Journal of Chemical Physics, 1995. **103**(23): p. 10252-10266.

64. Patra, M., et al., *Molecular dynamics simulations of lipid bilayers: Major artifacts due to truncating electrostatic interactions.* Biophysical Journal, 2003. **84**(6): p. 3636-3645.

65. Allen, M.P. and D.J. Tildesley, *Computer simulation of liquids*. 1987, Oxford [England] New York: Clarendon Press ; Oxford University Press. xix, 385 p.

66. Genco, I., et al., *Electroporation in symmetric and asymmetric membranes.* Biochim. Biophys. Acta., 1993. **1149**: p. 10-18.

67. Tu, K., et al., *Molecular dynamics investigation of the structure of a fully hydrated gel-phase dipalmitoylphosphatidylcholine bilayer.* Biophysical Journal, 1996. **70**(2): p. 595-608.

68. Feller, S.E. and R.W. Pastor, *On simulating lipid bilayers with an applied surface tension: Periodic boundary conditions and undulations.* Biophysical Journal, 1996. **71**(3): p. 1350-1355.

69. Kornberg, R.D. and Mcconnel.Hm, *Lateral Diffusion of Phospholipids in a Vesicle Membrane.* Proceedings of the National Academy of Sciences of the United States of America, 1971. **68**(10): p. 2564-&.

70. Ladha, S., et al., *Lateral diffusion in planar lipid bilayers: A fluorescence recovery after photobleaching investigation of its modulation by lipid composition, cholesterol, or alamethicin content and divalent cations.* Biophysical Journal, 1996. **71**(3): p. 1364-1373.

71. Muller, H.J. and H.J. Galla, *Chain-Length and Pressure-Dependence of Lipid Translational Diffusion.* European Biophysics Journal with Biophysics Letters, 1987. **14**(8): p. 485-491.

72. Vaz, W.L.C., R.M. Clegg, and D. Hallmann, *Translational Diffusion of Lipids in Liquid-Crystalline Phase Phosphatidylcholine Multibilayers - a Comparison of Experiment with Theory.* Biochemistry, 1985. **24**(3): p. 781-786.

Chapter Three

Coarse-grained MD simulation of mixed bilayer systems:

Understanding the in-plane fluctuation of bilayer edge

INTRODUCTION

Mixtures of short-chain phospholipids (DHPC[g]) and long-chain phospholipids (DMPC[h]) have been the focus of considerable interest recently. Sanders and Schwonek [1] in early 1990's introduced a mixed lipid system (DMPC and DHPC) called bicelles for use in NMR studies of biomembrane-associated macromolecules. Tjandra and Bax[2] developed a method to use the same bicelle mixture for NMR analysis of large soluble biomolecules, taking advantage of the slight alignment of the molecules imparted by the lipid aggregates in their nematic liquid crystalline phase. Despite the wide applications of bicelle systems in NMR experiments, questions persist about their thermodynamic phase behavior and microscopic morphology is still yet to be determined. Early publications [3] proposed that mixed DMPC/DHPC form discoidal structures that can easily be described by an "ideal-disc" model. This model assumes that the long-chain lipids (DMPC) exclusively occupy the center region of the disk and short-chain lipids (DHPC) occupy the rim of the disk. Recently, van Dam et al.[4, 5] and Nieh et al.[6, 7] have experimentally demonstrated that DMPC/DHPC mixtures undergo a series of different phases and morphologies over a wide range of temperature T, total lipid concentration c_{lp} and long tail:short tail lipid number ratio q. In addition to disks, cylindrical micelles or ribbons, porous sheets and vesicles, and branched network structures have been proposed.

Understanding the morphological transformation in mixed lipid systems requires some physical properties as input. The aggregate structure in a system that may have disk,

[g] DHPC: dihexanoylphosphatidylcholine, systematic name: 1,2-Diheptanoyl-*sn*-Glycero-3-Phosphocholine
[h] DMPC: dimyristoylphosphatidylcholine, systematic name: 1,2-Dimyristoyl-*sn*-Glycero-3-Phosphocholine

ribbon, and pore morphologies is sensitive to the free energy on the length and curvature of the bilayer edge. It is commonly known that line tension, or excess free energy per unit length, is sufficiently high in most pure lipid systems to drive the formation of vesicles from disks and to close pores. However, as these systems are believed to have stable edges, it is reasonable to assume that the line tension is greatly reduced or eliminated by the presence of the shorter-chain component; at vanishing line tension, subtle effects such as the bending elasticity of the edge may become important. By simulating the edge of a mixed bilayer with vanishing line tension and analyzing the shape fluctuations of the edge, we aim to learn more about these effects that may play important roles in determining morphology in bicelle systems.

Molecular dynamics simulation has been widely used in understanding structures and dynamics of self-assembled lipid systems. However, studying mixed lipid system using full atomistic simulations has limitations on time scale and length scale. The diffusion of lipids within bilayer to achieve segregation of different lipids to different environment requires longer timescale than practical with current computational power. The discoidal bicelles observed in experiment are on the order of 20nm in diameter (containing around 1000 lipids), which approaches the upper bound of practicality. To solve this dilemma, coarse-grained models, where a group of atoms is simplified and parameterized by one interacting site, have been developed by various groups[8-12].

Full atomistic and coarse-grained[13, 14] simulations on lipid bilayer edge have been done in our earlier work. A ribbon geometry was used in these simulations due to its simplicity to analyze the structure and energetics of the edge under periodic boundary conditions. Using a coarse-grained (CG) model of a bicelle-like mixture, we observed

the the domination of long-tail lipids in the bulk of the ribbon (i.e., the flat bilayer environment) and an enhancement of short-tail lipids at the edge region. Further analysis revealed that next to the bilayer rim, the long-tail lipid concentration and the bilayer thickness both reach a maximum before returning to their bulk values in the ribbon center. Line tension can be calculated from the anisotropy of pressure between the main axis along the ribbon edge and the perpendicular axes. The coarse-grained model in the previous work leads to systematically higher line tension than atomistic models calculated for lipid ribbons[13], pores[15, 16] and experiments. More importantly, even in the limit of a system composed purely of the shorter-chain component, the simulations indicated the bilayer structure to be stable, in qualitative disagreement with the experimental finding that DHPC forms small micelles[17, 18]. In order to achieve stable disks or pores in a bilayer system, the line tension of the edge must be reduced to a negligible quantity.

In this work a later version of the coarse-grained forcefield[19] with a more realistic line tension is used to investigate edge shape fluctuations on the order of a few hundred nanoseconds. Binary mixtures of DPPC[i]/DBPC[j] systems in which composition varied from 100% to 60% of the long-chain DPPC component are modeled, including both systems with high and negligible line tensions. We compared the fluctuations in ribbon edge shape and contour length to simple statistical theory and to a simple Monte Carlo model. At low % DBPC, the spectrum of fluctuations could be predicted quantitatively using the independently obtained value of the line tension from pressure

[i] DPPC: dipalmiotylphosphatidylcholine, systematic name: 1,2-Dipalmitoyl-*sn*-Glycero-3-Phosphocholine
[j] DBPC: systematic name: 1,2-Dibutaoyl-*sn*-Glycero-3-Phosphocholine, it has four methyl groups in each tail.

tensor calculation. For systems with low line tension, neither the fluctuations observed in the edge structure nor the partitioning of DBPC between the bilayer and its edge could be fully explained using simple models.

METHODS

Coarse-grained model and forcefield

We used the coarsed-grained (CG) model and forcefield developed by Marrink etal.[9] to calculate lipid-water systems in MD simulations. To represent phospholipids in this study, this model maps every 4 methylene/methyl groups in the two tails onto a single apolar particle; maps the glycerol ester linkage onto 2 nonpolar particles and maps the PC headgroup onto a positively and a negatively charged particle for choline and phosphate respectively. Four water molecules are represented by a single united atom with a corresponding mass of 72 amu. The forcefield parameters are chosen to well reproduce structural properties of lipid bilayers while using cheap short-ranged treatment for electrostatic interactions. In this study, the CG forcefield and topology (version 1.4) are from Marrink's website (http://md.chem.rug.nl/~marrink/coarsegrain.html). Following a later publication by Marrink and Mark[19], the phosphate-water LJ interaction energy was increased from 5.0 to 5.8 kJ/mol to improve the line tension calculation.

System construction and initialization

As the model can only represent tail chains in multiples of 4 carbons, we use DPPC and DBPC as our component in the binary mixture. These lipids have the same headgroup with decreasing number of methyl/methylene groups on the tails; the 16 carbons of the DPPC tails are represented by 4 CG sites, while the 4 carbons of the DBPC tails are represented by a single CG site.

Our initial systems were derived from 128 DPPC lipid bilayer provided by Marrink's website. To form a ribbon-shaped configuration, this bilayer patch was first replicated laterally. After that, two strips of lipids near the box boundary were removed along the one lateral axis (we hereafter denoted it as z axis). In case of binary mixture, a certain number of short-tail lipids (DBPC) were obtained by chopping terminal CG particles from each tail of randomly chosen DPPC lipids. The vacancy due to the removal was filled thereafter with randomly spaced water particles which have a minimum distance of 0.4nm among them so that the system density is close to $1 g/cm^3$. Energy minimization was performed using steepest decent algorithm before the systems were sent to production run. Table 3.1 summarizes systems in the CG MD runs in this study.

Molecular dynamics algorithm and technical details

Following Marrink's protocol[9], we used integration time step of 20 fs. The time scale of the calculations is on the order of hundreds of nanoseconds. Periodic boundary conditions are implemented in 3 dimensions. We added a shift function to coulombic force when the interaction distance falls between 0 nm and 1.2 nm so that the resulting force smoothly decays to zero in that range. Van der Waals interactions were treated

likewise except that the shift function was turned on between 0.9 nm and 1.2 nm. We used the grid type neighbor searching algorithm: atoms in the neighboring grid were updated every 10 time steps. Experimentally DPPC bilayer shows a fluid-like phase above 315K[20]. To simulate the DPPC bilayer in this phase, the system temperature is therefore coupled to 323K for different lipid types and water separately. Berendsen algorithm[21] was used for the temperature coupling with a time constant of 1 ps. We used a semiisotropic pressure coupling scheme: the box dimensions in the z axis, parallel to the edge, are fixed (zero compressibility), whereas the box dimensions in the other 2 dimensions are jointly scaled to an external pressure at 1 bar with compressibility set to 5.0×10^{-5} bar^{-1}, through the Bersendsen algorithm. According to this pressure coupling scheme, the line tension of the ribbon edge can be expressed as:

$$\Lambda = \frac{1}{2}\left\langle L_x L_y [\frac{1}{2}(P_{xx} + P_{yy}) - P_{zz}] \right\rangle \quad (1)$$

where the P_{xx}, P_{yy} and P_{zz} are the diagonal element of pressure tensor. Lx and Ly are box size in the x and y dimensions. For detailed description of line tension of lipid ribbons configuration, see Jiang et al[13].

The molecular dynamics simulations were performed using GROMACS[22, 23] (version 3.1.3). One to four processors (1.4-GHz 1600 MP Athlon) of a Beowulf-type linux cluster were used to carry out the simulations. Analysis tools include modified GROMACS utility programs, perl and linux shell scripts. The VMD package[24] was used for molecular graphics visualization.

Table 1a

DPPC #	DBPC #	Time (ns)	Box size x,y,z(nm)
966	0	200	18.7,8.5.20.4
1432	0	200	21.6,8.4,30.0
1205	0	100	21.9,8.2,25.0
716	0	100	21.2,8.5,15.0
870	588	200	18.6,8.0,30.0 (0-100ns)
			21.9,12.1,30.0 (100-200ns)
722	481	100	20.9,8.0,25.0
430	286	200	20.8,8.1,15.0

Table 1b

DBPC%	Time (ns)	DPPC #	DBPC #	Box (nm)
10	300	870	96	25.6,8.0.20.2
15	300	822	144	24.9,8.0,20.4
20	200	772	194	24.3,8.2,20.4
25	300	724	242	24.8,8.1,20.0
30	200	676	290	24.0,8.3,20.4
35	200	628	338	23.9,8.1,20.4
37	100	604	362	23.6,8.2,20.4
40	100	580	386	23.5,8.2,20.4

Table 3.1. Summary of MD simulation runs. Box size is the averaged value over the runs.

Spatial Spectral Analysis

During the course of the simulations, the ribbons were free to rotate around the z axis and to drift translationally in the x-y plane. Therefore before the analysis of the edge fluctuations, ribbon coordinates were first translated so that the ribbons' center of mass is the Cartesian origin and then were rotated around the z axis to the point that the longer primary axis of inertia of the ribbon (defined by the phosphorus atoms projected onto x-y plane) lies parallel to the x axis and the shorter one parallel to y axis. Hereafter in this paper, y denotes the direction of bilayer normal; x denotes the direction orthogonal to both bilayer normal and the edge direction, the z axis.

To describe the in plane shape undulations of the edge, we segmented the ribbon into small equal slices along the z dimension. The position of the lipid is defined by its phosphate position in the headgroup which fall into each slice. The two "edge points", representing the edge positions in each slice, is defined as the two points with maximum and minimum lateral displacements to the edge axis. By connecting the edge points of both edges by line segment, one can extract the shape contour of the edge and contour length is the summation of those line segment lengths. A Fourier transform of the shape fluctuation is performed to yield the mode intensity as a function of mode number.

In some cases, a very small number (less than 10) of short tail lipids in the ribbon binary mixtures diffused into the solvents for a few nanoseconds and then united with the ribbon again. These lipids were excluded from the shape fluctuation analysis for clarity.

THEORY OF BILAYER EDGE SHAPE FLUCTUATION

Although the bilayer is a two-dimensional surface, it is convenient to assume a flat bilayer, project the edge onto a plane, and expand the free energy in terms of the length and curvature of the edge in the plane. The lipid ribbon edge can hence be geometrically treated as a one-dimensional object and its thermal fluctuations reflect the material properties of the edge. Our analysis of these fluctuations is based on a large body of work characterizing fluctuations of two dimensional objects, i.e. bilayer and interface surfaces.[25]. We use the Monge representation *h(z)* to give the displacement of the edge from a flat reference axis *z*. The free energy associated with the ribbon edge is shown below:

$$F = \int_0^L f dl = F_0 + \int_0^L \left\{ \Lambda \left(1 + \frac{1}{2}(\nabla h)^2 \right) + \frac{1}{2}\kappa(\nabla^2 h)^2 \right\} dz \qquad (2)$$

The first term in the integrand is the line energy where Λ is the line tension, free energy per unit edge length. The second term is the bending energy where κ is the in-plane bending modulus of the edge. In eq. 2 we have used the approximation which is valid at small edge fluctuation:

$$dl = \sqrt{1 + (\nabla h)^2}\, dz \approx \left(1 + \frac{1}{2}(\nabla h)^2 \right) dz \qquad (3)$$

The integral is from 0 to the box size in the *z* dimension, L. and all the constant

terms are included in F_0. The Monge representation of *h(z)* can be expanded as a summation of Fourier series:

$$h(z) = \sum_q u_q e^{iqz} \tag{4}$$

where u_q is the intensity of the mode with wave number q. q spans in the range of [- ∞, + ∞], with discrete values spaced by 2π/L. Substitution of eq. 4 into eq. 2 yields：

$$F = F_0 + \frac{1}{2}\Lambda\int_0^L (\sum_q u_q (iq) e^{iqz})(\sum_{q'} u_{q'} (iq') e^{iq'z}) dz$$

$$+\frac{1}{2}\kappa\int_0^L (\sum_q u_q (-q^2) e^{iqz})(\sum_{q'} u_{q'} (-q'^2) e^{iqz}) dz \tag{5}$$

note the second and third term in the equation above have a product of two summations in their integrand. Due to orthogonality, all the cross terms vanishes when $|q| \neq |q'|$. It is easy to show that when $q = q'$, the term goes to zero since $\int_0^L e^{2iqz} dz = 0$. Therefore only two terms survive when q and q' only differ in sign (q=-q'). Finally, Eq 4 can be rewritten as:

$$\begin{aligned} F = F_0 + \frac{1}{2}\Lambda L(\sum_{q>0} q^2 \mid u_q^2 \mid + \sum_{q<0} q^2 \mid u_q^2 \mid) \\ +\frac{1}{2}\kappa L(\sum_{q>0} q^4 \mid u_q^2 \mid + \sum_{q<0} q^4 \mid u_q^2 \mid) \end{aligned} \tag{6}$$

The average configurational free energy in each harmonic term in this summation corresponds to kT/2 according to the equipartition theorem. As positive and negative q value correspond to the conjugate term in fourier series, their mode amplitude is equal as shown in the following:

$$\left\langle u_q^2 \right\rangle = \left\langle u_{-q}^2 \right\rangle = \frac{k_B T}{L}\left(\Lambda q^2 + \kappa q^4\right)^{-1} \tag{7}$$

It is important to note that the wave amplitude scales as q^{-2} when Λ dominates and scales as q^{-4} with vanishing line tension $\Lambda \approx 0$. We therefore calculate the correlation of 2 points' position as a function of their distance:

$$C(\Delta z) = \left\langle h(z)h(z+\Delta z)\right\rangle = \left\langle \sum_q u_q e^{iqz} \cdot \sum_{q'} u_{q'} e^{iq'(z+\Delta z)} \right\rangle \tag{8}$$

where the bracket ‹› denotes the statistical average of all the contour positions on the edge(i.e. integration over the z dimension). When $|q| \neq |q'|$, the cross terms on the right of eq. 7 will vanish because of orthogonality. When q equals q' , eq. 7 can be rewritten as:

$$C(\Delta z) = \left\langle \sum_q {u_q}^2 e^{2iqz+iq\Delta z} \right\rangle = \sum_q \frac{1}{L}\int_0^L {u_q}^2 e^{2iqz+iq\Delta z} dz$$

$$= \sum_q \left\{ \left\langle {u_a}^2 \right\rangle e^{iq\Delta z} \frac{1}{L}\int_0^L e^{2iqz} dz \right\} = 0 \tag{9}$$

note that in the above derivation, qL are multiple of 2π. As only terms where q=-q' give non-zero contribution, eq. 7 can be rewritten as:

$$C(\Delta z) = \left\langle \sum_q u_q u_{-q} e^{iq\Delta z} \right\rangle = 2\sum_{q>0} \left\langle |u_q|^2 \right\rangle \cos q\Delta z \tag{10}$$

Substituting $\left\langle u_q^{\,2} \right\rangle$ by eq. 6 yields:

$$C(\Delta z) = \left\langle h(z)h(z+\Delta z) \right\rangle = \sum_{q>0} \frac{2k_B T \cos qz}{L(\Lambda q^2 + \kappa q^4)} \tag{11}$$

similar in eq. 6, the theory predicts that the Fourier transform of the position correlation function shows -2 and -4 power law dependence on positive value of *q* at high and low line tension regime respectively. Hereafter in this paper, *q* refers to the absolute value of *q* in Fourier (reciprocal) space.

A MONTE CARLO MODEL TO SIMULATE BILAYER EDGE FLUCTUATIONS

Because the theory described above is limited to the regime of small amplitude fluctuations, we also developed a Monte Carlo scheme to simulate the bilayer edge fluctuation shown in Figure 3.1. Each point in the figure represents the position of the edge in each slice, similar in the definition of edge position in each slice from MD data. These “edge points” are equally spaced in the edge direction and are only allowed to move vertically. In each MC step, several points along the edges are randomly chosen to move a displacement (both positive and negative) within a limit of 0.5nm. The edge is represented by connecting the “edges points” all together. The edge length is therefore the summation of bond length. Periodic boundary condition is applied by connecting the both ends. To avoid very large bond length, we set a maximum bond length of 3nm.

The Hamiltonian of this model is shown below.

$$H = \Lambda \sum_{i=1}^{n} l_i \qquad \text{(for high } \Lambda \text{ systems)}$$
$$= \sum_{i=1}^{n} \frac{1}{2} \frac{\kappa \theta_i^2}{\overline{l_i}} + \frac{1}{2} \gamma (\sum_{i=1}^{n} l_i - L_0)^2 \qquad \text{(for low } \Lambda \text{ systems)} \tag{12}$$

the term on the first line of eq.12 is the line energy term, namely the line tension times the length of the edge. The first term on the second line is the bending energy term which accounts for the curvature of the edge. θ is the angle of neighboring 3 atoms. $\overline{l_i}$ in the denominator of this term is defined as the mean bond length of the two bonds forming the angle. By including $\overline{l_i}$ we properly weighted configurations with different curvature radius. The second term for low line tension system assumes system has a preferred contour length of L_0 and there is a harmonic energy with the deviation from this preferred contour length. Parameter γ controls the strength of the harmonic term. After trying different combinations of these parameters, we found that neglecting the bending term and harmonic term in the Hamiltonian can well reproduce the fluctuation spectrum in high line tension systems. As a result, we split equations 12 for systems at high and low line tension individually: it has one adjustable parameter Λ for high line tension system and has 3 adjustable parameters:, κ, γ and L_0 for low line tension systems. They will be used as input in MC simulation later in this paper.

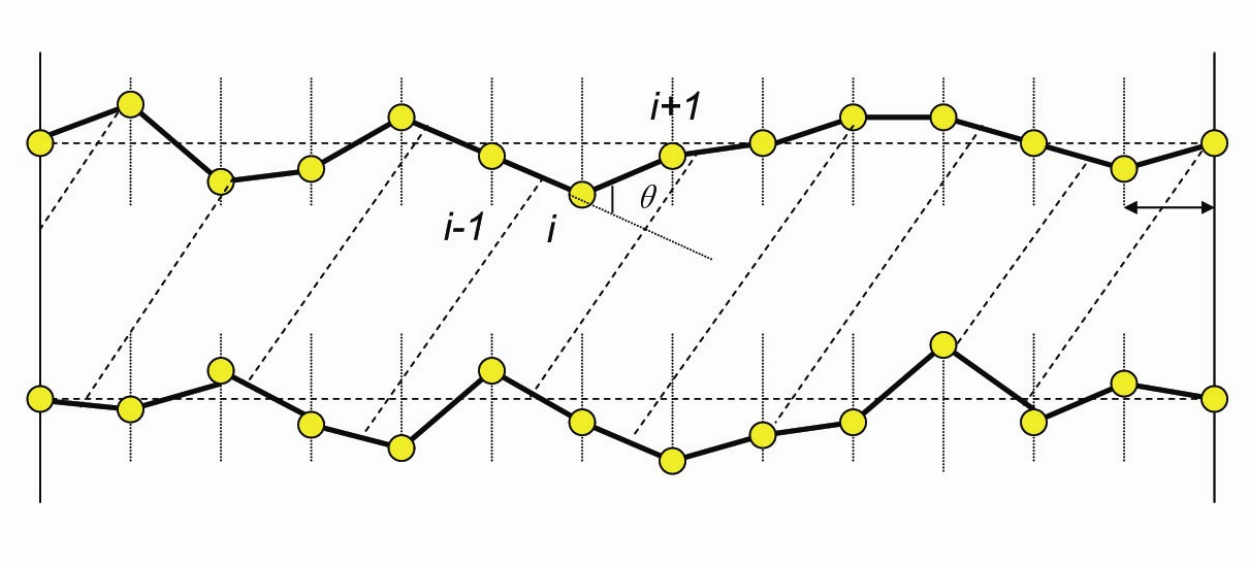

Figure 3.1. Cartoon showing the simple monte carlo model. The yellow dots represent the edge points in each slice in md simulation.

RESULTS

Equilibrium Dynamics

During the MD simulations of these ribbons, the edges of the ribbons underwent a variety of configurations. Snapshots from one of these simulations, composed of 65% DPPC, are shown in Figure 3.2. In the mixed systems, the short tail lipids (S) quickly established equilibrium between the edge region and bilayer bulk region at the beginning of the simulations. We see S lipids moved back and forth between the two regions until a stable state is reached. As have been seen in previous simulation[14], a preponderance of S lipids was observed in the edge region and majority of bulk region was occupied by long tail lipids (L). In other words, we observe partial segregation of two lipid species with rapid equilibrium process of the S lipids taking place between the edge and the bulk region in the mean time.

To investigate whether the edges have propagated thoroughly in its configurational space within our simulation time, we calculate the ensemble average of correlation of edge point at time t and its position at a later time t+Δt, $\langle h(t;z)\cdot h(t+\Delta t;z)\rangle$ as shown in Figure 3.3. Here the bracket means averaging over each time steps along the trajectories and each edge point along the edge contour. Systems with the same lipid number ratio but different edge length are graphed. The top graph in Figure 3.3 shows in pure DPPC systems this correlation decays more slowly as the edge length increases. This is not surprising because the system with longer edge contour comprises more modes and therefore requires more time to fully develop them, especially those with longer wavelength. Consequently, we observed that 40nm curve

does not reach zero within 40 ns while 20nm and 30nm curves do so within 20 ns. For this reason, we confine our analysis to ribbons 30nm and shorter.

Line tension

Eq. 1 provided a convenient way to calculate the line tension from the pressure anisotropy: the difference of pressure tensor in XY plane and Z axis must be compensated by a contraction force, which is defined as excess energy for a unit length. The calculation of error bars is based on the block averaging method [26]. DPPC/DBPC systems reached the zero line tension region (<5pN) with a number ratio of 1.5. The pure DPPC systems show a line tension around 50pN. This value agrees well with atomistic simulations of DPPC ribbons[15] , whereas it is higher than experimental value (10~30 pN) of similar lipid type[27, 28].

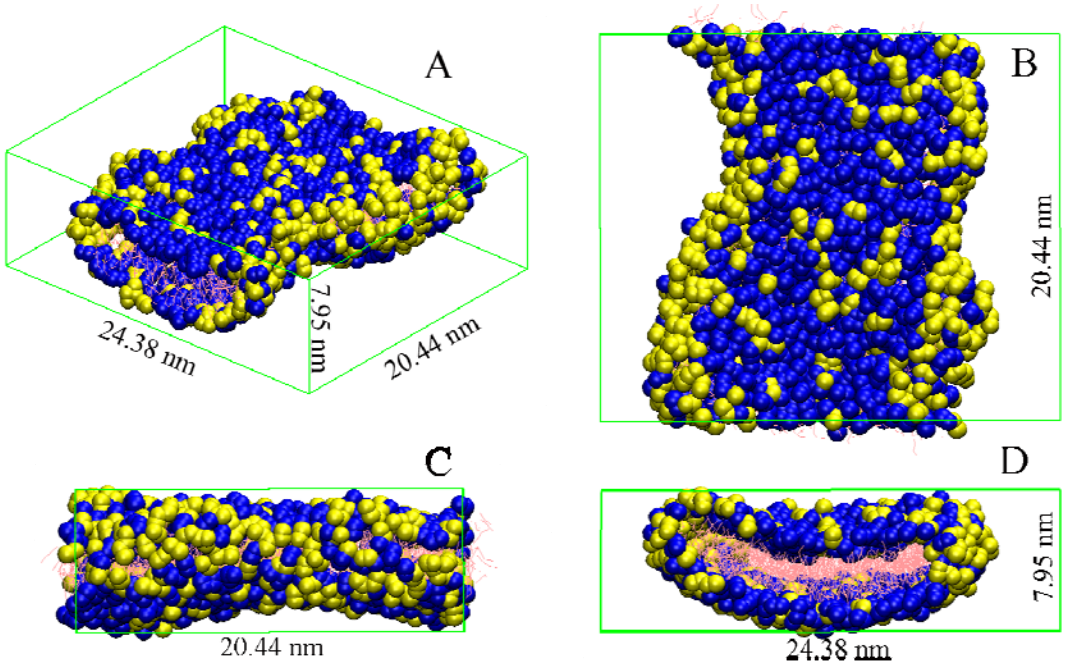

Figure 3.2. Snapshot of one MD simulations. System composed of 65% DPPC and 35% DBPC and has total of 966 lipids. Blue and yellow spheres represent DPPC and DBPC headgroups, respectively. Alkyl chains are represented by pink lines. Waters are not shown for clarity.

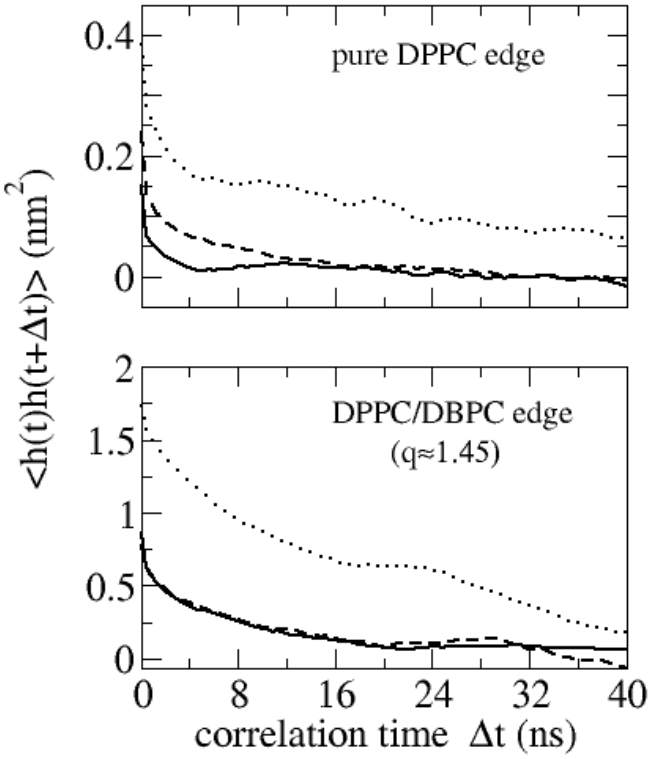

Figure 3.3. Equilibrium Dynamics of bilayer edge. y axis is the time correlation of edge point. Solid lines: box size in edge dimension of 20nm. dashed lines:30nm. dotted lines:40nm

DBPC%	Λ (pN)	κ (10^{-28} Jm)	γ (10^{-2} J/m^2)	R0 (nm)
10	46.07*	0	0	N/A
15	41.71*	0	0	N/A
20	31.49*	0	0	N/A
25	24.30*	0	0	N/A
30	24.21*	0	d0	N/A
35	0.00	0.08	1.0	20.70
37	0.00	0.08	0.77	20.71
40	0.00	0.2	0.35	21.00

Table 3.2. Parameters used in MC simulations to fit position correlation function of edge points and contour length distributions. * means the line tension values obtained from MD simulation pressure tensor calculations.

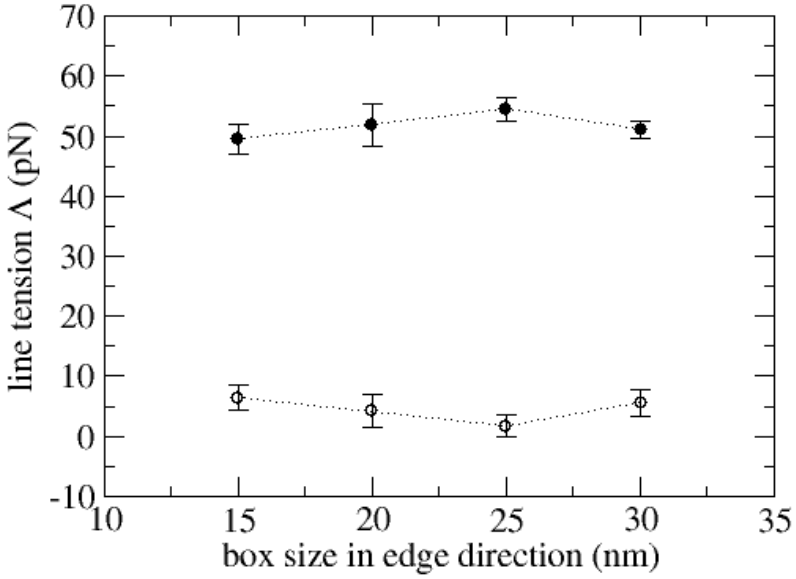

Figure 3.4. Line tension as a function of systems size and composition. Filled circles represent pure DPPC systems. Open circles represent mixed DPPC/DBPC system (58.6%)

Figure 3.4 shows the line tension dependencies on box z dimension and system composition. Although the line tension is strongly influenced by system composition, it fluctuates very little as system size expands. The line tension values set our systems into 2 categories: (1) high line tension region (~50pN) (2) low line tension region (<5pN). To further investigate how line tension varies with composition, we gradually change the number ratio in DPPC/DBPC systems while keeping the total number of lipid constant. The result is shown in Figure 3.5a. The line tension smoothly decreases from around 46 pN to 20 pN until a sudden drop below 0 pN.

Partitioning of short-tail lipids

We calculate the DBPC percentage in the bulk region (a 4nm wide strip in the center of the ribbon) for ribbons of increasing total DBPC concentration, as shown in Figure 3.5b. The percentage of DBPC in the bulk is consistently lower than the total percentage of DBPC, consistent with the enhancement of DBPC at the edge. The rise in bulk DBPC is uninterrupted even as the line tension vanishes between 30 and 35% total DBPC.

Edge Contour length

Figure 3.5c gives the mean edge contour length as a function of system DBPC percentage. The contour length basically remains unaltered until the percentage of DBPC reached 30% and starts to increase promptly with higher DBPC percentage, consistent with line tension drop in Figure 3.5a. The distribution also becomes broader in the low line tension regime.

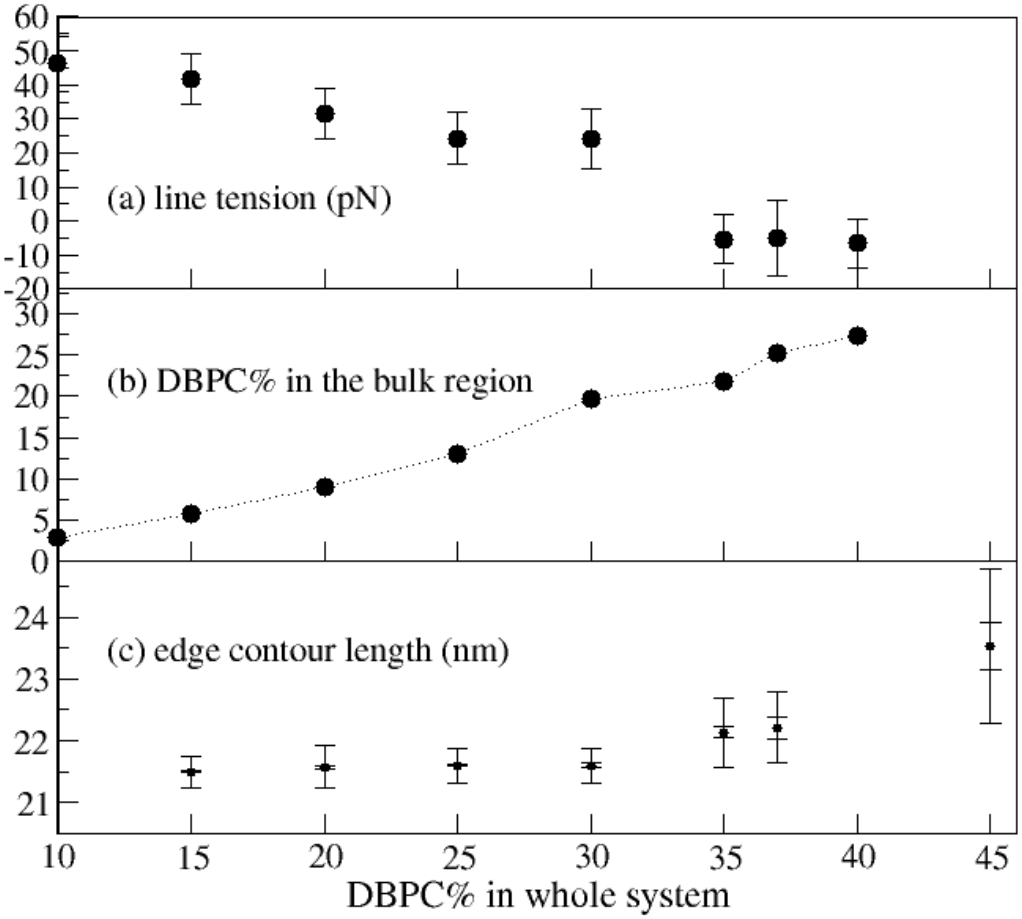

Figure 3.5. System property as a function of system composition. (a) Line tension as a function of DBPC lipid percentage in the whole system. Line tension is calculated from the pressure tensor, as given by Eq. 1. (b) DBPC lipids percentage in the bulk region as a function of DBPC percentage in the whole system. The bulk region is defined as a strip region that spans 4nm across the center of the bilayer. (c) Mean edge contour length as a function of DBPC percentage in the whole system. Inner bars give standard error; outer bars show standard deviation.

Position Correlation function fourier transform

As discussed in the Methods section, to quantitatively analyze the in-plane fluctuations of the edge we represented the projection of each ribbon edge as a function $h(z)$. We then calculated the position correlation function $C(z)=\langle h(z)h(z+\Delta z)\rangle$, averaging over both edges and the full production run, from MD simulations at both high line tension region and low line tension region. Fourier transform of this function is plotted in Figure 3.6. In Figure 3.6a, we observe that for all the four systems of different edge length the mode intensity behaves as q^{-2} at small wave number, agreeing very well with theoretical prediction. To further test that, in Figure 3.7 we fitted the mode intensity data from MD and MC simulations to theory (eq. 9) by inputting the line tension Λ_{MD} value calculated from pressure tensor (eq. 1) and neglecting the bending term ($\kappa \approx 0$). The results show very good agreement with theory at wave number less than 0.1 nm^{-1}. A plateau is seen for higher wave numbers. Figure 3.6a also shows that the modes with the same q have larger amplitudes at smaller box boundary size along the edge, which is consistent with eq.4. In Figure 3.6b, the mode intensity behaves differently from what theory predicts. The q^{-2} scaling no longer exists at small q regions but does not show q^{-4} scaling as predicted from theory when $\Lambda \approx 0$ (in the case of Figure 3.6b, Λ is close to zero) if fluctuations were controlled by an in-plane bending rigidity κ. These results indicate that at $\Lambda \approx 0$, the in-plane fluctuations of the edge are not controlled by a simple bending parameter alone. In contrast with Figure 3.6a, the mode intensity in Figure 3.6b does not decrease with increasing ribbon length, so no free energy model based on a (positive) quadratic dependence on mode amplitude and a linear dependence on edge

length will fit the data. We therefore turned to simple Monte Carlo simulation of a 1-dimensional representation of the edge to test other free energy models.

Fitting edge fluctuation at high line tension region (DPPC percentage $\geq$70%)

Results from above show that edge correlation function agrees very well with theoretical predictions at large wave length and high line tension. We therefore use the line tension, calculated from pressure tensor (eq. 1), as the input in Monte Carlo simulations to check our Monte Carlo methods. Both Fourier transform of fluctuation correlation function and edge length distribution from Monte Carlo simulation show very good agreement with that from molecular dynamics data, as shown in Figure 3.7 for systems in the high line tension regime, at 90% and 80% DPPC. The single line tension parameter fitting works very well until DPPC percentage drops below 70%. We are confident that at high line tension region, line energy is dominating force that controls the shape of the edge.

Fitting edge fluctuation at low line tension region (DPPC percentage $\leq$65%)

Figure 3.5a shows that line tension drops below zero as DPPC percentage in systems is equal or less than 65%. As this occurs, it is apparent through visual observation and through the sudden increase in edge contour length Figure 3.5c, the edge enters a regime of large amplitude fluctuations, qualitatively different from the high line tension regime. In our Monte Carlo simulations, we set line tension equals zero and tune the κ, γ and L_0 in eq. 12. Fitting results show that including the harmonic term in eq.12 is essential to fit both fourier transform of fluctuation correlation function and edge length distribution from MD simulations.

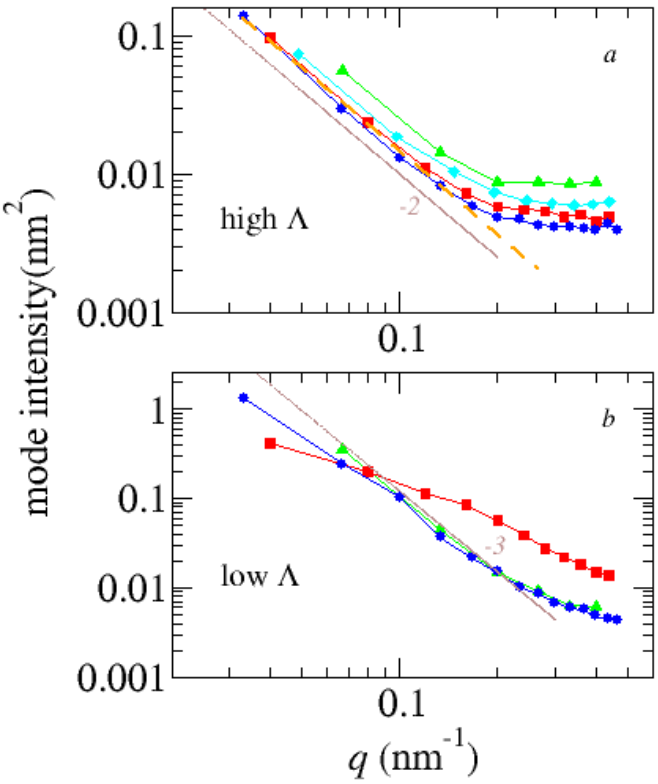

Figure 3.6. Fourier transform coefficient(mode intensity) of Hcorr function of different system size in the edge direction. Blue represents system at 30nm in edge direction. Red :25 nm Cyan:20nm. Green:15nm. Panel a: systems composed of pure DPPC lipids. Dashed line gives prediction of Eq. 11 based on line tension calculated using Eq. 1 for 30 nm system. Panel b: system contains 58.6% DPPC and has low line tension(<5pN). Dash line is power law with exponent -3 for reference.

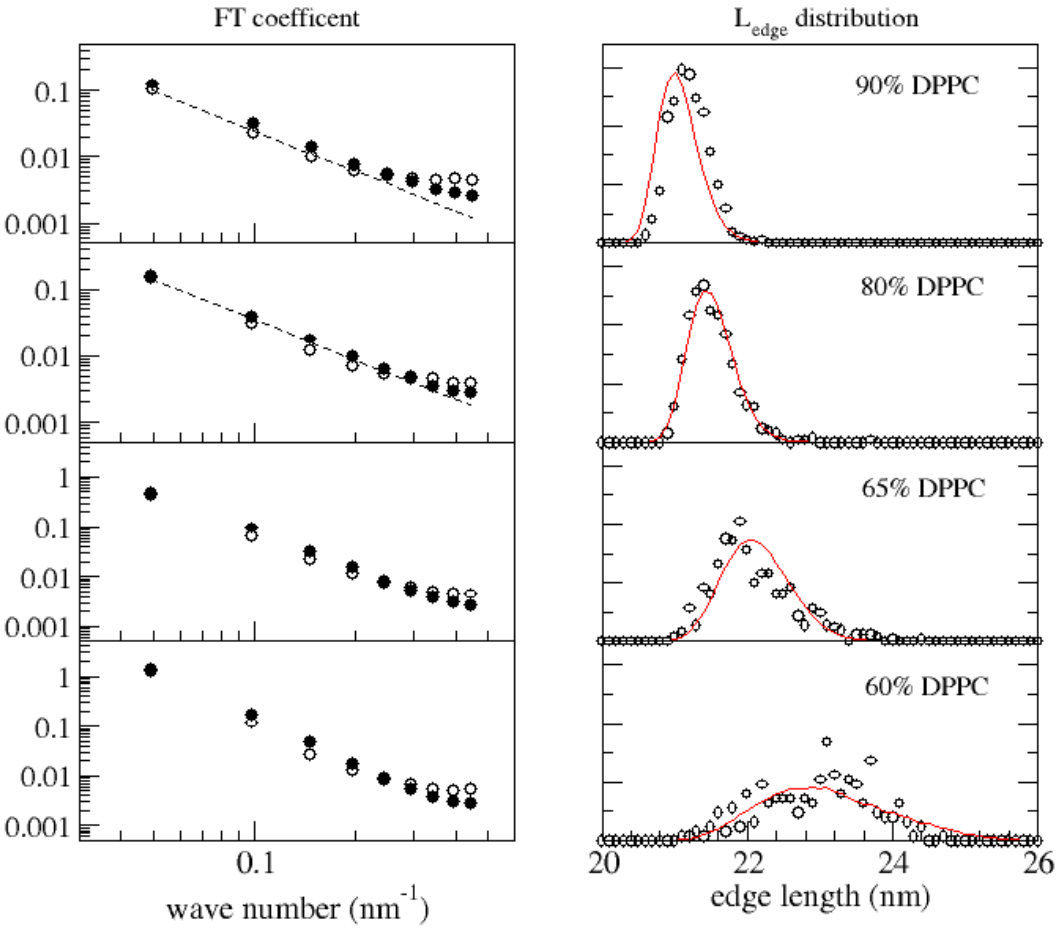

Figure 3.7. Fourier transform coefficient and edge contour length distribution for DPPC/DBPC binary mixture. In the left-hand column, open and solid dots are results from MD and MC respectively. Dashed lines are from theoretical analysis using Eq. 11 with line tension obtained from Eq. 1. In the right-hand column, black circles are data from MD simulations and red lines represent best fits of the data from MC simulations. Parameters used in MC simulations are shown in Table 3.2.

DISCUSSION

As in a previous study using a similar model,[14] increasing the concentration of shorter tailed lipid stabilized the bilayer edge, as indicated by a reduction in line tension. In the present work, the line tension is reduced to zero (in fact, a negative value) at moderate fraction of shorter tailed lipids, leading to a great increase in shape fluctuations. In the positive line tension regime, the amplitudes of random thermal fluctuations are limited by the excess free energy of the increased contour length associated with these fluctuations. Both a simple expression (Eq. 11) based on the equipartition theorem and a simple Monte Carlo model do a good job of predicting the long-wavelength amplitudes using the line tension, obtained independently from pressure tensor following Eq. 1, as the only input.

When line tension drops below zero, however, the behavior of the edge is more complex. If we assume $\Lambda=0$, then the edge length could in principle diverge. Our original prediction was that the fluctuations would be limited by the in-plane bending elasticity of the edge; however, the q^{-4} dependence predicted from Eq. 11 was not observed in the amplitude spectrum. We realized that the condition $\Lambda=0$ does not mean a true absence of any contour length effects on energy within our small, fixed-composition system. The fluctuations of the edge are in fact limited by the availability of the short-tail lipid DBPC; increases to the edge contour length will lower the DBPC concentration in the edge and the bulk and re-introduce a line tension that will limit further increases. Reductions to the edge contour length will lead to an excess of DBPC that will lead to an effective line pressure. A harmonic dependence of free energy on edge length, to maintain the length in a range appropriate for the total system composition, would seem

to be appropriate. We do not have an expression analogous to Eq. 11 for the fluctuation spectrum of such a system, so we resorted to MC simulation of a simplified edge model with a known potential to model the MD results. We obtained a good fit to the contour length distributions upon varying γ and L_0 in eq. 12, but found simultaneous agreement with both edge length distribution and fluctuation amplitude spectrum only when the in-plane bending modulus was included in the Hamiltonian. The harmonic model force constants obtained were in the range 3 - 10 pN/nm, indicating that the edge contour length can fluctuate by one or several nanometers before restoring forces reach the significant level of ~ 10 pN. The in-plane bending elastic constant of the edge, $\kappa \sim 10^{-29}$ J m, corresponds to a persistence length of about 4 nm, of the same order as the bilayer thickness. (Persistence length of the edge cannot be directly related to the decay length of orientational correlations, as is commonly done for polymers with free ends, because the geometry of the system ensures that the correlations re-appear periodically.) Due to the multivariate nature of the fitting, we do not place any emphasis on the particular values obtained for κ, but the general conclusion is that even at negligible line tension, the edge contour will tend to be smooth on a length scale comparable to bilayer thickness, but not exhibit any significant rigidity over a larger length-scale. The fact that bending elasticity is not necessary to interpret the fluctuations of the edge at high line tension does not imply a lower bending elasticity, rather that the stronger damping effect of the line tension obscures any influence the bending elasticity may have.

Partitioning of long and short tail lipids between the bulk and the edge

Our MD simulations show that the edge of ribbon is predominately occupied by short tail lipids and bulk region predominately occupied by long tail lipids. If we can

treat the edge and the bulk as two phases within a pseudobinary system, as suggested by Triba et al.[29], then so long as both phases are stable and at equilibrium with each other (i.e., zero line tension) their compositions should not change: increasing the amount of short-chain component would increase the length of the edge without affecting the composition of the edge or the interior. In contrast to this appealing notion, the current results (Figure 3.5b) show an uninterrupted increase in the bulk DBPC fraction even in the regime of low or vanishing line tension. The assumption behind the two-phase model is that the chemical potential of each component in each "phase" is a simple function of the composition of that phase. This assumption is not strictly true, and the significant deviation from the model's prediction may arise from one of several phenomena.

One issue is that in order for the edge to increase its contour length in the box of fixed length, it has to curve. If the relative chemical potentials of the two lipid types are sensitive to the degree of curvature, then the composition of the interior at equilibrium with the edge may shift. More importantly, if the curvature increases the free energy of the edge, the resistance to bending may prevent the edge from expanding to its true equilibrium length and absorbing excess bulk DBPC. This is consistent with the observed negative line tension – the free energy of the system would decrease if the box were extended, allowing the edge to lengthen without bending. Although the simulation geometry is constrained in an unnatural way, experimental factors may also effectively constrain the in-plane edge curvature, as in the ideal bicelle disk model where composition determines disk radius.

Other possible mechanisms leading to the breakdown in the two-component two-phase model involve the coupling between edge and interior "phases". If this coupling is

significant, the chemical potentials of short and long lipids at the edge gain an additional dependence on the bulk composition. The minimum free energy of the system with coexisting phases can then no longer be obtained through a linear combination of phases with fixed composition. Such a coupling could arise from the influence of the interior composition on the bilayer thickness, which will in turn affect the stability and structure of the edge. If the edge could be made more stable by changing the thickness, as the edge becomes a greater fraction of the total system the composition of the bulk will change to better accommodate the edge. Bulk composition changes might influence the edge stability by changing bending rigidity as well as thickness. At high line tensions, the increase in edge length that will accompany most out-of-plane surface bending modes will suppress surface bending fluctuations of the ribbon. When line tension is no longer significant, fluctuations of the edge normal to the bilayer plane will incur an energy cost from the bending of the surface, which may explain why these out-of-plane fluctuations are weaker than in-plane fluctuations, as seen in Figure 3.2.

Protrusion contribution to fluctuation

The plateau of fluctuation amplitudes at $q > 0.3$ nm^{-1} in Figures.3.6 and 3.7 is a deviation from the predictions of the model that treats the edge as a continuum structure with a line tension. As a small wavelength effect it is likely to come from molecular level fluctuations, analogous to the lipid protrusions from a bilayer sheet as addressed in previous papers. [30, 31] In those analyses, the effect of molecular protrusions on the mean square amplitude of fluctuations in Fourier space was found to be the addition of a term proportional to $(1 + bq^2)^{-1}$. When bq^2 is not too large, a plateau like the one

observed is expected. Fluctuations with q-independent amplitude could arise from random noise, which may be a contributor to the plateau value in the MD data and is the only explanation available for the plateau in the MC data, where molecular protrusion modes are not represented.

CONCLUSIONS

We have performed molecular dynamics simulations on mixed-lipid systems using a coarse-grained forcefield to investigate the behavior of a stable bilayer edge. The system edge behavior can be divided into 2 regimes based on its fluctuations property and line tension: (1) *high line tension regime*. When DBPC% ≤ 30%, although fluctuation of the edges has a trend to become larger, the amplitude of fluctuation remained small. Line tension calculated in this regime is ≥ 24 pN. (2) *Low line tension regime*. When DBPC% is from 35% to 60%, line tension becomes negligible and edges show very strong fluctuations. By fitting the MD data with a simple MC model, we discover that in regime (1) line tension is the dominating factor that determines the edge fluctuations. This result is confirmed by a theoretical model as well. However, in regime (2) the edge is controlled by a harmonic term that has a preferred edge length and by a bending term. The in-plane bending rigidity of the stable edge leads to an apparent persistence length of the order of the bilayer thickness. We observed that short-tail lipid concentration in the bulk of ribbon increases with the total short-tail lipid concentration in the systems even in the low line tension regime, where a two-component two-phase model would predict a plateau. Several possible explanations for this effect are proposed, but in any case the results call into question of the common assumption that in experimental bicelle systems that bilayer

edge and interior compositions are fixed over the range of compositions at a given temperature.

REFERENCE

1. Sanders, C.R. and J.P. Schwonek, *Characterization of Magnetically Orientable Bilayers in Mixtures of Dihexanoylphosphatidylcholine and Dimyristoylphosphatidylcholine by Solid-State Nmr.* Biochemistry, 1992. **31**(37): p. 8898-8905.
2. Tjandra, N. and A. Bax, *Direct Measurement of Distances and Angles in Biomolecules by NMR in a Dilute Liquid Crustalline Medium.* Science, 1997. **278**: p. 1111.
3. Vold, R.R. and R.S. Prosser, *Magnetically oriented phospholipid bilayered micelles for structural studies of polypeptides. Does the ideal bicelle exist?* Journal of Magnetic Resonance Series B, 1996. **113**(3): p. 267-271.
4. van Dam, L., G. Karlsson, and K. Edwards, *Morphology of magnetically aligning DMPC/DHPC aggregates-perforated sheets, not disks.* Langmuir, 2006. **22**(7): p. 3280-3285.
5. van Dam, L., G. Karlsson, and K. Edwards, *Direct observation and characterization of DMPC/DHPC aggregates under conditions relevant for biological solution NMR.* Biochimica Et Biophysica Acta-Biomembranes, 2004. **1664**(2): p. 241-256.
6. Harroun, T.A., et al., *Comprehensive examination of mesophases formed by DMPC and DHPC mixtures.* Langmuir, 2005. **21**(12): p. 5356-5361.
7. Nieh, M.P., et al., *Magnetically alignable phase of phospholipid "Bicelle" mixtures is a chiral nematic made up of wormlike micelles.* Langmuir, 2004. **20**(19): p. 7893-7897.

8. Shelley, J.C., et al., *A Coarse Grain Model for Phospholipid Simulations.* J. Phys. Chem. B, 2001. **105**(19): p. 4464-4470.

9. Marrink, S.J., A.H. de Vries, and A.E. Mark, *Coarse grained model for semiquantitative lipid simulations.* Journal of Physical Chemistry B, 2004. **108**(2): p. 750-760.

10. Murtola, T., et al., *Coarse-grained model for phospholipid/cholesterol bilayer.* Journal of Chemical Physics, 2004. **121**(18): p. 9156-9165.

11. Izvekov, S. and G.A. Voth, *A multiscale coarse-graining method for biomolecular systems.* Journal of Physical Chemistry B, 2005. **109**(7): p. 2469-2473.

12. Brannigan, G., P.F. Philips, and F.L.H. Brown, *Flexible lipid bilayers in implicit solvent.* Physical Review E, 2005. **72**(1): p. -.

13. Jiang, F.Y., Y. Bouret, and J.T. Kindt, *Molecular dynamics simulations of the lipid bilayer edge.* Biophysical Journal, 2004. **87**(1): p. 182-192.

14. de Joannis, J., F.Y. Jiang, and J.T. Kindt, *Coarse-grained model simulations of mixed-lipid systems: Composition and line tension of a stabilized bilayer edge.* Langmuir, 2006. **22**(3): p. 998-1005.

15. Wohlert, J., et al., *Free energy of a trans-membrane pore calculated from atomistic molecular dynamics simulations.* Journal of Chemical Physics, 2006. **124**(15): p. -.

16. Leontiadou, H., A.E. Mark, and S.J. Marrink, *Molecular dynamics simulations of hydrophilic pores in lipid bilayers.* Biophysical Journal, 2004. **86**(4): p. 2156-2164.

17. Lin, T.L., et al., *The use of small-angle neutron scattering to determine the structure and interaction of dihexanoylphosphatidylcholine micelles.* J. Am. Chem. Soc., 1986. **108**(12): p. 3499-3507.

18. Tausk, R.J.M., et al., *Physical chemical studies of short-chain lecithin homologues. 2. Micellar weights of dihexanoyl- and diheptanoyllecithin* Biophysical Chemistry 1974. **1**(3): p. 184-203.

19. Marrink, S.J. and A.E. Mark, *Molecular view of hexagonal phase formation in phospholipid membranes.* Biophysical Journal, 2004. **87**(6): p. 3894-3900.

20. Lewis, R.N.A.H. and R.N. McElhaney, in *The Structure of Biological Membranes*, P. Yeagle, Editor. 1992, CRC Press Boca Raton,FL.

21. Berendsen, H.J.C., et al., *Molecular-Dynamics with Coupling to an External Bath.* Journal of Chemical Physics, 1984. **81**(8): p. 3684-3690.

22. Berendsen, H.J.C., D. Vanderspoel, and R. Vandrunen, *Gromacs - a Message-Passing Parallel Molecular-Dynamics Implementation.* Computer Physics Communications, 1995. **91**(1-3): p. 43-56.

23. Lindahl, E. and O. Edholm, *Molecular dynamics simulation of NMR relaxation rates and slow dynamics in lipid bilayers.* Journal of Chemical Physics, 2001. **115**(10): p. 4938-4950.

24. Humphrey, W., A. Dalke, and K. Schulten, *VMD: Visual molecular dynamics.* Journal of Molecular Graphics, 1996. **14**(1): p. 33-&.

25. Safran, S.A., *Statistical thermodynamics of surfaces, interfaces, and membranes*. Frontiers in physics ; v. 90. 1994, Reading, Mass.: Addison-Wesley Pub. xvii, 270 p.

26. Allen, M.P. and D.J. Tildesley, *Computer simulation of liquids*. Oxford science publications. 1989, Oxford [England] New York: Clarendon Press ; Oxford University Press. xix, 385 p.

27. Zhelev, D.V. and D. Needham, *Tension-Stabilized Pores in Giant Vesicles - Determination of Pore-Size and Pore Line Tension.* Biochimica Et Biophysica Acta, 1993. **1147**(1): p. 89-104.

28. Genco, I., et al., *Electroporation in Symmetrical and Asymmetric Membranes.* Biochimica Et Biophysica Acta, 1993. **1149**(1): p. 10-18.

29. Triba, M.N., D.E. Warschawski, and P.F. Devaux, *Reinvestigation by phosphorus NMR of lipid distribution in bicelles.* Biophysical Journal, 2005. **88**(3): p. 1887-1901.

30. Lipowsky, R. and S. Grotehans, *Renormalization of Hydration Forces by Collective Protrusion Modes.* Biophysical Chemistry, 1994. **49**(1): p. 27-37.

31. Brannigan, G. and F.L.H. Brown, *A consistent model for thermal fluctuations and protein-induced deformations in lipid bilayers.* Biophysical Journal, 2006. **90**(5): p. 1501-1520.

Chapter Four

Two-step hybrid configurational-bias Monte Carlo and molecular dynamics simulations

INTRODUCTION

The phase behavior of mixed lipid assemblies has drawn great attention recently as it provides a prototype to study the cell membrane in living organisms. The cell membrane is a combination of lipids, cholesterol, membrane proteins and carbohydrates that serve as a barrier to control the flux of nutrients, waste and information in and out of the cytoplasm. In the fluid mosaic model[1], the cell membrane is described as a two dimensional fluid in which membrane components can diffuse more or less freely. Recently, cholesterol-rich or protein-rich domains, known as "lipid rafts", are proposed to function in signal transduction [2].

Mixtures of lipids that share the same headgroup but differ in their tails length are considered as the simplest model systems of mixed bilayers. Mixed bilayer micelles composed of DMPC[k] and DHPC[l], called "bicelles", shows tendency to form nematic phases that align in the presence of a magnetic field and therefore can be used as media under which large biological molecules align in NMR experiments; high resolution NMR structure can therefore be solved[3-6]. However, structural properties of mixture lipid systems are difficult to elucidate due to bicelle's complex phase behavior in fluid-like phase and limited capability of experimental techniques[7, 8]. Morphologies, such as ideal disk model[9, 10], perforated sheets[11], wormlike micelles[12], or multilamellar vesicles(MLV) [13] are proposed but cannot be confirmed unambiguously by experiments.

For decades, molecular simulation has been a very useful tool to understand the lipid assemblies and their phase behavior. However, conventional MD simulation faces the

[k] DMPC: dimyristoylphosphatidylcholine, systematic name: 1,2-Dimyristoyl-*sn*-Glycero-3-Phosphocholine
[l] DHPC: dihexanoylphosphatidylcholine, systematic name: 1,2-Diheptanoyl-*sn*-Glycero-3-Phosphocholine

challenge of sufficiently sampling of configurations at equilibrium. The equilibration process may take on the order of microseconds when diffusive mixing is required. Therefore mixed Monte Carlo and molecular dynamics methodologies have been developed. Smart MC[14] method uses the force experienced by particle to bias the direction of Monte Carlo moves. Replica-exchange method is another example of mixing the two methods: configurations from MD simulation at two temperatures are swapped with a probability based on their weights in configurational space. LaBerge and Tully developed a procedure that treats part of systems(e.g. solvent) with MC moves and rest of system(e.g. hydrocarbons) with MD moves[15]. This procedure avoided the expensive integration of equation of motion in some degrees of freedom. However, this method is limited in lipid/solvents systems as solvents have strong interactions with headgroups of lipids. Recently, an isomolar-semigrand emsemble molecular dynamics (iSGMD) has been developed and apply to methane/ethane mixtures[16]. In this method a coupling variable λ, which transforms particles from one type to the other, is included in the system Hamiltonian and evolves with time. However this method still cannot cross the local barriers efficiently during the transformation process. A sequential hybrid MC and MD method was invented for fast sampling of ensemble average[17]. This method is efficient only with continuum treatments of solvents and can not deal with systems with explicit degrees of freedom. Chiu et al. developed a method using alternating blocks of MD and configurational-bias Monte Carlo method and applied it to lipid bilayers[18]. This method requires re-insertion of water molecules after every successful mutation which could leads to significance artifacts near the bilayer interface.

In this chapter, a method that integrates the CBMC method with MD simulation will be described in detail. As CBMC samples configurations of polymeric molecules by adding or

removing each segment, this method can be applied to switch the lipid type by growing or shrinking their tail length. Unlike other hybrid methods, this method lets each CBMC step alternates with MD step while keeping the water degrees of freedom untouched. We have used this method to investigate the mixed lipid bilayer [19] and shown its applicability to binary lipid bilayer of DPPC/DLPC over a wide range of compositions, in which two lipid components have di-16 and di-12 carbon tails respectively. The lipid bilayer has 128 lipids and converges to a composition at equilibrium within 1ns of MD steps. A thorough investigation of the structural properties of bilayer components has been performed. The number density of acyl carbons indicates the significant transbilayer interactions of lipids between the two leaflets. However the radial distribution data shows almost uncorrelated pairing between either same lipids type or different lipid type. Reasons for this weak correlation may come from the insignificant difference between the two lipid types and it pushed us to investigate more challenging systems composed of lipid species that differ by 8 carbons in their tail length, for example DMPC/DHPC system. However, as the acceptance rate decays exponentially with increasing molecular size difference in CBMC, a direct application of the previous one-step mutation scheme on DMPC/DHPC would become very inefficient. We therefore developed this two-step mutation scheme that helps to facilitate the transition from long-tail lipid to short-tail lipid by introducing an intermediate species. The intermediate species establishes equilibria with both long-tail and short-tail lipids at the same time; and the intermediate species is kept at low level by carefully tuning the composition parameter so that the predominant components of the system is still a binary mixture of long and short tail lipid. Application of the two-step mutation scheme has been applied to lipid bilayers and lipid bilayers with edge defects over a range of compositions. The simulation

results show that the edge of the ribbon is predominantly occupied by the short-tail lipid. The line tension value is strongly dependent on the composition of the system. Our method has provided the way to study the lateral distribution of lipids at equilibrium using the atomistic models.

METHODS

Configurational-bias Monte Carlo Algorithm

Configurational-bias Monte Carlo technique was first introduced by Siepman and Frenkel[20-23] based on earlier technique developed by Rosenbluth and Rosenbluth in 1955[24]. In the current work, this method is used to regrow a chopped short tail lipid to a long tail lipid or reversibly, to chop a long tail lipid to a short-tail lipid. In our method, configurational-bias Monte Carlo steps (MC steps) are used between MD steps. The forward move (growing) procedure is shown as follows:

(1) For the next extension site along the tail, generate k different positions on the sphere centered at the preceding site with the radius equal the bond length. The probability of generating these position is proportional to $\exp(-\beta U_{bonded})$. β equals 1/kT and U_{bonded} is the bonded interactions within the same molecule. This term includes the potentials associated with the bond angle and bond dihedral angles.

(2) The selection of the one of the k sites is proportional to its Boltzmann weight of nonbonded interactions $\exp(-\beta U_{nonbonded})$. $U_{nonbonded}$ is sum of Lennard-Jones interactions of the new sites. We assume there that the net charge on each site is zero, as is typical for the tail sites of lipids represented through united-atom forcefields.

(3) Accept the trial move with a probability acc(S->L) = min[1, $W\alpha^{-1}exp(-\beta U_{end})$] . W is the Rosenbluth weight of the growing part of the new chain.

$$W = \prod^{nchop} \frac{1}{k} \sum_{i=1}^{k} \exp(-\beta U_{i,nonbonded})$$

$$\alpha = exp(\beta\mu_S)/exp(\beta\mu_L)$$

where U_{end} is the potential energy change of changing the terminal carbon site from methyl to methylene groups. In the reverse move if a long tail lipid is chosen, its tails will be chopped with an acceptance ratio of min[1,$W^{-1}\alpha exp(\beta U_{end})$] . W is calculated in a similar way as the growing procedure in which $k - 1$ positions are generated from its weighted distribution of bonded interactions and the existing one is substituted as the k th position.

In practice, the activity ratio α is the important input parameter that controls the relative composition of the two lipid types.

Verification of the CBMC Method

The algorithm described above samples a semigrand-canonical ensemble. Within this ensemble, the probability weight for a given structure is proportional to exp(-βU)exp[β(μ_S-μ_L)N_S], according to detailed balance:

$$\frac{acc(L\to S)}{acc(S\to L)}=\frac{P(N_s+1,N_{tot}-N_S-1)}{P(N_S,N_{tot}-N_S)}\frac{\alpha_{S->L}}{\alpha_{L->S}}$$

$$=\frac{\exp(-\beta U_S)}{\exp(-\beta U_L)}\frac{\exp(\beta\mu_S)}{\exp(\beta\mu_L)}\frac{\exp(-\beta U_{CH3})}{\exp(-\beta U_{CH2})}\frac{\prod_1^{nchop}\frac{\exp(-\beta\Delta U_{bonded})}{\sum_{i=1}^{k}\exp(-\beta\Delta U_{i,bonded})}\frac{\exp(-\beta\Delta U_{nonbonded})}{\sum_{i=1}^{k}\exp(-\beta\Delta U_{i,nonbonded})}\frac{1}{k}}{1}$$

$$=\frac{\exp(-\beta U_S)}{\exp(-\beta U_L)}\alpha\exp(\beta U_{end})\frac{\exp(-\beta(U_L-U_S))}{\prod_1^{nchop}\frac{1}{k}\sum_{i=1}^{k}\exp(-\beta\Delta U_{i,bonded})}$$

$$=W^{-1}\alpha\exp(\beta U_{end}) \qquad (1)$$

Clearly, the proposed acceptance ratio satisfies detailed balance. Notice that the *1/k* factor in *W* is on account of the discrete sampling of the *k* trial positions in each consecutive step on the sphere centered at preceding site with a bond radius of bond length. In the current study, *k* is set to 4 to balance the expense of calculation and statistical accuracy.

Stochastic (Langevin) Dynamics

System temperature is maintained at 323K using stochastic (Langevin) dynamics[25] method with thermostat time constant of 0.2ps. Langevin dynamics is typically written in the following form:

$$m_i\vec{a}_i=\vec{F}_i-\xi v_i+\vec{R}_i \qquad (2)$$

Where m, a and v are the particle mass, acceleration and velocity respectively. The system dynamics is determined by three types of forces: F, the force calculated from gradient of the potential energy function, ξv, the friction force and R, the random force. Langevin dynamics provides statistically correct constant temperature but does not

rescale the velocities based on the total kinetic energy for all the particles; therefore it is suitable for our system with variable number of atoms.

Implementation of one-step MCMD method

The particle removal in CBMC is achieved by turning off the nonbonded interactions of terminal acyl carbons in the short-tail lipid. These carbons are not really deleted in the simulation but become "invisible" to the real particles and therefore are called "ghost atoms". Switching a real atom to a ghost atom, the turning off step, is implemented by changing the atom type from carbon type to hydrogen type. The ghost atoms are only topologically linked to the end of real atoms and will have no influence on the configurational distribution of the existing real segments of molecules. After the real atoms are switched to the ghost atoms, the new terminal site will be changed from CH2 to CH3 type. The partition function of the unchopped and chopped molecule can be written as the following:

$$Q_{long(L)} = Q_{real(bonded+nonbonded)} Q_{terminal-real(bonded-ghost,nonbonded-ghost)} \quad (3)$$

$$Q_{short(S)} = Q_{real(bonded+nonbonded)} Q_{terminal-ghost(bonded-real)} \quad (4)$$

As indicated in equation 4, the ghost atoms will result in a shift of chemical potential of short-tail lipid, and the shift only depends on intramolecular bonded interactions. Equation 4 also indicates that since the partition function of the short-tail lipid is the product of the partition function from the real part and the ghost part, at equilibrium, the ghost part will not affect the distribution of tail configuration in the real part. As we see

in equation 3, the lipid is in unchopped state, the terminal carbons are treated as real atoms and they are sampled with non-bonded interactions. When a transition (from unchopped →chopped) is made, the positions of the ghost carbons reflect both bonded and non-bonded energies and may not be at equilibrium. Based on this reason, it is possible that a net energy will flow from the real part to the ghost part; however, in practice, this effect will not be a problem due to the following two reasons: (1) new velocity will be assigned to each particle from Maxwell-Boltzmann distribution after every MC move to compensate the energy lost and the stochastic MD steps between MC steps will also compensate the energy lost.(2) nonbonded interactions between the terminal carbons are all short-ranged, their contributions to the partition function are insignificant relative to bonded interactions. This problem has been avoided in the latest version of the code by choosing new ghost particle positions from a Boltzmann distribution after each successful chop move. In the particle growing procedure, the atomtype of the ghost tails will be switched back to normal CH2 or CH3 type and therefore the nonbonded interaction will be counted again. To take advantage of the existing forcefield calculation code in GROMACS, our Monte Carlo code that change the particle forcefield parameter is inserted before the neighbor search and force calculation (Figure 4.1). Table 4.1 lists the input parameters we added for the two-step CBMC subroutine.

Implementation of two-step MCMD method

Implementation of two-step MCMD is based on previously developed one-step mutation code[19]. The data structure t_mc is added to the code (in file mc.c), which

Input parameter	Description	default value
mctype	choose 0 - conventional MD 1 - bybrid MCMD 2 - pure MC	1
mcchop1	number of carbon atoms to be chopped on tail 1	4 for DPPC/DLPC 8 for DMPC/DHPC
mcchop2	number of carbon atoms to be chopped on tail 2	same as above
mcfreq	the MD steps between MC attempts	1
mcrepeat	the number of MC attempt if not succeed	1
mcSnum0	the number of short-tail lipid in the starting configuration.This value is ignored if a chops.dat file is present in current directory.	N/A
mcBnum0	the number of long-tail lipid in the starting configuration. This value is ignored if a chops.dat file is present in current directory.	N/A
mckmax	the number of attempted positions for each stepwise site growth	4
mctemperature	temperature that matches the langevin dynamics	300 or 323K
mcactivityratioSL	the activity ratio between the long-tail and short-tail lipid	N/A
mcactivityratioBL	the activity ratio between the long-tail and intermediate lipid	N/A

Table 4.1. Description of the input parameters in two-step MCMD code.

contains all the necessary input parameters of the simulation and some array that can be shared by data of the same type. Each lipid in simulation is in one of the three states: 0-full lipid (long-tail lipid); 1-half chopped lipid (intermediate) or 2-fully chopped lipid (short-tail lipid). The states of lipids are recorded in an array called bLSB in mc.c file. This array is updated every time a CBMC attempt is succeeded and is written to a chops.dat file together with coordinates saved on another file dtraj.gro. When a simulation is started, the MCMD searched the chops.dat file in the current folder first. If it is found, the last line in chops.dat, which contains the lipid state (0, 1 or 2) will be read into the program and the corresponding lipid in the starting configuration .gro file (start.gro) in it will be changed to that state by switching its forcefield parameters. If chops.dat is not present in current directory, the code will read mcSnum0 as the number of fully chopped lipid and change the first mcSnum0 lipids to state 2 in the start.gro file; it then reads mcBnum0 and changes the next mcBnum0 lipids to state 1 in the start.gro file; the rest lipids are treated as full lipids. Chopping the lipid type is realized by changing the atom type of a few atoms at the end of each tail to hydrogen type (chopped atoms become ghost atoms) which has no nonbonded interactions with other atoms; the carbon united atom preceding the lasted chopped atom along the tail is then mutated from CH2 type to CH3 type. Similarly, growing a chopped lipid to a longer one turns on the nonbonded interactions by changing the atom type from ghost type back to its original atom type and the nonbonded interactions is then restored.

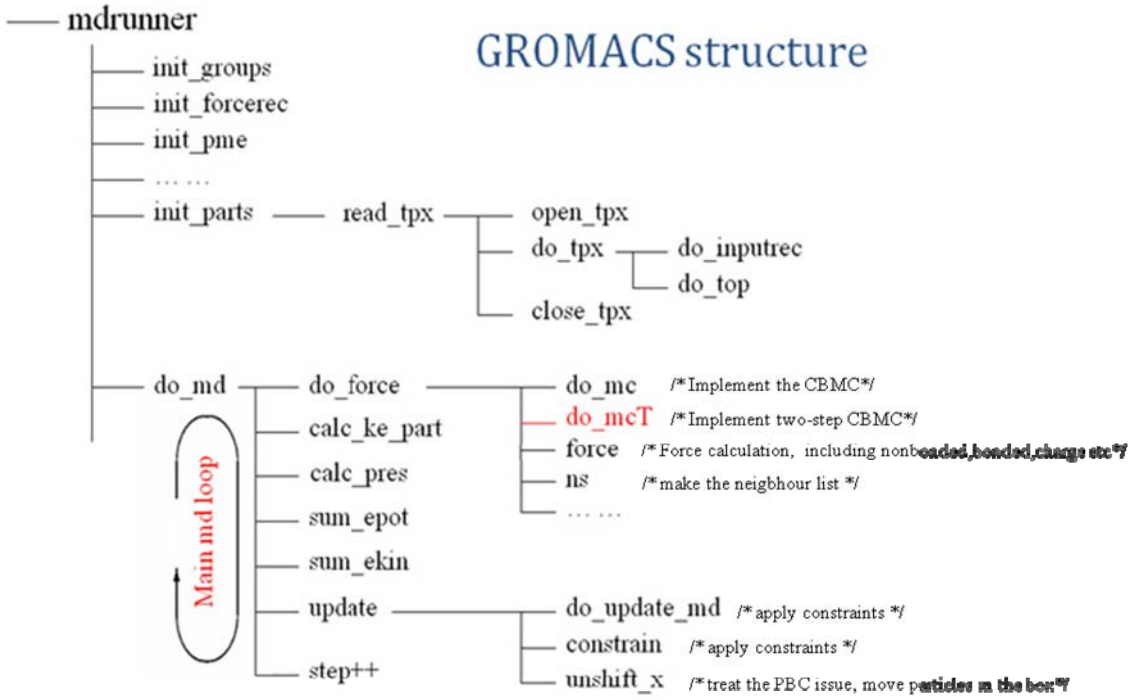

Figure 4.1 The code structure of GROMACS.

The Two-Step Mutation

The MCMD method has been applied to lipid bilayers of DLPC and DPPC systems in which the two lipid types differ by four carbons in their tail length.[19] Although we observed that system gradually converged to equilibrium composition within 2 nanosecond MD time, the Monte Carlo acceptance ratio maintains 0.1%. As W is the product of consecutive attempts to add or remove segments of a chain, the acceptance ratio will decrease geometrically as the difference in tail lengths between the long and short lipids increases. To avoid the low acceptance ratio in such systems, we further developed a two step mutation algorithm in which an intermediate molecule (molecule B) type is introduced.

$$L \underset{}{\overset{\alpha_2}{\rightleftharpoons}} B \overset{\alpha_3}{\rightleftharpoons} S \tag{5}$$

$$L \overset{\alpha_1}{\rightleftharpoons} S \tag{6}$$

In (1), we set up two equilibriums at the same time in which α_2 and α_3 are the activity ratio for each. The product of α_2 and α_3 is equivalent to the activity ratio of direct equilibrium between L and S which determines the relative composition of L and S in (6): $\alpha_1 = \alpha_2\ \alpha_3$

There are three types of lipid in two-step MC algorithm: L, S and B, representing long, short and intermediate lipid. For each attempt MC move, one lipid molecule is selected at random. If a long tail lipid or short tail lipid is selected, a growing and chopping procedure similar to one-step mutation will be performed. If an intermediate lipid is chosen, then this lipid will have equal probability to either grow to long tail lipid

or be chopped to short tail lipid. The intermediate molecule tail length is therefore chosen as the halfway between long tail lipid and short tail lipid. In simulation, α_1 and α_2 is chosen to control the equilibrium composition of L, S and L,B. The third activity ratio that controls the B, S equilibrium is $\alpha_3 = \alpha_1 / \alpha_2$.

In the production runs, α_1 and α_2 are carefully chosen so that the overall L: S ratio is close to preferred value and the intermediate molecule maintain very few in the system. In the Results, we reproduce the same system composition with 2 carbons chopped in each step as the one-step mutation in which 4 carbons are chopped at one time[19].

Line tension calculation

Line tension along the ribbon edge can be express by the following equation.

$$\Lambda = \frac{1}{2}\left\langle L_x L_y [\frac{1}{2}(P_{xx} + P_{yy}) - P_{zz}] \right\rangle \quad (7)$$

P_{xx}, P_{yy} and P_{zz} are the diagonal componensts of the instantaneous pressure tensor. L_x and L_y are box sizes in the x and y dimensions. The prefactor of ½ accounts for the two edges in the ribbon geometry. As linetension is macroscopically defined as the free energy penalty for unit increment of edge length, its value can be obtained by measuring the effective force in the z (the edge) dimension statistically. This effective force will be the difference of actual force arising from the bulk (the average of P_{xx} and P_{yy}) and the force from the z dimension, the edge direction. The bracket in equation 7 means to average over the frames along the simulation trajectory. Typically the line tension is positive and the edge will not be favored or stable. In some cases, the composition of lipid assembly falls into the ratio at which the

line tension could be close to zero, indicating the edge length increase is not subject to free energy contribution from the pressure tensor. Conversely, in some systems, negative line tension, or namely line pressure, can be observed, indicating a decrease in free energy when edges begin to form.

Forcefield and implementation details

Simulations are performed using the forcefield and topology parameters derived from DPPC lipid by Berger et al[26]. DMPC, DLPC and DHPC used the same parameters with 2, 4 and 8 methylene groups removed from each tail of DPPC lipid. Topology files are modified due to the removal accordingly. Single point charge (SPC) model[27] is used for the water molecules. Acyl groups in the hydrophobic tails are simplified by united atom models with charge-free sites, which saves CPU time when calculating nonbonded interactions. During MD simulations, all bonds are subject to all-bonds constraints using LINCS[28](for lipids) or SETTLE[29](for waters). The electrostatic forces are treated using Particle Mesh Ewald[30], with a 1.0 nm cutoff in real space, 0.12nm grid size in Fourier space and fourth-order interpolation. Neighbor list is updated every MD step using grid type algorithm.

The integration time step is composed of 2fs MD step and a CBMC mutation attempt. Stochastic (Langevin) dynamics method [25] is used to keep system temperature at 323K with a thermostat time constant of 0.2 ps. Langevin dynamics has the advantage of dissipating undesired thermal energies without rescaling the velocities of particles system-wide and therefore is suitable to our systems that contain variable number of particles. Berendsen's semiisotropic pressure coupling scheme is applied in the XY and Z

(bilayer normal) direction independently with compressibility set to 4.5×10^{-5} bar^{-1}. The pressure is coupled to 1bar with a time constant of 1 ps. Isotropic pressure coupling should be avoided as the dependence of the pressure tensor in XY and Z dimension will push equilibrium between the long and short lipid towards the direction of more lipid being chopped.

The source code is implemented based on GROMACS 3.2.1. Simulations were performed on single processor (Dual-Core 2.0GHz AMD Opteron) of our Beowulf-type linux cluster. Linux Shell scripts and python scripts are used for analysis purposes. The VMD package[31] is used for molecular visualization.

System initiation

bilayer

The testing bilayer structure of 128 lipids in fluid phase is downloaded from the Tieleman's website at the University of Calgary: http://moose.bio.ucalgary.ca/index.php?page=Downloads. [32]

Ribbon

Three parallel starting structures for lipid ribbons are used for convergence test. One structure is from previous DMPC/DDPC structures with equilibrated distribution of long and short lipids. The two structures with edges are from our previous runs of pure DMPC ribbons with different number of DMPC chopped to intermediate species DDPC. The box dimension along the edge direction, defined as Z in this paper, is set to a fixed value at 6.14125nm. Ribbons edge is subject to semiisotropic pressure coupling to 1 bar

on the XY dimension at compressibility of 4.5×10^{-5} bar^{-1} and Z dimension at compressibility of zero. All the systems mentioned above are set at constant temperature at 300K using Langevin dynamics algorithm.

RESULTS

(I) Verification of two-step MCMD: parallel test on DLPC/DPPC bilayer system

activity ratio, $\alpha=\exp[\beta(\mu_S-\mu_L)]$	DPPC/DLPC	% intermedidate (DMPC)	time(ns)	mean area per lipid ($Å^2$)
1163	(A)3.71	11.7%	5.4ns	66.54±1.26
	(B)3.44	*N/A*	*10ns*	*66.68±0.18*
3490	(A)1.08	5.9%	6.4ns	66.74±0.30
	(B)0.95	*N/A*	*10ns*	*67.10±0.11*
9307	(A)0.38	4.6%	5ns	67.63±0.25
	(B)0.33	N/A	*10ns*	*67.01±0.34*

Table 4.2: Comparison of the results from two-step MCMD (dataset A) and previous one-step MCMD (dataset B in italicized font) on DPPC/DLPC systems.

A good way of testing the two-step algorithm would be a comparison with previous one-step mutation between DPPC and DLPC bilayer (differ in 4 carbons in each of their tails). The two-step algorithm is therefore designed to establish two equilibriums: DPPC/DMPC and DMPC/DLPC with tails differ in 2 carbons. The activity ratio α is set to 3469, which corresponds to a 50:50 overall composition of L:S. The two-step mutation starts from a composition far from equilibrium composition (q=1) but converge to q=1 composition within 0.5ns. In the two-step mutation simulation, the percentage of intermediate species is less than 10%, therefore its presence should have very little effect to the ratio of both L and S lipids, especially when the amount of L and S are close. This figure shows that the two-step algorithm can reproduce previous one-step results and we are confident to extend the application of two-step mutations to more challenging systems such as DMPC/DHPC mixtures with edges.

(II) Simulation of DMPC/DHPC Ribbon systems

To further investigate the DMPC/DHPC lipid distributions at equilibrium with the presence of edge defects, we performed the simulations using 2-step mutation algorithm over a range of system compositions, as summarized in Table 4.2.

α1	α2	time	DMPC%	DHPC%	line tension(pN)
0.5e8	1e3	(I) 15ns	66.6%	23.6%	3.6±11.1
		(II) 12ns	57.3%	32.2%	10.3±9.8
1e8	1e3	(I) 20ns	51.7%	38.1%	24.4±7.8
		(II) 30ns	49.0%	42.8%	20.2±6.9
		(III) 10ns	54.4%	36.3%	26.3±13.6
2e8	1e3	(I) 30ns	42.9%	51.7%	16.8±8.2
		(II) 40ns	40.0%	53.5%	-3.1±5.5
		(III) 17ns	36.5%	55.7%	21±10.2
4e8	1e3	(I) 20ns	27.5%	67.14%	7.8±7.8
		(II) 20ns	18.2%	78.1%	10.2±7.9
		(III) 10ns	27.1%	67.8%	52.3±13.3

Table 4.3. Results from two-step MCMD simulations on DMPC/DHPC/DDPC(intermediate) ribbons assemblies. α1 and α2 are the activity ratio between DMPC/DHPC and DMPC/DDPC respectively. At each activity ratio, two or three parallel systems starting from different configurations are simulated with two-step MCMD method. Line tension is calculated from equation 7. The percentage of DMPC and DHPC are the averaged composition over the last 2ns simulation data. The line tension is the averaged value over the whole trajectory.

Snapshots

Snapshots from two-step mutations are shown in Figure 4.2. As expected, DDPC lipids near the edge are quickly switched to DHPC lipids and remained as DHPC lipids for quite a long time. A low level of DHPC lipids is also observed in the central bulk region. Similar enhancement of the DHPC near the shoulder of the edge is also observed. In addition, the ribbon exhibits a small dip in the central ribbon with increasing DHPC amount at or closeby.

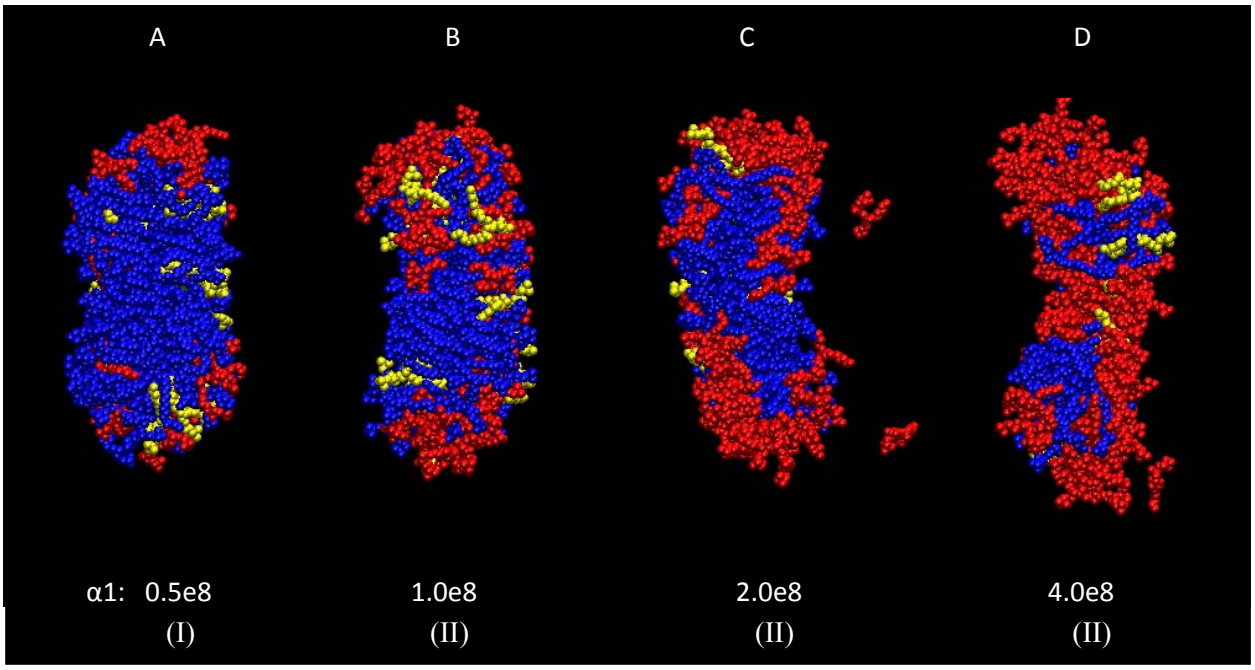

Figure 4.2. Snapshots of the final structure from DMPC/DHPC/DDPC(intermediate) ribbon simulations at different activity ratios. The Roman numerals at the bottom are the corresponding runs in Table 4.2. Blue: DMPC lipid; Red: DHPC lipid; Yellow: DDPC lipid. Note that two DHPC lipids diffuse into solvents from both edges in C. One lipid diffuses into solvent from lower edge in D. Water pore is observed in D which is shown in Figure 4.6. (water pore has not formed so far in the other two runs with different starting configurations but the same activity ratio)

Composition convergence

To test the efficiency of two-step MCMD method and the rate of composition convergence of mixed lipid ribbons, simulations on four systems at different activity ratios are performed. As shown in Figure 4.3, the system undergoes significant composition changes in the first a few nanoseconds and reached a stable composition afterwards. As mutation between L (or S) to intermediate require only one step switch, the percentage of the intermediate species converges faster than the convergence of direct mutations between L and S lipid. As the intermediate has the equal probability of either growing to L or shrinking to S, the overall equilibrium process between L and S should be 4 times longer than one step mutation, giving an average of one mutation per 4 or 8 picoseconds. As the proportion of the intermediate is kept low, this rate will decrease further.

In Figure 4.2D, we observed that the equilibrium quickly established in the first 1 or 2ns and composition maintained constant until a steady increase of S lipid amount occurred after 10ns. As discussed later, this is due to the formation of a water pore in the middle of the ribbon; the pore creates more edges and further switches more L to S around its rim.

Line tension

Line tension is defined as the free energy cost per unit edge length and therefore its value will affect the stability of the edge. Computationally, line tension can be calculated from MD data: the pressure tensor difference in the edge direction and

direction perpendicular to the edge, as shown in equation 3. The results are shown in table 4.2 and the error bar is calculated with the block averaging method [33].

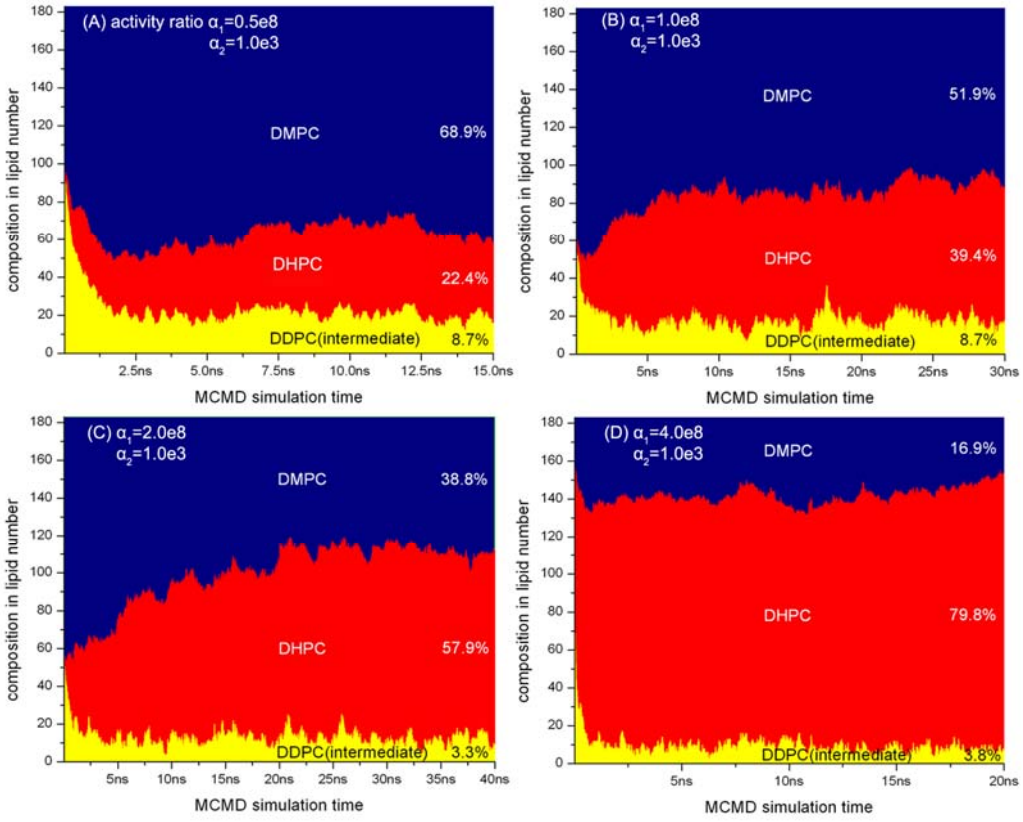

Figure 4.3. Composition convergence with time from simulations on DMPC/DHPC/DDPC(intermediate) ribbon assemblies at four difference compositions. Blue, Red and Yellow represent DMPC,DHPC and DDPC component respectively. The percentage on the right is the composition at the end of each runs. Activity ratio is shown on the upperleft corner of each sub-figure.

Edge composition profile

To show the distribution of the lipid components, we plot the site density as a function of distance from the ribbon center towards the edge, as shown in Figure 4.4. Lipids are oriented in the XY plane so that one of its principle axes is aligned with Y direction and their centers of mass are superimposed to the box center. The two red peaks at the edge position show the apparent partition of DHPC. It is interesting to see that the segregation is more pronounced when less S is present in the system. In Figure 4.4A and 4B, the height ratio of the DHPC peak is roughly 3 times the plateau of DHPC in bulk region; but this ratio decreases to 2 in Figure 4.4C and 1.3 in Figure 4.4D. The integration of the density in Figure 4.4 gives the relative amount of the lipid in different part of the ribbon. Figure 4.4 indicates a saturation point of short-chain lipid in the edge and segregation of two lipid type becomes weakened if extra short-chain lipids are introduced to the system.

Edge bulging effect

To better understand the lipid distribution of the edge and the time-averaged shape of the ribbon structure, we have generated a graph of overlapped positions of the phosphorus atoms from lipids in the x and y coordinates over the trajectory of 15 or 20ns with an interval of 20ps, as shown in Figure 4.5. As rotation and translation occurred during the simulation, the ribbons were translated and rotated with their center of mass superimposed with the center of the box and their larger principle axis parallel with Y axis. Figure 4.5 shows how the shape of ribbon cross section changes as system composition changes. It shows that the thinning in the bulk center becomes more and more prominent with increasing short-tail lipids.

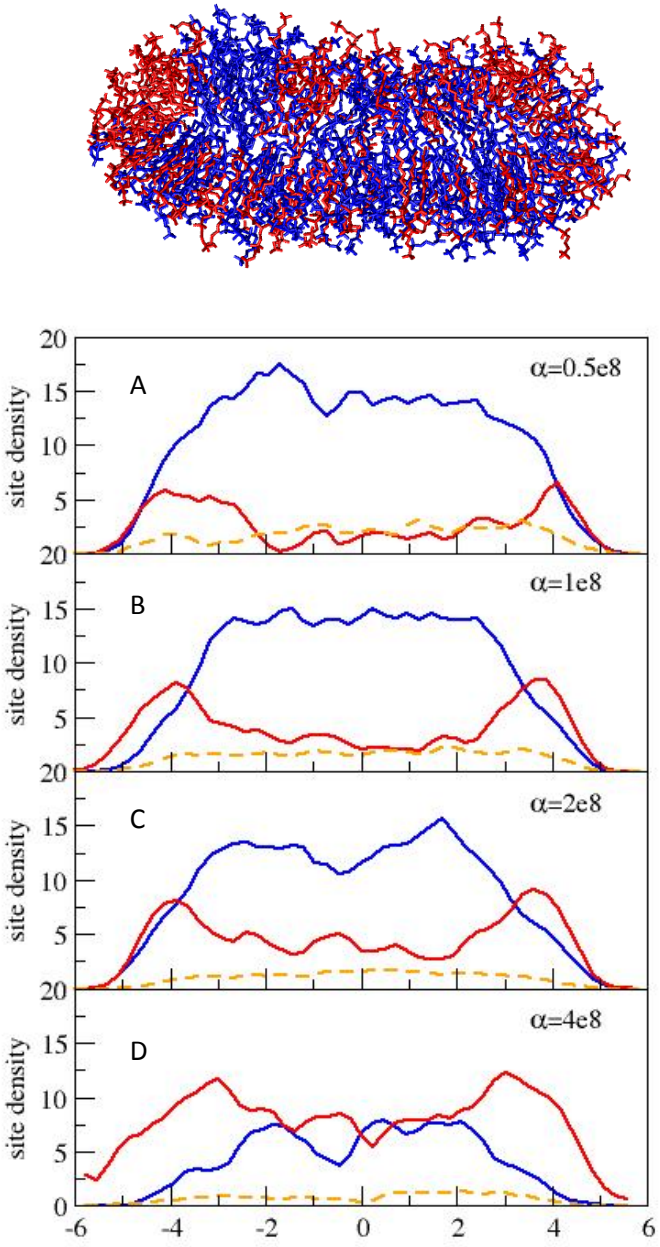

Figure 4.4 Site density profile of different lipid compenents as a function of distance to the geometrical center(the zero point in x axis) along the direction across the bilayer edge. Blue curve: DMPC. Red Curve DHPC. Yellow dashed curve:DDPC(intermediate).

Edge fluctuation

Fluctuation of the edge is closely related to edge free energy. As fluctuation introduced more edges to the system, one would expect large fluctuation of the edge at low edge line tension and small fluctuations as high edge line tension. Consistently, we observe the amplitude of the edge fluctuation increases with increasing DHPC percentage. When the line tension is small, long wavelength fluctuation is restrained by the box size. We observe strong local curvatures present along the edge throughout simulation, indicating the persistent length of the edge should be smaller than the box size (6nm). Large amplitude of in-plane fluctuation induced out-of-plane bending as shown in the snapshot in Figure 4.2D.

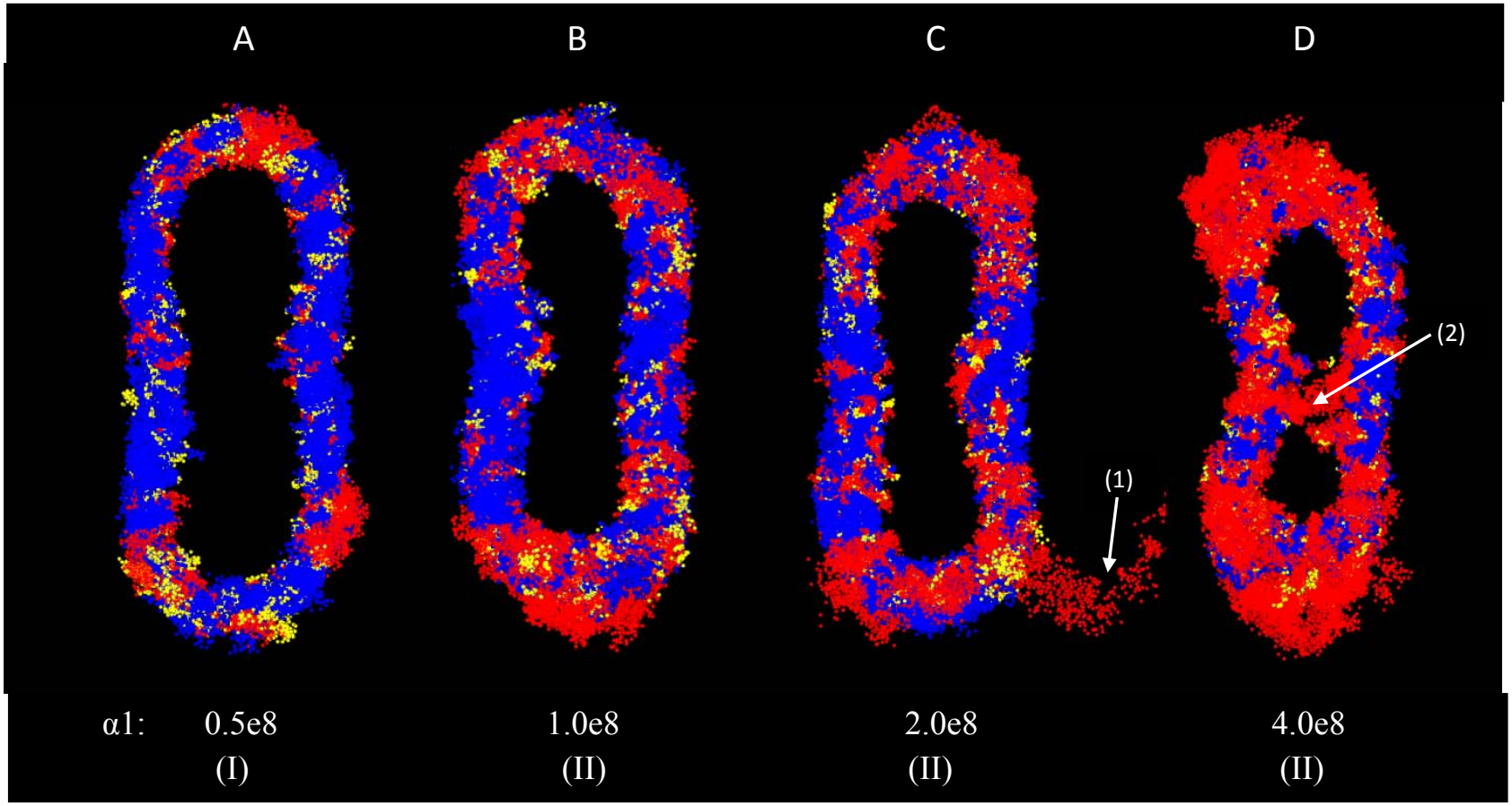

Figure 4.5. Overlapped scatter plot of phosphorus atoms generated from the trajectories, indicating the positions of the headgroups. Blue: DMPC headgroups. Red: DHPC headgroups. Yellow: DDPC headgroups. The trailing part in the lower-right part of C depicts the trajectory of a DHPC diffusing way from the ribbon edge (Arrow 1). Arrow 2: formation of water channel in the ribbon bulk center.

Water pore formation

At low line tension and high composition of short-tail lipid DHPC present in the systems, the lipid ribbon assembly undergoes significant reorganization in the bulk region as well as large in-plane and out-of-plane fluctuations on the edge. As shown in Figure 4.6, a pore gradually formed and developed within the first 20ns. The figure shows the composition of the lipid assembly converges very quickly within the first 1 or 2ns and remains unchanged afterwards. From 1ns to 10ns, before the appearance of the pore, the long-tail lipid DMPC (shown in blue) is more or less randomly distributed in the bulk region. The pore appears immediately before 10ns right in the midpoint between the two edges. Note that the central of the bulk region connects the two bulging edges (see description of edge bulging effect above) and therefore is smallest in thickness and rich in DHPC. The pore steadily grows after its formation and water molecules begin to penetrate through the bilayer. Water penetration helps the pore continue to grow and its side effect is to push more DMPC switched to short-tail lipid so as to reduce the line tension along the pore rim. The pore's existence induces significant change in lipid distribution. At the end of 20ns, the rim of the edge is almost exclusively occupied by DHPC. The shape of pore is irregular and keeps distorting itself while growing. The pore provides another way of extending the edge; the size of the pore becomes roughly 2.5nm in diameter at 20ns and continues to grow. The steady-growing pore edge indicates the system has reached the zero line tension regime; and the two edge contours become more rugged and prone to larger fluctuation amplitude after the appearance of the pore. Limited by system size and periodic boundary condition, one edge becomes very close to the image of another edge and may eventually merge. With the growing pore, this could lead

to a complete rupture of the ribbon geometry, resulting in a possible interconnected morphology which has been proposed from experimental observations.

DISCUSSION

Efficiency of the method

From the result of DPPC/DLPC binary mixture, each MC step takes about 70% CPU time of one MD step; the acceptance rate of one-step mutation for such system (differ by four carbons in each tail) is on the order of 0.1%, which is high enough for the hybrid MCMD method to give significant improvements over pure MD to investigate equilibrium properties of mixed lipid systems[19]. In two-step mutation scheme, as the intermediate can has dual directions to mutate, the equilibration process of DMPC/DHPC would take longer than DPPC/DLPC system depending on the amount of intermediate lipid present. For equally distributed system (L:Intermediate:S=33%:33%:33%), we would expect equilibration process takes about 4 times longer than one-step mutation (L:S=50%:50%) and time required for equilibration would increase linearly with decreasing amount of intermediate.

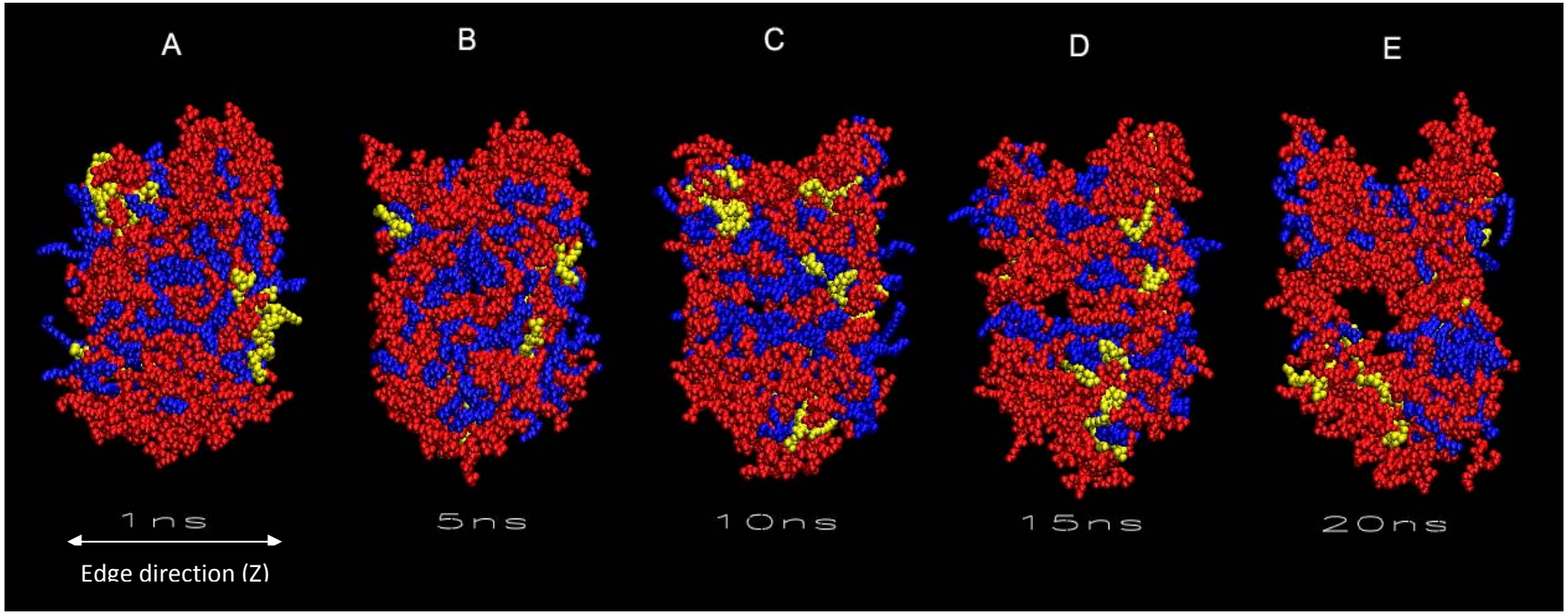

Figure 4.6. The process of water pore formation. Activity ratio between DMPC/DHPC set to 4.0e8. Water molecule is not shown for clarity. Blue: DMPC. Red: DHPC. Yellow DDPC (intermediate), the horizontal direction is the edge direction denoted by Z.

Edge bulging

We observe edge bulging effect in previous simulations[34, 35] and current study. The edge bulging is the consequence of the reorganization between different lipid type. The bulging of the edge helps to avoid strong curvature in the edge and potential steric repulsions due to limited volume in the edge cap. We also found the bulging effect introduced curvature and thinning in the bulk center. The thickness fluctuation in the bulk then facilitates enhancement of short-tail lipid in the bulk center and eventually leads to the formation of the water pore.

Lipid diffusion into solvents

In the condition of high percentage of short-tail lipid present in the ribbon, we observed individual S lipids (DHPC) diffuse into solvents on occasion. Two lipids escaped from the both edges of ribbon assembly where the local concentration of short-tail lipid is very high. One of them merged back to the assembly shortly but soon diffused away, indicating the short-tail lipid may more or less reached equilibrium between the assembly state and the fully solvated solution state. We can therefore estimate the critical micelle concentration (CMC) of DHPC. Experimentally, there exists a small range of concentrations separating the limit below which no micelle aggregates form and above which virtually no free surfactant can be found. The CMC is a concentration where micelles and free lipid can coexist. Our simulation provides an estimated CMC of ~10mM, which is close to experimental value of 14mM[36, 37].

CONCLUSIONS

We have extended the one-step CBMC-MD method for mixed lipid systems to two-step mutation method that supports simulations of lipid mixtures which have significant difference in the tail length of their components. This two-step scheme introduces an intermediate species that facilitates the transition between long-tail lipid and short-tail lipids. This mechanism was shown to be consistent with previous one-step mutation results [19] when applied to the same system of DPPC/DLPC. We have applied this method on DMPC/DHPC systems with edge defects over a series of molar ratios of the components. The number density profile from different lipid type reproduces the segregation phenomena of long and short-chain lipid type at the edge and indicates a saturation threshold beyond which free energy difference between the edge and the bulk will be weaken and more short-tail lipids are accumulating in the bulk center. At high percentage of short-tail lipid present in system, the edge shows large fluctuations and a water pore began to form after 10ns simulation, indicating the system has reached a zero line tension regime at that composition. The current method allows us to investigate "bicelle" system at different line tension condition and therefore provides insights to complex phase behavior and morphologies observed in experiments.

It will be of interest to apply the current method to investigate the structure of disk-shaped aggregates of DMPC and DHPC, as well as to explore the pore structure without the complication of the ribbon edges. The two-step approach more generally might eventually be useful for mixtures in which tail saturation, rather than tail length, is changed during mutations, or even for mixtures of lipids having different head-groups.

REFERENCE

1. Singer, S.J. and G.L. Nicolson, *Fluid Mosaic Model of Structure of Cell-Membranes.* Science, 1972. **175**(4023): p. 720-&.
2. Simons, K. and E. Ikonen, *Functional rafts in cell membranes.* Nature, 1997. **387**(6633): p. 569-572.
3. Tjandra, N. and A. Bax, *Direct Measurement of Distances and Angles in Biomolecules by NMR in a Dilute Liquid Crustalline Medium.* Science, 1997. **278**: p. 1111.
4. Sanders, C.R. and J.P. Schwonek, *Characterization of Magnetically Orientable Bilayers in Mixtures of Dihexanoylphosphatidylcholine and Dimyristoylphosphatidylcholine by Solid-State Nmr.* Biochemistry, 1992. **31**(37): p. 8898-8905.
5. Bax, A., *Weak alignment offers new opportunities in NMR structure determination of proteins and nucleic acids.* Abstracts of Papers of the American Chemical Society, 2003. **226**: p. U241-U241.
6. Bax, A., *Weak alignment offers new NMR opportunities to study protein structure and dynamics.* Protein Science, 2003. **12**(1): p. 1-16.
7. Harroun, T.A., et al., *Comprehensive examination of mesophases formed by DMPC and DHPC mixtures.* Langmuir, 2005. **21**(12): p. 5356-5361.
8. Nieh, M.P., et al., *SANS study of the structural phases of magnetically alignable lanthanide-doped phospholipid mixtures.* Langmuir, 2001. **17**(9): p. 2629-2638.

9. Vold, R.R. and R.S. Prosser, *Magnetically oriented phospholipid bilayered micelles for structural studies of polypeptides. Does the ideal bicelle exist?* Journal of Magnetic Resonance Series B, 1996. **113**(3): p. 267-271.

10. Luchette, P.A., et al., *Morphology of fast-tumbling bicelles: a small angle neutron scattering and NMR study.* Biochimica Et Biophysica Acta-Biomembranes, 2001. **1513**(2): p. 83-94.

11. vanDam, L., G. Karlsson, and K. Edwards, *Morphology of Magnetically Aligning DMPC/DHPC Aggregates-Perforated Sheets, Not Disks.* Langmuir, 2006. **22**(7): p. 3280-3285.

12. Nieh, M.P., et al., *Magnetically alignable phase of phospholipid "Bicelle" mixtures is a chiral nematic made up of wormlike micelles.* Langmuir, 2004. **20**(19): p. 7893-7897.

13. Harroun, T.A., et al., *Comprehensive Examination of Mesophases Formed by DMPC and DHPC Mixtures.* Langmuir, 2005. **21**(12): p. 5356-5361.

14. Rossky, P.J., J.D. Doll, and H.L. Friedman, *Brownian Dynamics as Smart Monte-Carlo Simulation.* Journal of Chemical Physics, 1978. **69**(10): p. 4628-4633.

15. LaBerge, L.J. and J.C. Tully, *A rigorous procedure for combining molecular dynamics and Monte Carlo simulation algorithms.* Chemical Physics, 2000. **260**(1-2): p. 183-191.

16. Morrow, T.I. and E.J. Maginn, *Isomolar-semigrand ensemble molecular dynamics: Application to vapor-liquid equilibrium of the mixture methane/ethane.* Journal of Chemical Physics, 2006. **125**(20): p. -.

17. Guarnieri, F. and W.C. Still, *A Rapidly Convergent Simulation Method - Mixed Monte-Carlo Stochastic Dynamics.* Journal of Computational Chemistry, 1994. **15**(11): p. 1302-1310.

18. Chiu, S.W., et al., *Application of combined Monte Carlo and molecular dynamics method to simulation of dipalmitoyl phosphatidylcholine lipid bilayer.* Journal of Computational Chemistry, 1999. **20**(11): p. 1153-1164.

19. de Joannis, J., et al., *Equilibrium distributions of dipalmitoyl phosphatidylcholine and dilauroyl phosphatidylcholine in a mixed lipid bilayer: Atomistic semigrand canonical ensemble simulations.* Journal of Physical Chemistry B, 2006. **110**(51): p. 25875-25882.

20. Siepmann, J.I. and I.R. Mcdonald, *Monte-Carlo Simulations of Mixed Monolayers.* Molecular Physics, 1992. **75**(2): p. 255-259.

21. Martin, M.G. and J.I. Siepmann, *Predicting multicomponent phase equilibria and free energies of transfer for alkanes by molecular simulation.* Journal of the American Chemical Society, 1997. **119**(38): p. 8921-8924.

22. Stubbs, J.M. and J.I. Siepmann, *Aggregation in dilute solutions of 1-hexanol in n-hexane: A Monte Carlo simulation study.* Journal of Physical Chemistry B, 2002. **106**(15): p. 3968-3978.

23. Siepmann, J.I. and D. Frenkel, *Configurational Bias Monte-Carlo - a New Sampling Scheme for Flexible Chains.* Molecular Physics, 1992. **75**(1): p. 59-70.

24. Rosenbluth, M.N. and A.W. Rosenbluth, *Monte-Carlo Calculation of the Average Extension of Molecular Chains.* Journal of Chemical Physics, 1955. **23**(2): p. 356-359.

25. Vangunsteren, W.F., H.J.C. Berendsen, and J.A.C. Rullmann, *Stochastic Dynamics for Molecules with Constraints Brownian Dynamics of Normal-Alkanes.* Molecular Physics, 1981. **44**(1): p. 69-95.

26. Berger, O., O. Edholm, and F. Jahnig, *Molecular dynamics simulations of a fluid bilayer of dipalmitoylphosphatidylcholine at full hydration, constant pressure, and constant temperature.* Biophysical Journal, 1997. **72**(5): p. 2002-2013.

27. Berendsen, H.J.C., et al., *In Intermolecular Forces*, ed. B. Pullman. 1981, Dordrecht, The Netherlands: D. Reidel Publishing Company. 331–342.

28. Hess, B., et al., *LINCS: A linear constraint solver for molecular simulations.* Journal of Computational Chemistry, 1997. **18**(12): p. 1463-1472.

29. Miyamoto, S. and P.A. Kollman, *Settle - an Analytical Version of the Shake and Rattle Algorithm for Rigid Water Models.* Journal of Computational Chemistry, 1992. **13**(8): p. 952-962.

30. Darden, T., D. York, and L. Pedersen, *Particle Mesh Ewald - an N.Log(N) Method for Ewald Sums in Large Systems.* Journal of Chemical Physics, 1993. **98**(12): p. 10089-10092.

31. Humphrey, W., A. Dalke, and K. Schulten, *VMD: Visual molecular dynamics.* Journal of Molecular Graphics, 1996. **14**(1): p. 33-&.

32. Tieleman, D.P. and H.J.C. Berendsen, *A molecular dynamics study of the pores formed by Escherichia coli OmpF porin in a fully hydrated palmitoyloleoylphosphatidylcholine bilayer.* Biophysical Journal, 1998. **74**(6): p. 2786-2801.

33. Allen, M.P. and D.J. Tildesley, *Computer simulation of liquids*. 1987, Oxford [England] New York: Clarendon Press ; Oxford University Press. xix, 385 p.

34. Jiang, F.Y., Y. Bouret, and J.T. Kindt, *Molecular dynamics simulations of the lipid bilayer edge.* Biophysical Journal, 2004. **87**(1): p. 182-192.

35. de Joannis, J., F.Y. Jiang, and J.T. Kindt, *Coarse-grained model simulations of mixed-lipid systems: Composition and line tension of a stabilized bilayer edge.* Langmuir, 2006. **22**(3): p. 998-1005.

36. Chou, J.J., J.L. Baber, and A. Bax, *Characterization of phospholipid mixed micelles by translational diffusion.* Journal of Biomolecular Nmr, 2004. **29**(3): p. 299-308.

37. Burns, R.A., et al., *Monomer-to-Micelle Transition of Dihexanoylphosphatidylcholine - C-13 Nmr and Raman Studies.* Journal of the American Chemical Society, 1982. **104**(2): p. 430-438.